ETAM
ΕΛΛΗΝΙΚΟ ΤΜΗΜΑ ΑΝΤΙΣΕΙΣΜΙΚΗΣ ΜΗΧΑΝΙΚΗΣ
HELLENIC ASSOCIATION FOR EARTHQUAKE ENGINEERING

in collaboration with

AFAD T.C. İÇİŞLERİ BAKANLIĞI AFET VE ACİL DURUM YÖNETİMİ BAŞKANLIĞI

TEE

TÜRKİYE DEPREM MÜHENDİSLİĞİ DERNEĞİ
EARTHQUAKE ENGINEERING ASSOCIATION OF TURKEY

NATIONAL TECHNICAL UNIVERSITY OF ATHENS

The February 6th Kahranmanmaras earthquake sequence in Turkiye

Technical Report

Editors & Reconnaissance Mission Coordinators:
Aristidis Papachristidis, Anastasios Sextos

Authors: Garini E., Gazetas G., Giarlelis C., Marinos V., Moretti M., Palieraki V., Pitilakis D., Stefanidou S., Thanopoulos P., Tsiatas G., Tsopelas P., Vintzileou E., Vougioukas E., Zeris C., Cekinmez M., Papachristidis A., Sextos A.

DOI: 10.13140/RG.2.2.33692.91526

Table of Contents

1. Introduction and Scope

Following the devastating Kahramanmaraş earthquake sequence that took place on February 6th, 2023 in Turkyie, a joint reconnaissance mission was organized by the **Technical Chamber of Greece** (TCG / TEE), in collaboration with **National Technical University of Athens** (NTUA) and the **Hellenic Association for Earthquake Engineering** (HAEE / ETAM). The reconnaissance team (Fig. 1.1) involved a team of 17 engineers and researchers (members of NTUA and/or the Board of HAEE), who traveled to the affected area for 5 days across over 1500 km in regions affected by the disaster (Fig. 1.2).

This field work was organized in close collaboration with AFAD in Turkiye, and covered the cities of Pazarcik, Gaziantep, Gölbaşı, Adiyaman, Kahranmanmaras, Antakya, Iskenderun, Nurdağı, and Islahiye. The team assessed both geotechnical failures and structural damage and performed Rapid Visual Inspections for around 500 residential buildings. The field mission took place in close collaboration with **AFAD**, which is the sole authority on disasters and emergencies in Turkyie (**Prof. O. Tatar**, General Manager and **Dr. Recep Cakir**) and the **Earthquake Engineering Association of Turkey** (**Prof. Altug Erberik**, President of the Association).

Coordination was also made with scientific international teams such as the Geotechnical Extreme Events Reconnaissance (GEER) Association and Middle East Technical University (**Prof. Haluk Sucuoglu** and **Prof. Kemal Onder Cetin**). The authors of this report would like to warmly thank the above organizations and international experts for their support and collaboration before, during and after the mission. Acknowledgements are also extended to **Prof. Andreas Boudouvis** (Rector, NTUA), **Prof. Evaggelos Sapountzakis** (Vice rector, NTUA), **Prof. Nikolaos Lagaros** (Dean, NTUA) and the **Embassy of Greece at Ankara** for their administrative and scientific support. Sincere thanks are also due to the **Technical Chamber of Greece**, which funded the campaign, and particularly to President **George Stasinos** and the coordination and **Liana Anagnostaki**, Head of International Relations, without the help of which this reconnaissance mission would not be feasible.

Figure 1.1 The joint TEE/NTUA/ETAM mission at the epicentral area of the Kahranmanmaras earthquake sequence (April, 2023).

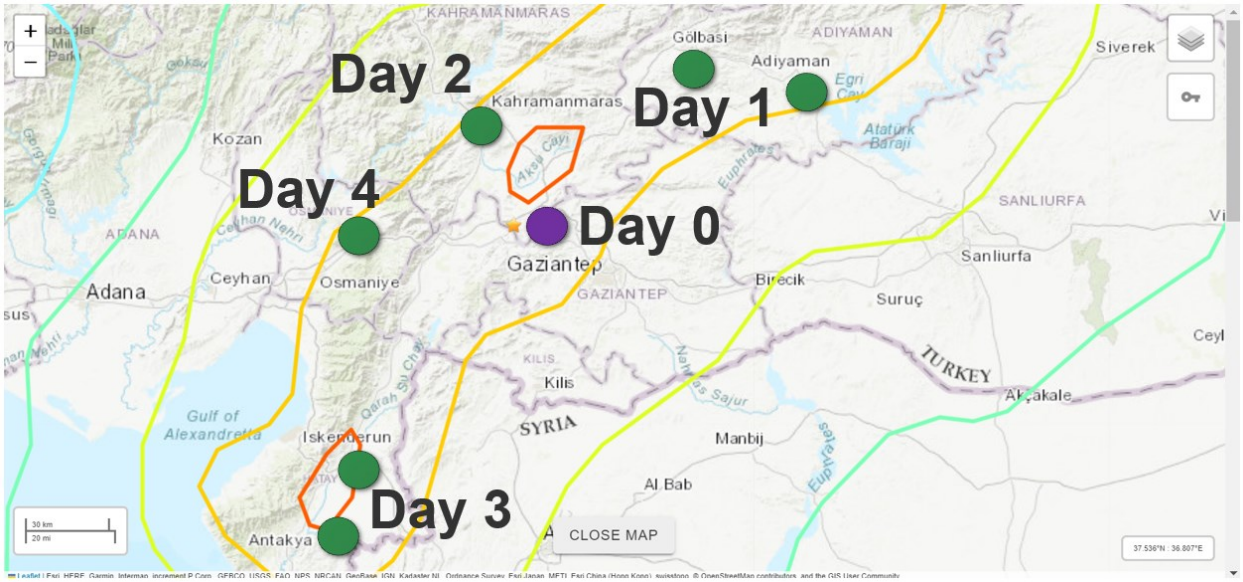

Figure 1.2 Itinerary of the reconnaissance mission across Southeast Turkiye.

2. Strong Ground Motions and Near - Fault Effects

Chapter Authors: ***Evangelia GARINI*** *and* ***George GAZETAS***

Two major strong motion Networks operate in Turkey: the AFAD and the KOERI. In particular, AFAD [Disaster and Emergency Management Presidency] is the Turkish National Strong Motion Network and comprises 856 recording stations nationwide (Figure 2.1). KOERI stands for the Kandilli Observatory and Earthquake Research Institute and counts 249 recording stations (Figure 2.2). Therefore, a total of 1105 recording stations are operating in Turkey. Herein, we will present and discuss the recordings from the AFAD Network.

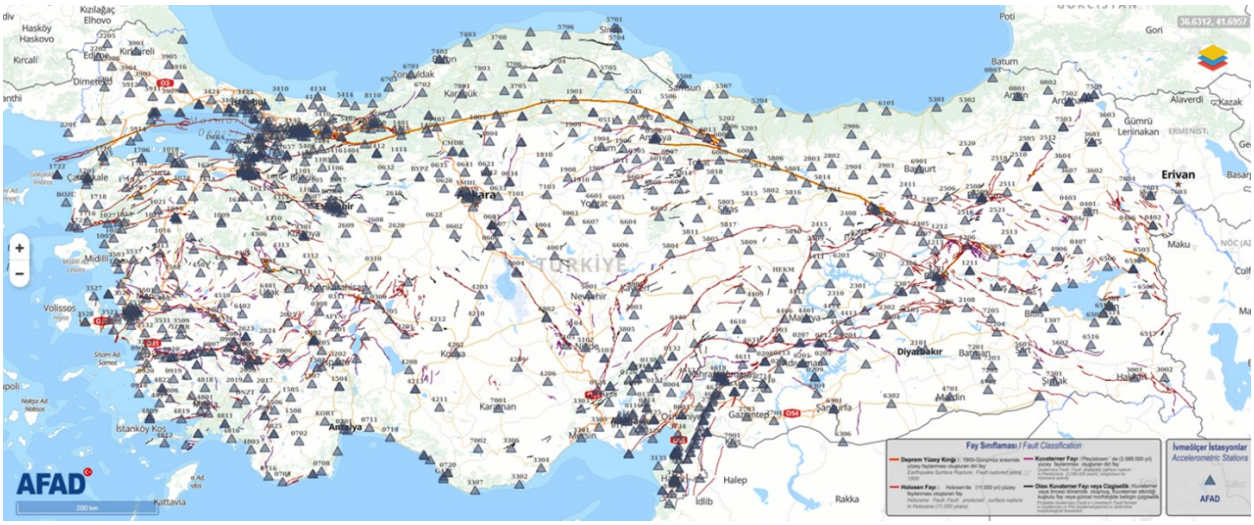

Figure 2.1 Map of the AFAD strong motion Network. The recording stations are shown with blue triangles.

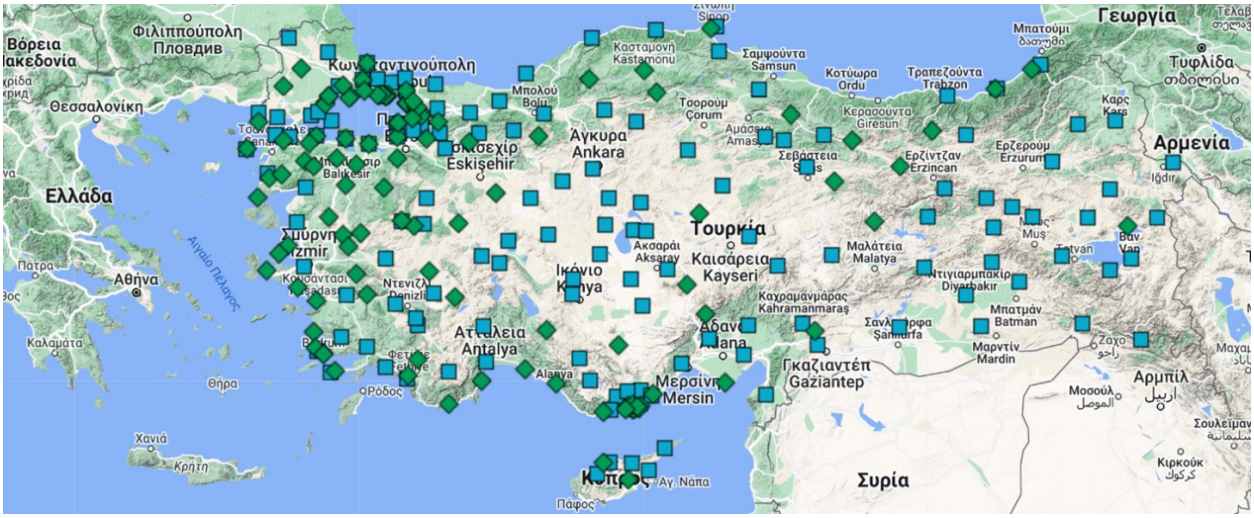

Figure 2.2 Map of the KOERI strong motion Network.

2.1 Recordings from the M_w7.8 Pazarcik EQ

During the M_w7.8 Pazarcik earthquake of February 6th 2023, a total of 379 recordings have been reported by AFAD (https://tadas.afad.gov.tr/event-detail/17966). Distribution of Peak Ground Acceleration (PGA) and Peak Ground Velocity (PGV) recorded in the Pazarcik event, are shown in Figures 2.3 and 2.4 respectively.

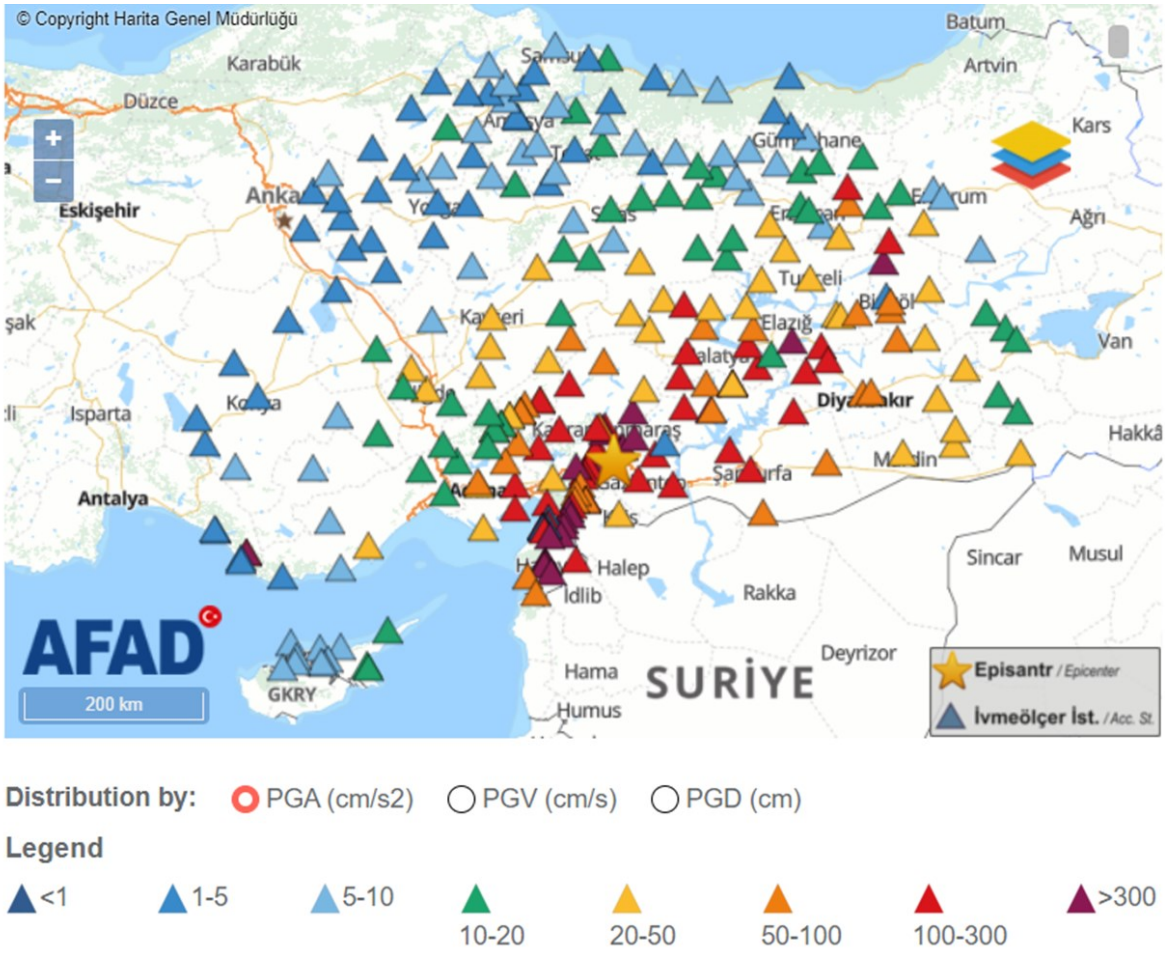

Figure 2.3 Recorded PGAs at the AFAD stations during the Mw7.8 Pazarcik seismic event (Source: https://tadas.afad.gov.tr/event-detail/17966).

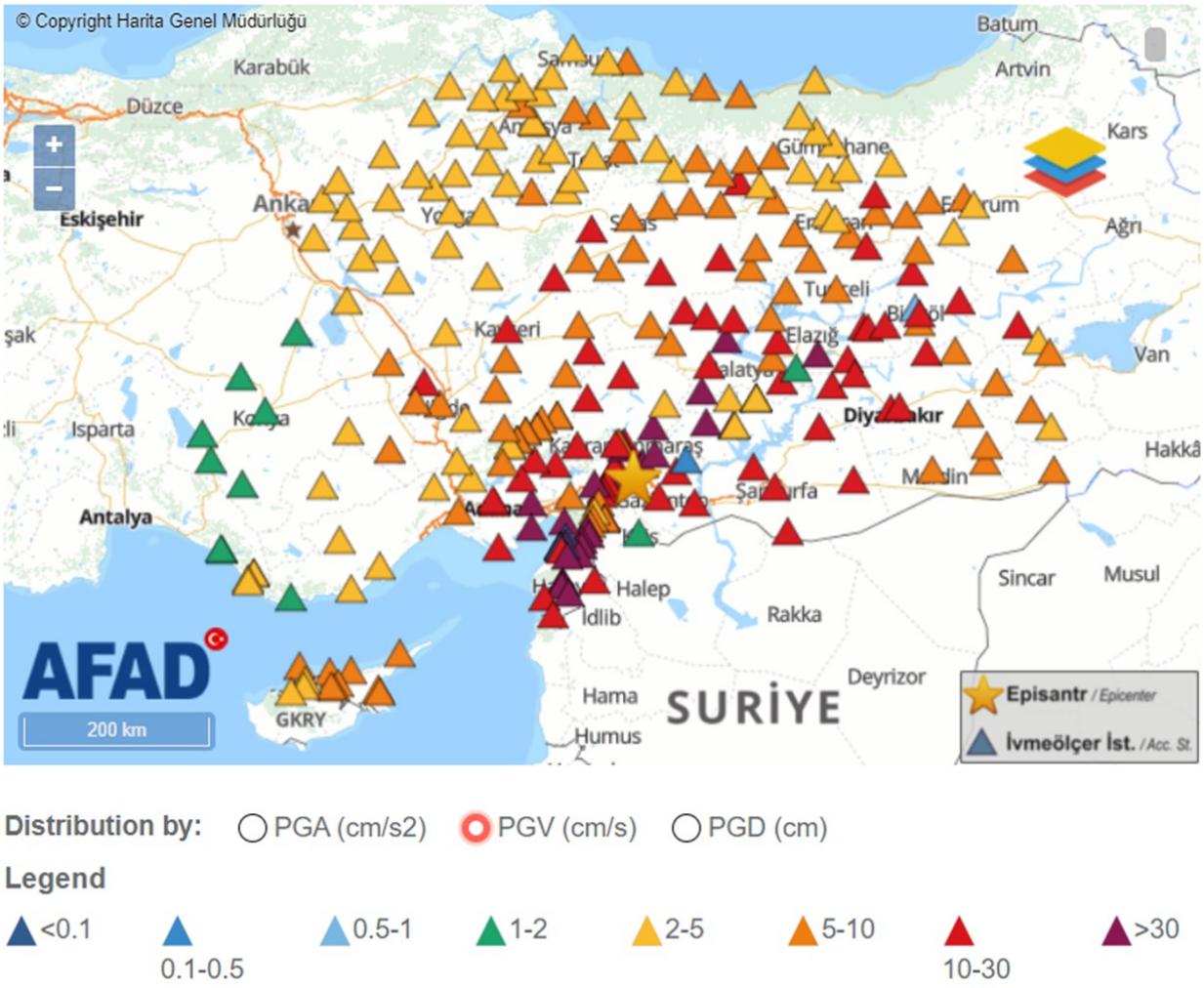

Figure 2.4 Recorded PGVs at the AFAD stations during the Mw7.8 Pazarcik seismic event (Source: https://tadas.afad.gov.tr/event-detail/17966).

The highest peak acceleration was recorded in station 4614 in Pazarcik city, with 30 km epicentral distance but only 5 - 6 km fault distance from both the first and second rupture segments as Figure 2.5 shows. The recorded peak horizontal accelerations in station 4614 were: 2.15 g and 2.13 g in the HNE and HNN components respectively. The peak vertical component of 1.58 g was also very high.

Acceleration and velocity time-histories of the two horizontal components of station 4614 are illustrated in Figures 2.6 and 2.7. The corresponding elastic response spectra are pictured in Figure 2.8. Observe the large spectral accelerations (greater than 1 g) for the period range [0.0 - 0.7 s]. Many near-fault records are captured with AFAD network: 33 stations recorded PGAs greater than 0.3 g (Table 2.1) from the Pazarcik earthquake.

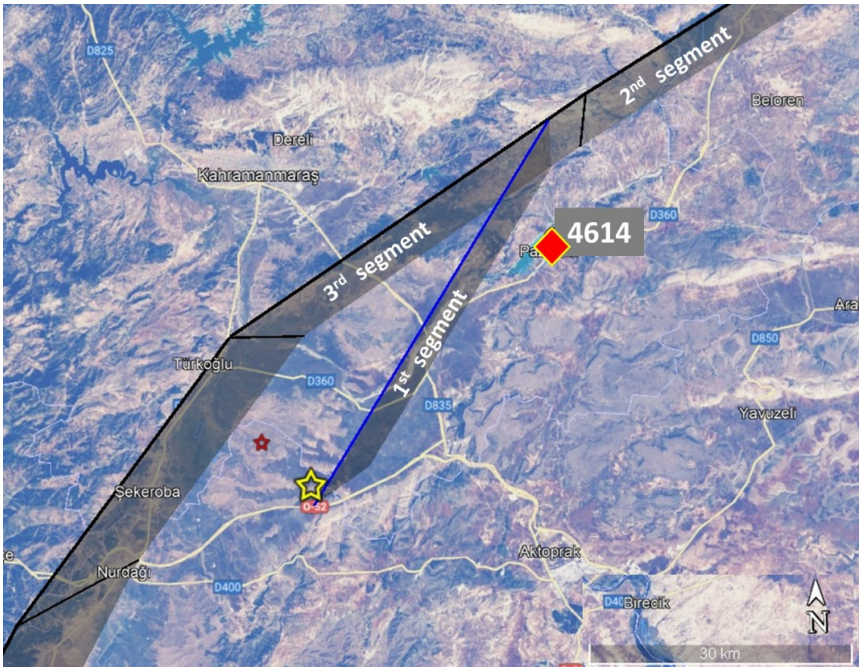

Figure 2.5 Map of the rupturing fault segments during Mw7.8 Pazarcik earthquake along with the location of station 4614 in which the greatest PGAs were recorded.

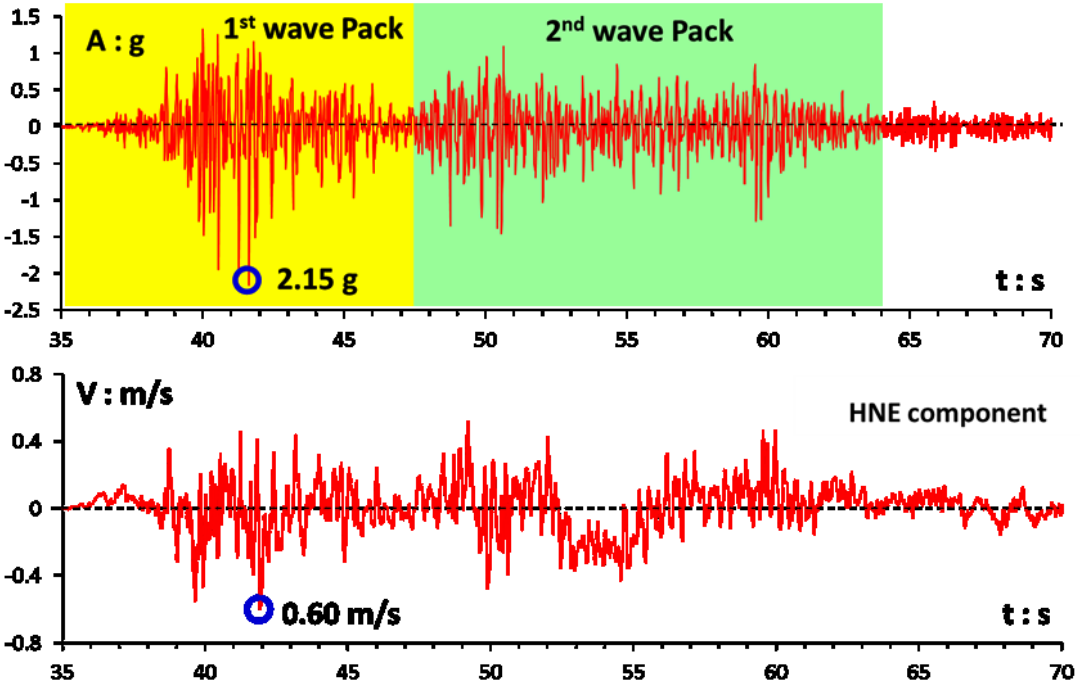

Figure 2.6 Acceleration (top) and velocity (bottom) timehistories of the horizontal component HNE recorded in station 4614 during Pazarcik earthquake.

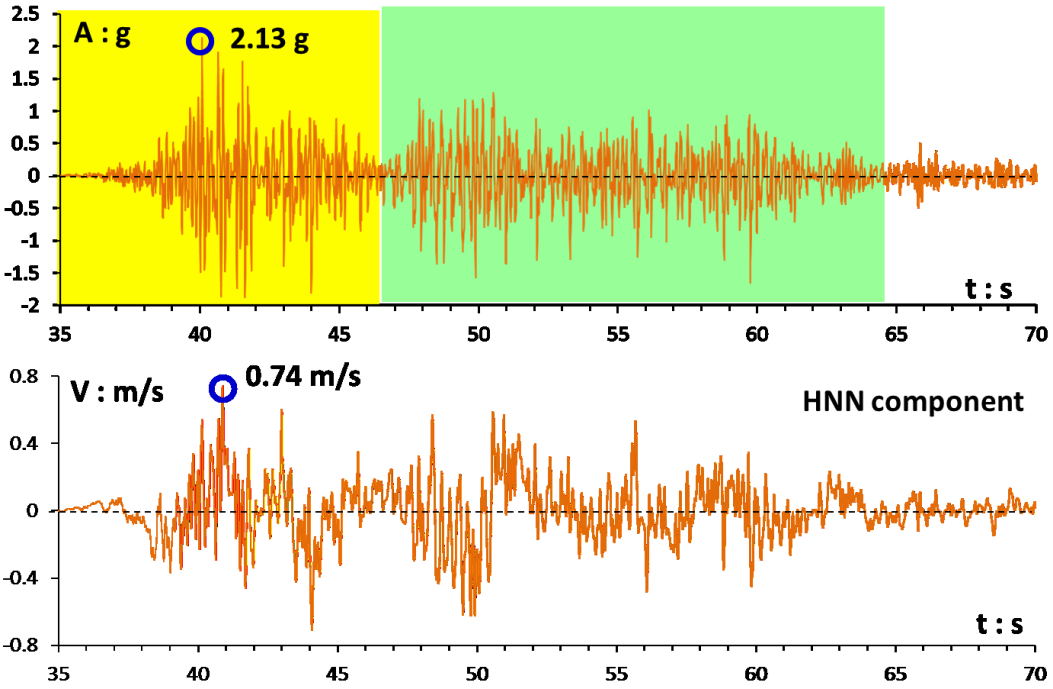

Figure 2.7 Acceleration (top) and velocity (bottom) timehistories of the horizontal component HNN recorded in station 4614 during Pazarcik earthquake.

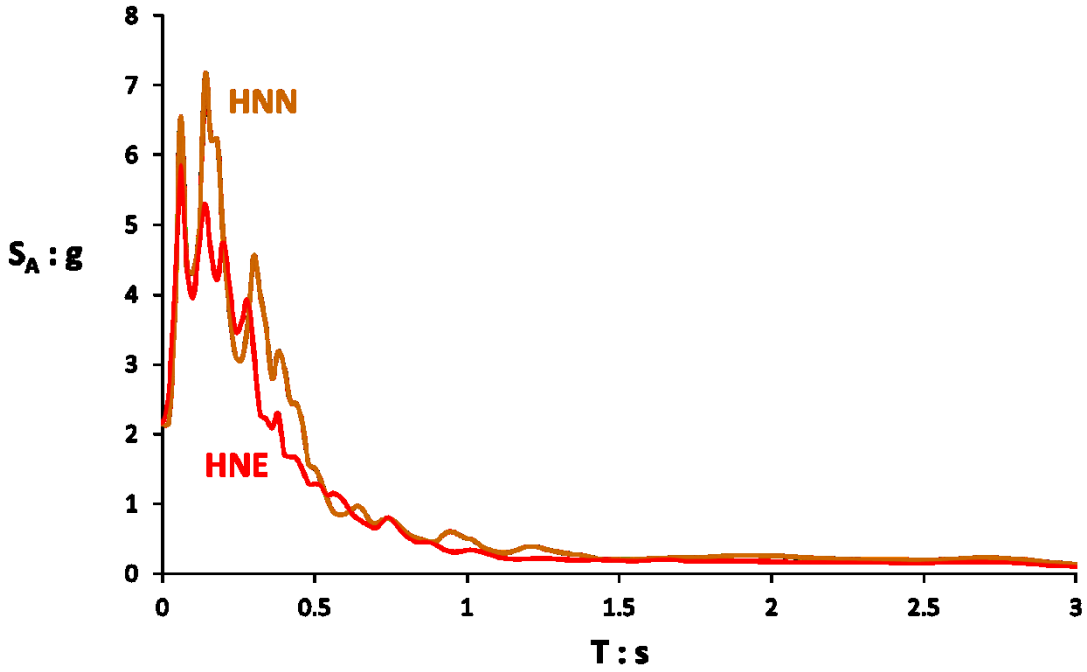

Figure 2.8 Acceleration spectra of the HNE and HNN components of station 4614 during Pazarcik earthquake.

Table 2.1 Stations with recorded PGA over 0.3 g, from the M_w7.8 Pazarcik earthquake.

Station Code	PGA_NS (g)	PGA_EW (g)	PGA_UP (g)
4614	**2.02**	**2.04**	**1.58**
3129	**1.35**	**1.20**	**0.72**
3126	**1.18**	**1.00**	**0.92**
3141	**0.96**	**0.87**	**0.72**
3125	**0.82**	**1.12**	**1.15**
NAR	0.78	0.62	0.48
3135	**0.74**	**1.37**	**0.59**
3123	0.66	0.59	0.87
2718	0.65	0.63	0.59
3142	0.65	0.74	0.46
3144	0.61	0.76	0.45
4616	0.61	0.43	0.39
3145	0.59	0.69	0.61
4615	0.58	0.56	0.66
3139	0.58	0.50	0.38
3124	0.57	0.64	0.58
2712	0.56	0.59	0.31
3136	0.53	0.40	0.22
3132	0.52	0.51	0.35
3146	0.48	0.35	0.34
201	0.47	0.88	0.32
2715	0.46	0.34	0.26
4625	0.45	0.47	0.34
3137	0.43	0.67	0.45
3143	0.38	0.35	0.41
4621	0.36	0.30	0.25
3131	0.36	0.37	0.15
4632	0.36	0.30	0.20
4624	0.36	0.31	0.16
4611	0.35	0.32	0.17
4629	0.34	0.25	0.12
4619	0.30	0.19	0.18
4620	0.30	0.32	0.19

2.1.1 Accelerographs along the Fault

The Mw7.8 Pazarcik event started from the rupturing of a small fault segment close to Pazarcik city (see Fig.2.5) and then rupture ***jumped*** to the well-known East Anatolian Fault, where a bilateral fracture moved towards North-East to Malatya (the second segment) and South-West to Antakya (the third segment). The phenomenon of a rupturing jump from one fault to another is not a new one (Fliss et al. 2005; Rice et al. 2001 & 2005). It was recognized and studied in detail among others for the 1992 Landers earthquake (Fialko 2004; Perfettini & Avouac 2007; Wollherr et al. 2019). In several locations the fault emerged at the ground surface, such as in Sekeroba,

Turkoglu, Hassa, Kirikhan, Gölbaşi, and others (Garini & Gazetas, 2023). A total of at least 210 km length of fault appear to have been ruptured in the M_w7.8 seismic event [METU 2023 report].

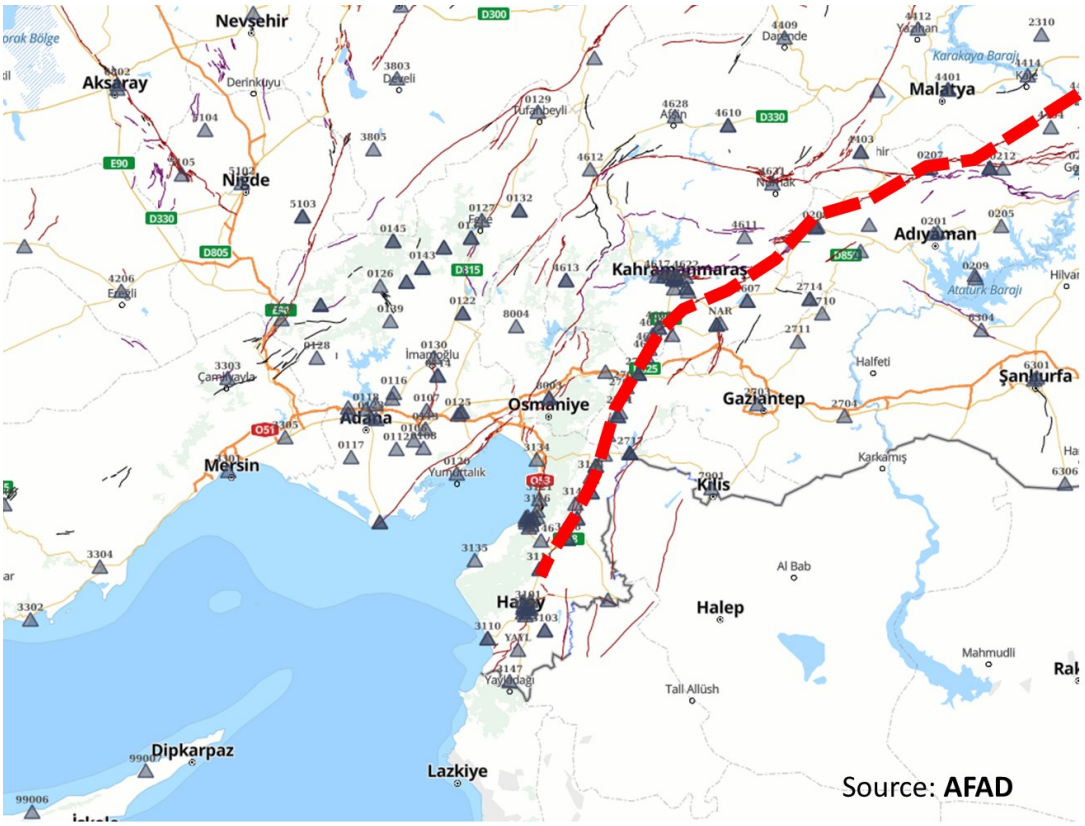

Figure 2.9 Map of the recording stations and the East Anatolian Fault segment (dashed red line) that cracked in the M_w7.8 Pazarcik earthquake.

More than 15 stations were located *on* or *near-field* the rupturing zone, as can be seen in Figure 2.9. Near-fault phenomena such as ***forward-directivity*** and ***supershear*** were captured in the acceleration and velocity timehistories of the recorded stations (Rosakis et al. 2023; Garini & Gazetas 2023). Forward-rupture directivity was manifested by the presence of large amplitude, long period pulses in acceleration and velocity timehistories recorded normal to fault plane. On the other hand, supershear appeared by well-defined velocity pulses in direction parallel to fault plane. In addition, when supershear occurred the parallel recordings were the dominating compared with the normal ones. Keep in mind that supershear can happen simultaneously with forward directivity, for instance in the Antakya 3126 station (Abdelmeguid et al. 2023; Wang et al. 2023).

Forward directivity effect was present in many recordings at stations along the first and third fault segment of M_w7.8 earthquake. On the contrary, supershear was only noticed in the NAR station in Pazarcik, the 3145 station in Balarmudu close to Kirikhan, as well as the stations of

Antakya especially 3124, 3123, 3129, according to the study of Rosakis et al. 2023 and Abdelmeguid et al. 2023.

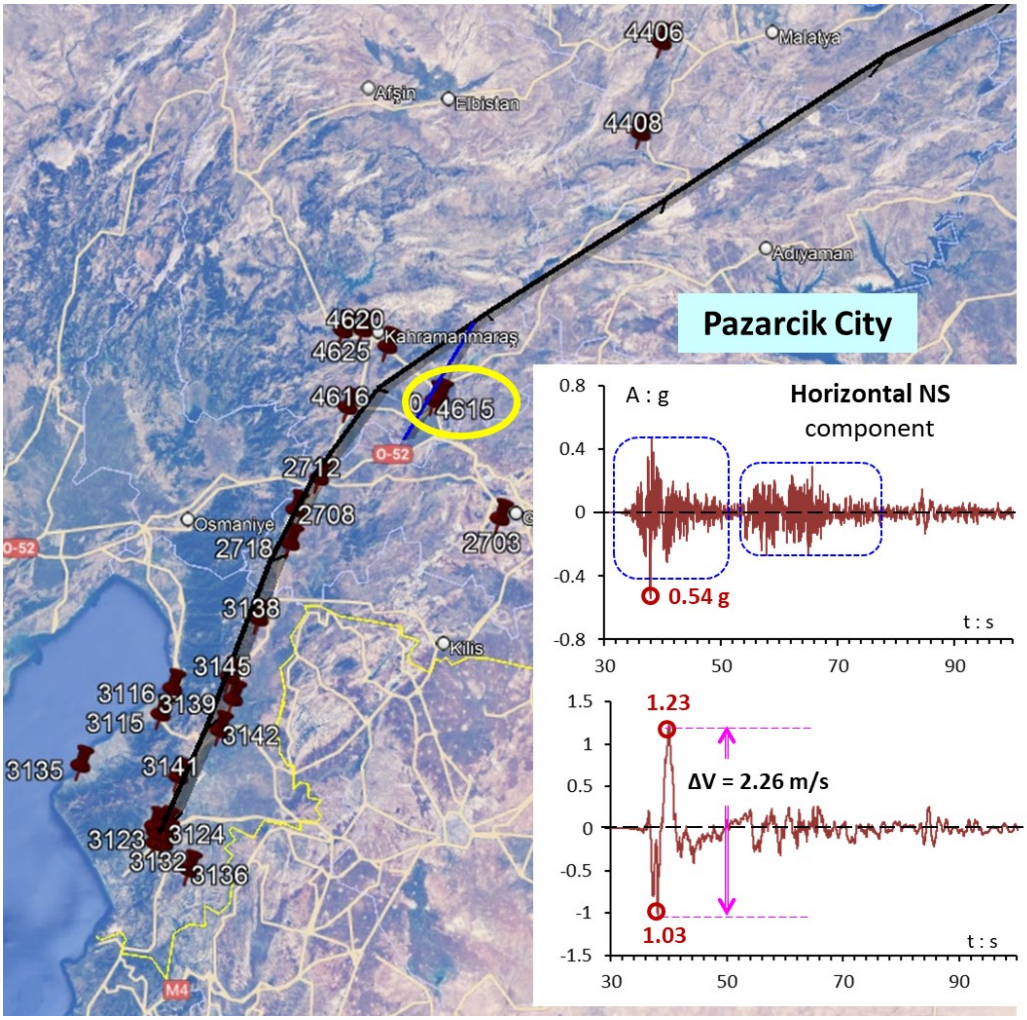

Figure 2.10 Location of station 4615 close to the first rupturing segment of M_w7.8 Pazarcik earthquake, along with the recording acceleration and velocity timehistories of the NS component of station 4615.

To demonstrate the evolution of acceleration records along the rupturing faults, Figures 2.10-2.13 present the recording accelerations and velocities in four characteristic locations: in station 4615 close to Pazarcik city, station 4616 in Turkoglu, and in stations 3123 and 3129 in Antakya. The distinct wave packets arising from the rupturing of the first and the second and third segments can be noticed in the acceleration timehistories of stations 4615 and 4616. On the contrary, Antakya recordings in stations 3123 and 3129 exhibit a sole sequence of acceleration pulses which are of large amplitude and period—a sign of the forward directivity effect.

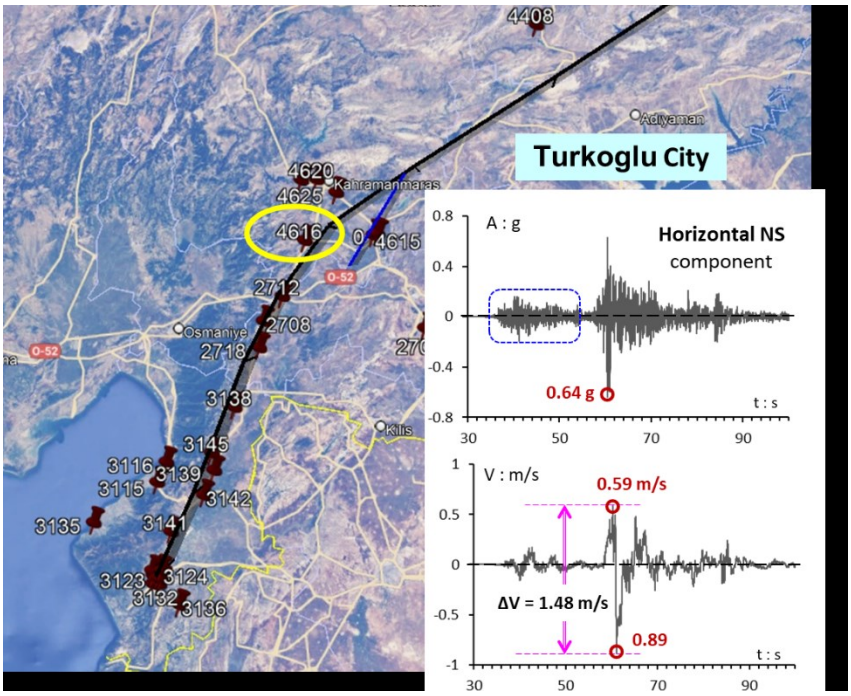

Figure 2.11 Location of station 4616 close to the third rupturing segment of M_w7.8 Pazarcik earthquake, along with the recording acceleration and velocity timehistories of the NS component of station 4616.

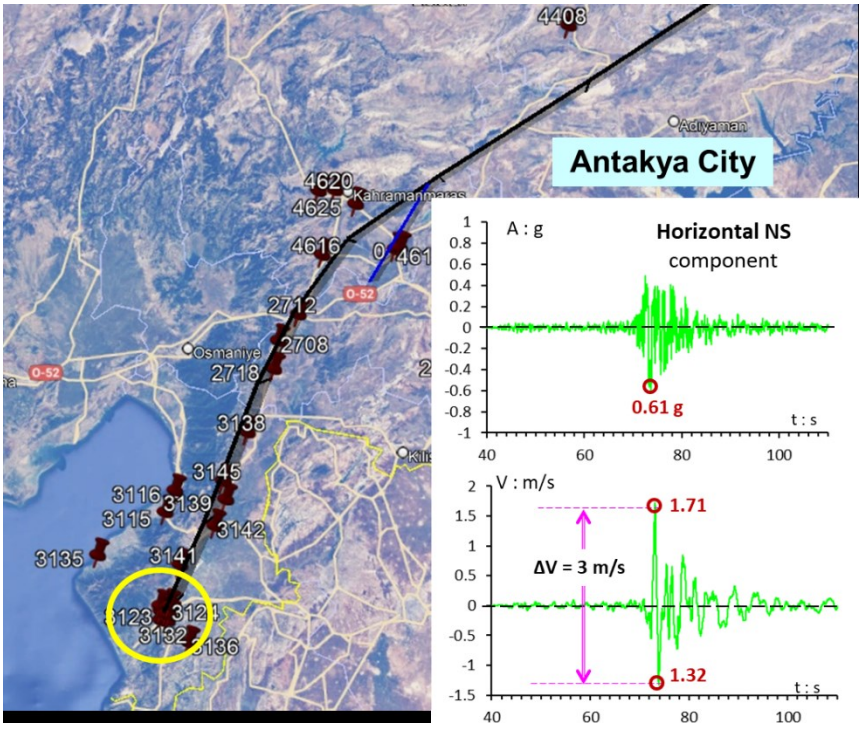

Figure 2.12 Location of station 3123 in Antakya, along with the recording acceleration and velocity timehistories of the NS component during the M_w7.8 Pazarcik earthquake.

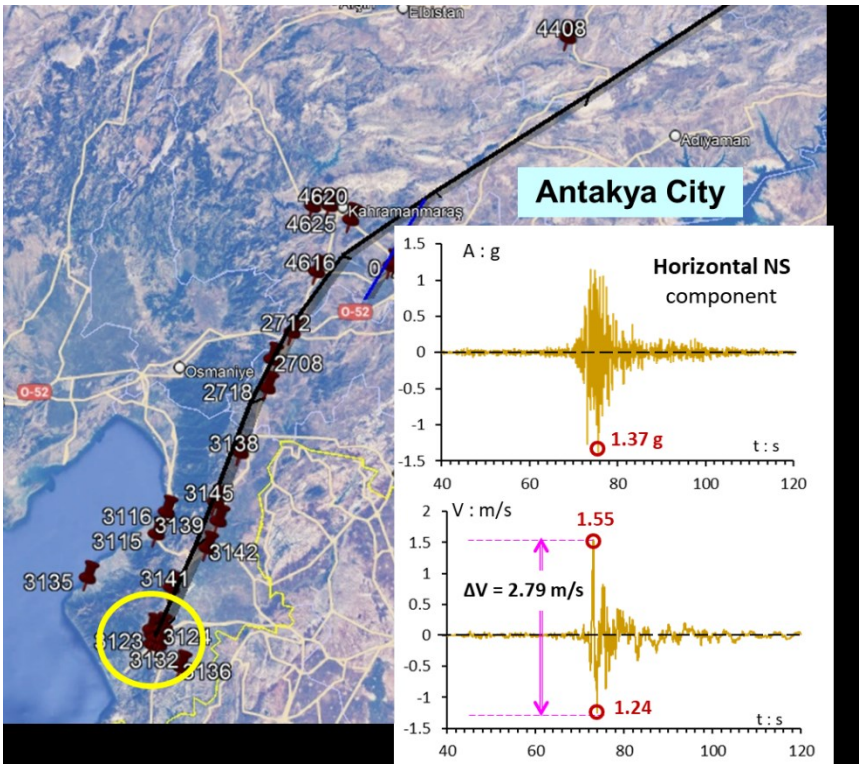

Figure 2.13 Location of station 3129 in Antakya, along with the recording acceleration and velocity timehistories of the NS component during the M_w7.8 Pazarcik earthquake.

2.1.2 Accelerographs at several major Turkish cities

Figures 2.14-2.23 picture characteristic recordings from the M_w7.8 seismic event, providing acceleration and velocity timehistories of all three components (NS, EW horizontal and vertical components) along with their elastic response spectra. The depicted stations, namely are:

Station	$V_{S,30}$	City	Prefecture
2712	Unknown	Nurdagi	Gaziantep
2718	Unknown	Islahiye	Gaziantep
3142	539 m/s	Kirikhan	Hatay
3145	533 m/s	Kirikhan	Hatay
4620	484 m/s	Onikişubat	Kahramanmaraş
4565	346 m/s	Dulkadiroğlu	Kahramanmaraş
4408	654 m/s	Doğanşehir	Malatya
3116	870 m/s	Iskenderun	Hatay
3125	448 m/s	Antakya	Hatay
3129	447 m/s	Antakya	Hatay

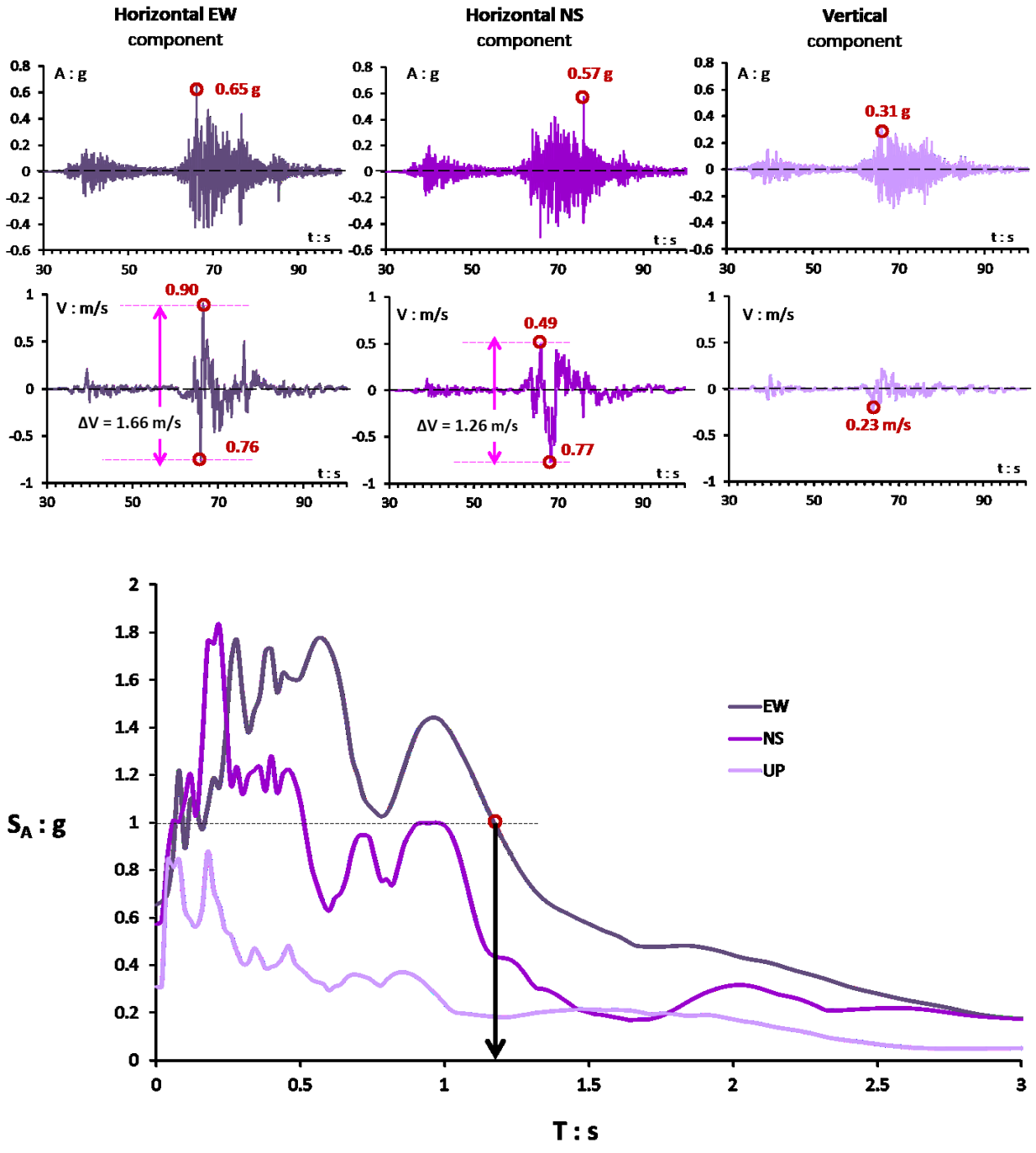

Figure 2.14 Acceleration and velocity timehistories of the two horizontal and one vertical components of station 2712 in Nurdagi, along with their elastic response spectra, as recorded in M_w7.8 Pazarcik earthquake.

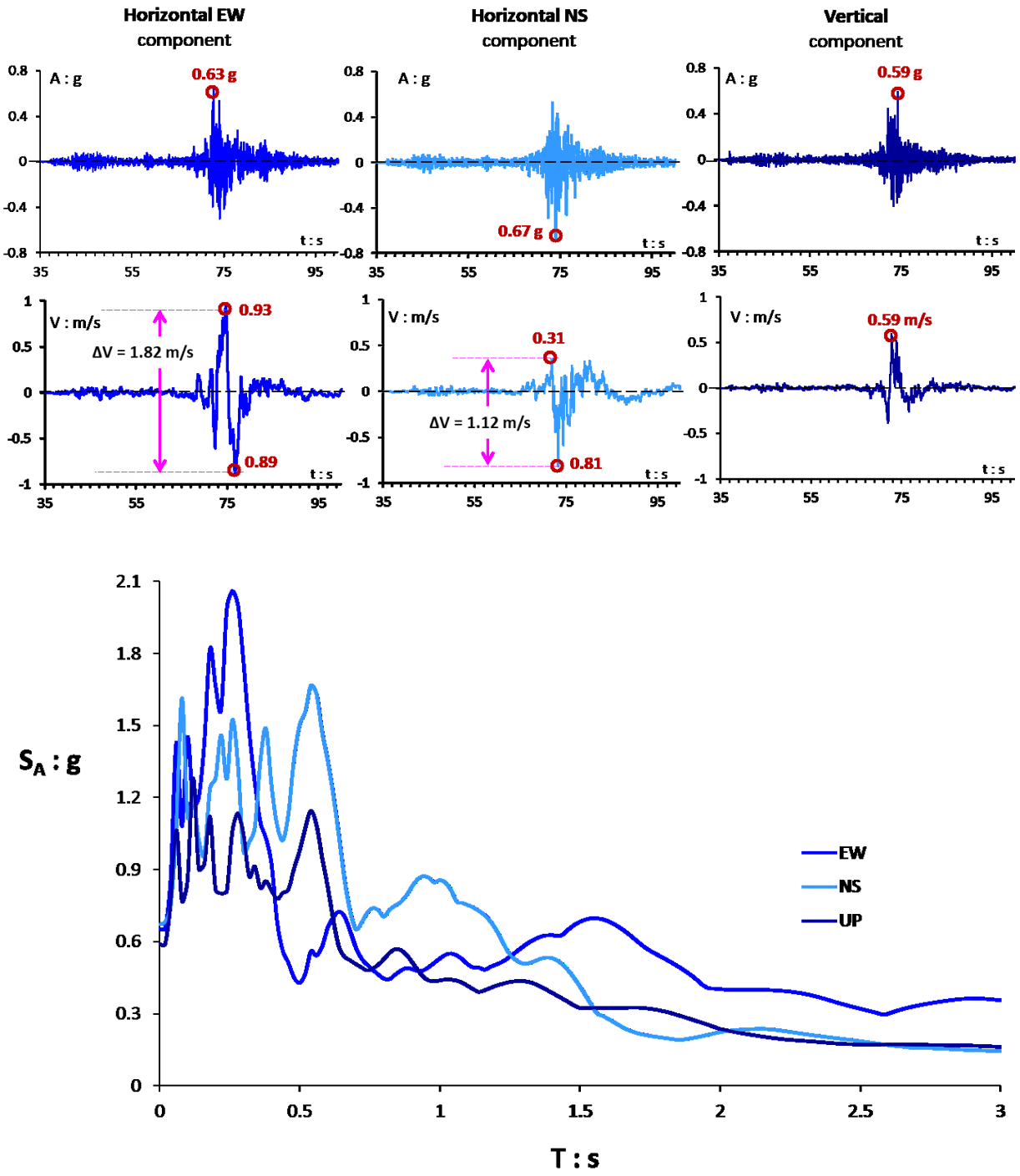

Figure 2.15 Acceleration and velocity timehistories of the two horizontal and one vertical components of station 2718 in Islahiye, along with their elastic response spectra, as recorded in M_w7.8 Pazarcik earthquake.

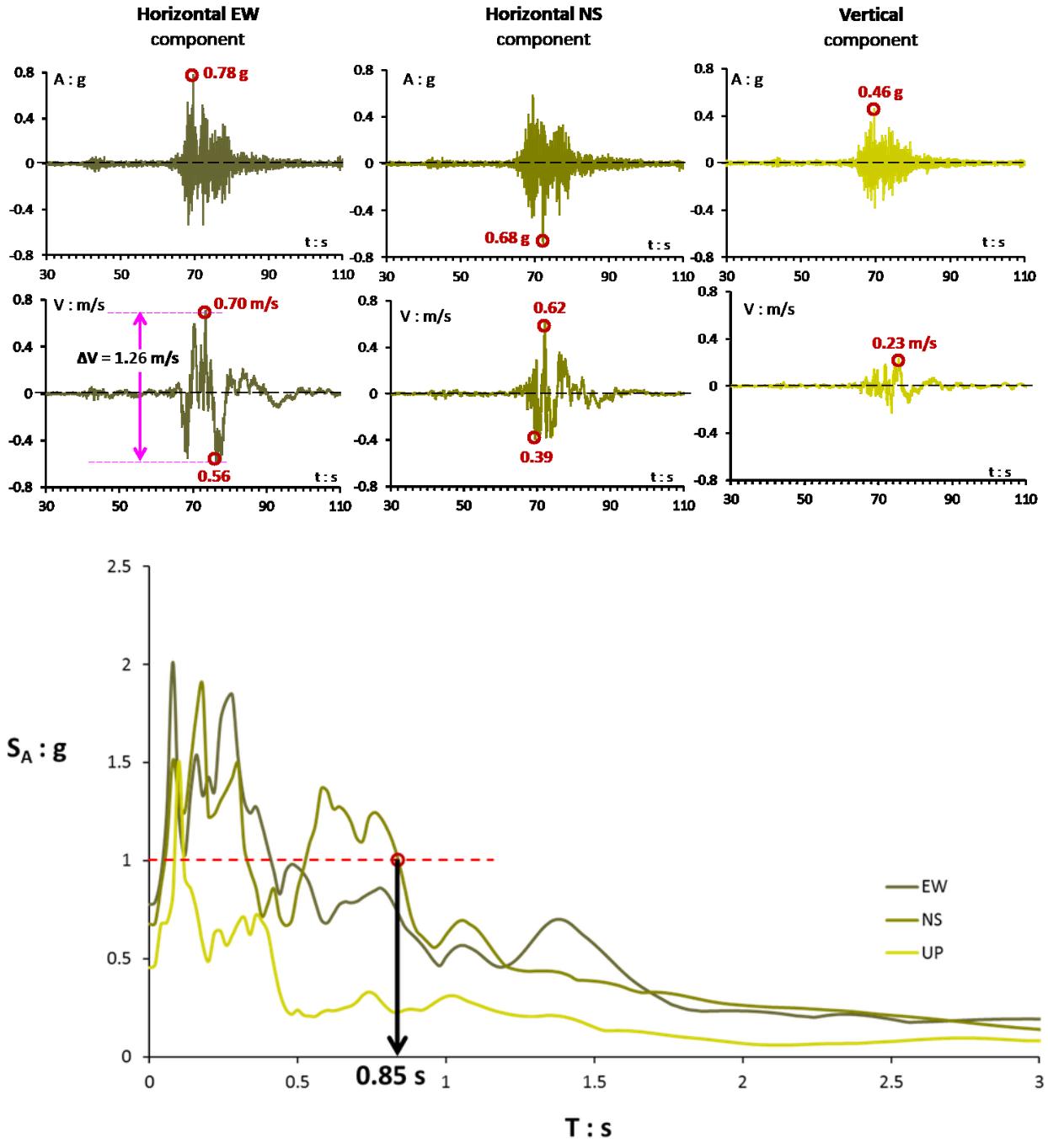

Figure 2.16 Acceleration and velocity timehistories of the two horizontal and one vertical components of station 3142 in Kirikhan, along with their elastic response spectra, as recorded in M_w7.8 Pazarcik earthquake.

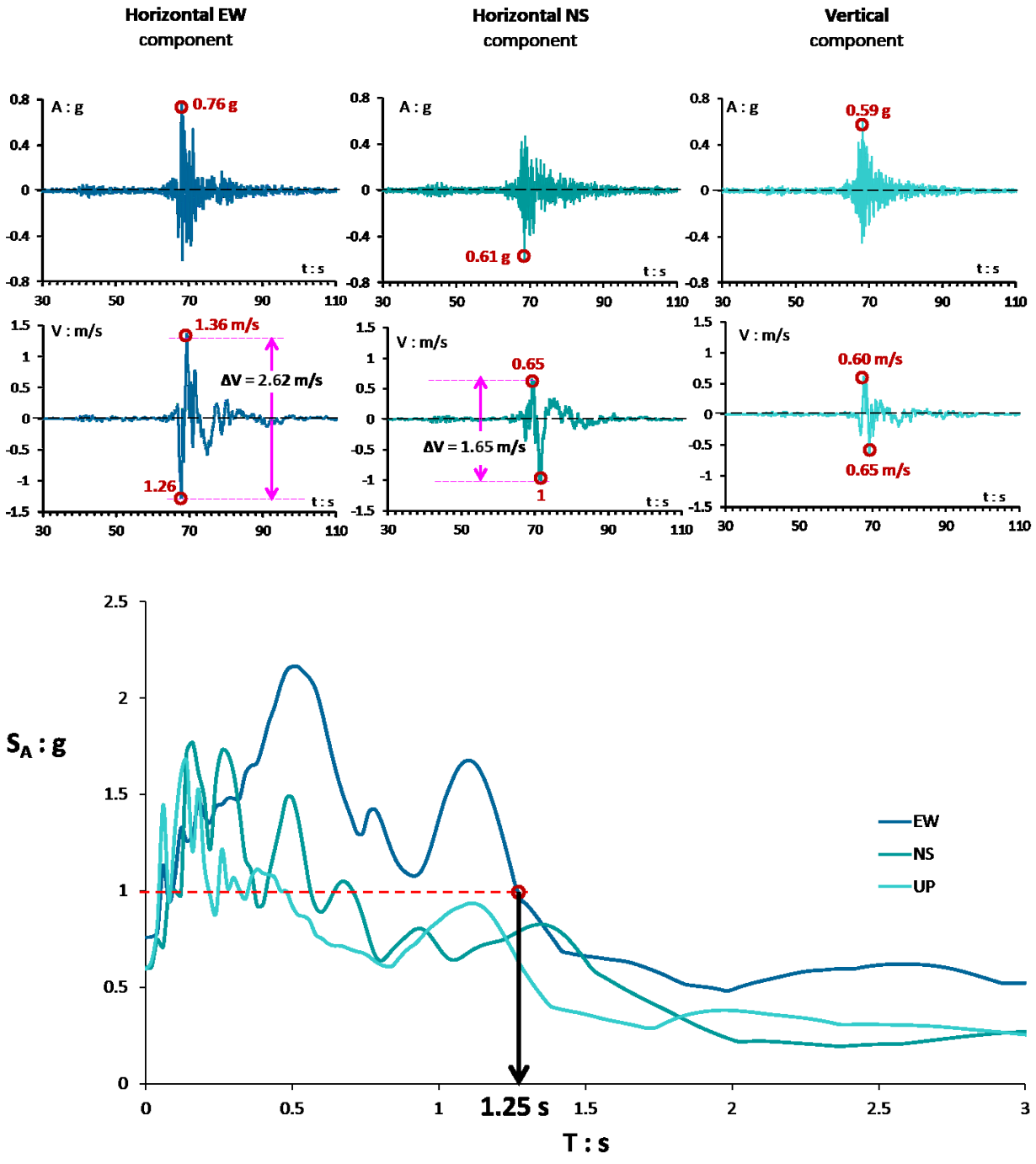

Figure 2.17 Acceleration and velocity timehistories of the two horizontal and one vertical components of station 3145 in Kirikhan, along with their elastic response spectra, as recorded in M_w7.8 Pazarcik earthquake.

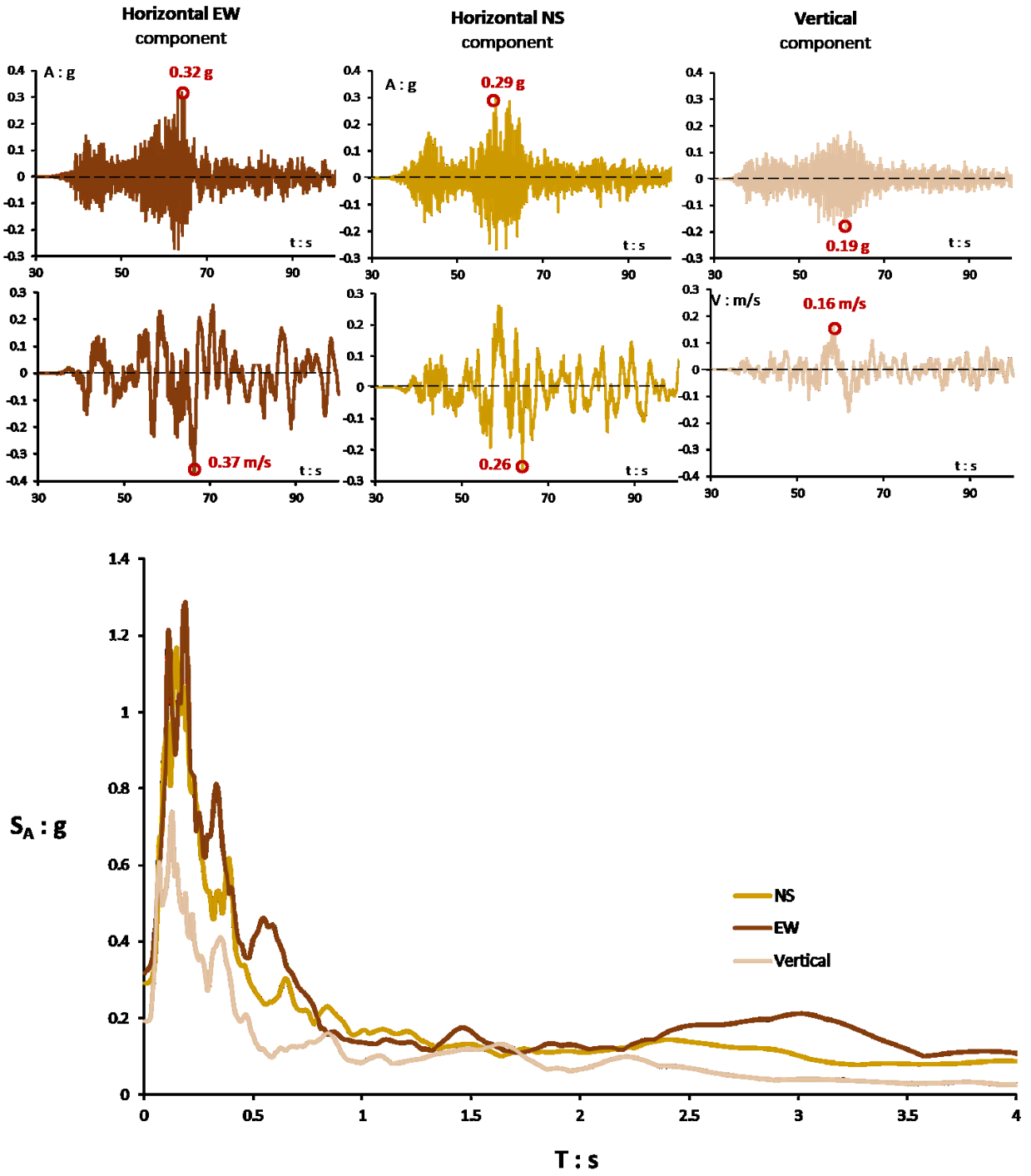

Figure 2.18 Acceleration and velocity timehistories of the two horizontal and one vertical components of station 4620 in Kahramanmaras, along with their elastic response spectra, as recorded in M_w7.8 Pazarcik earthquake.

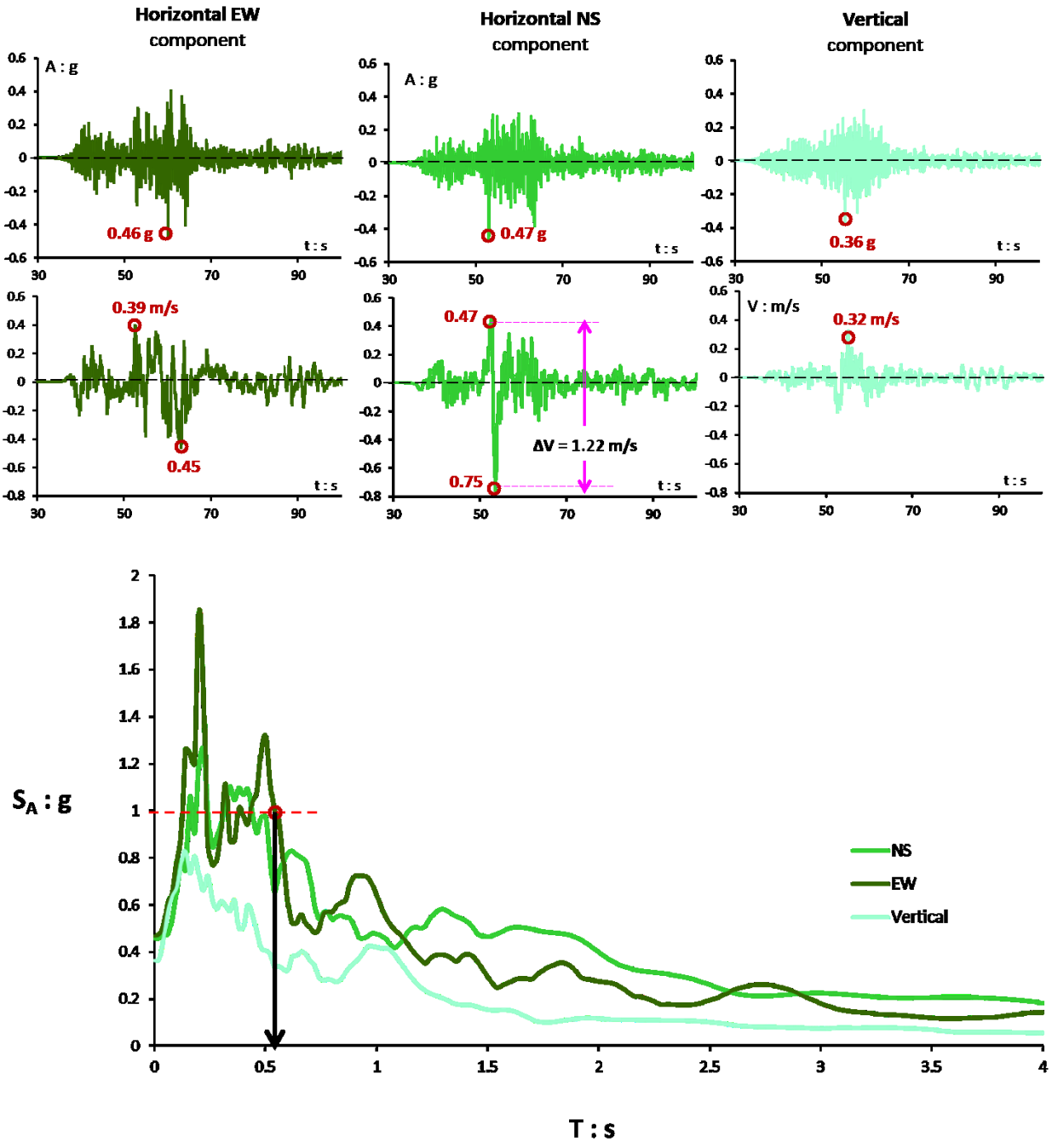

Figure 2.19 Acceleration and velocity timehistories of the two horizontal and one vertical components of station 4625 in Kahramanmaras, along with their elastic response spectra, as recorded in M_w7.8 Pazarcik earthquake.

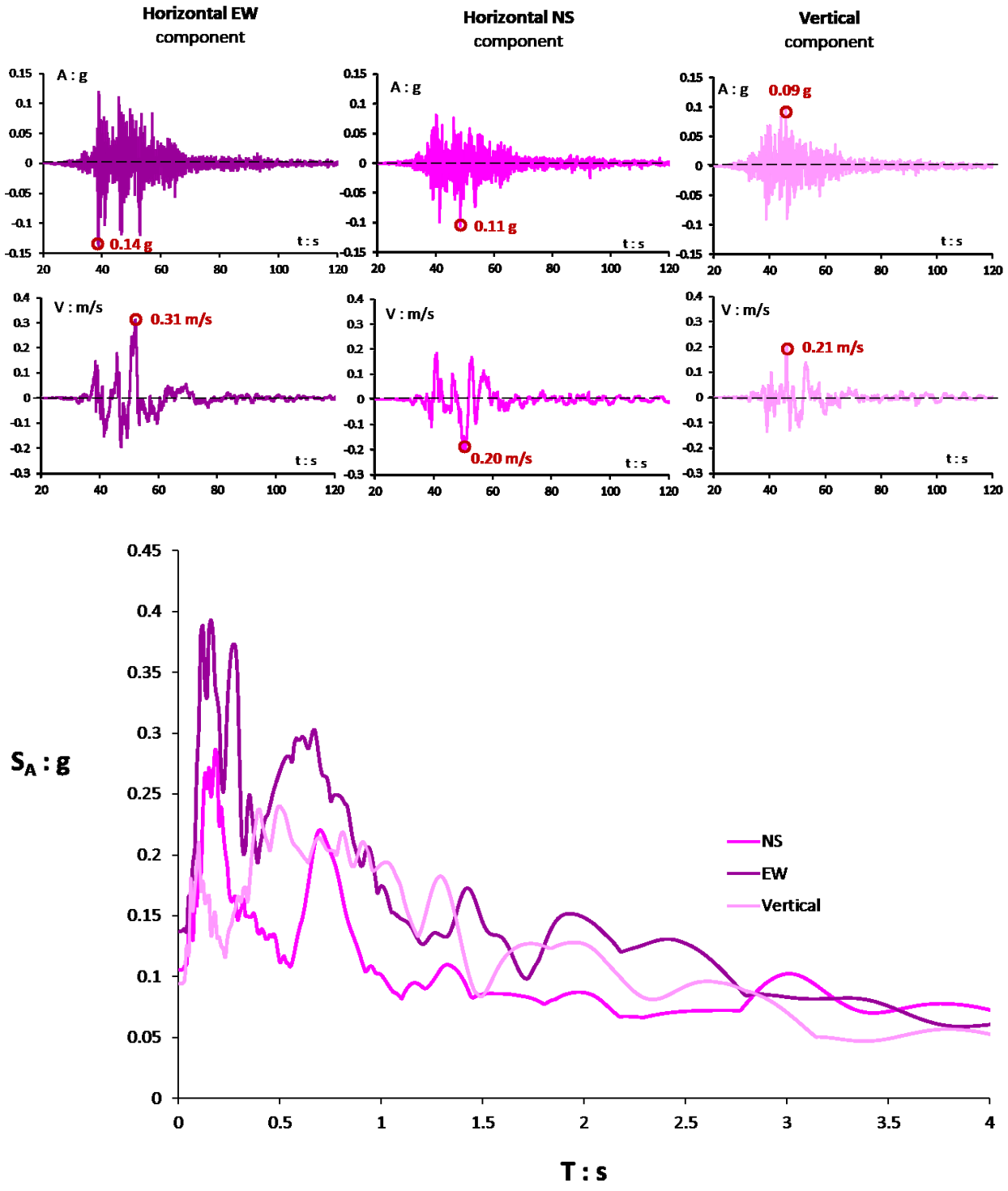

Figure 2.20 Acceleration and velocity timehistories of the two horizontal and one vertical components of station 4408 in Malatya, along with their elastic response spectra, as recorded in M_w7.8 Pazarcik earthquake.

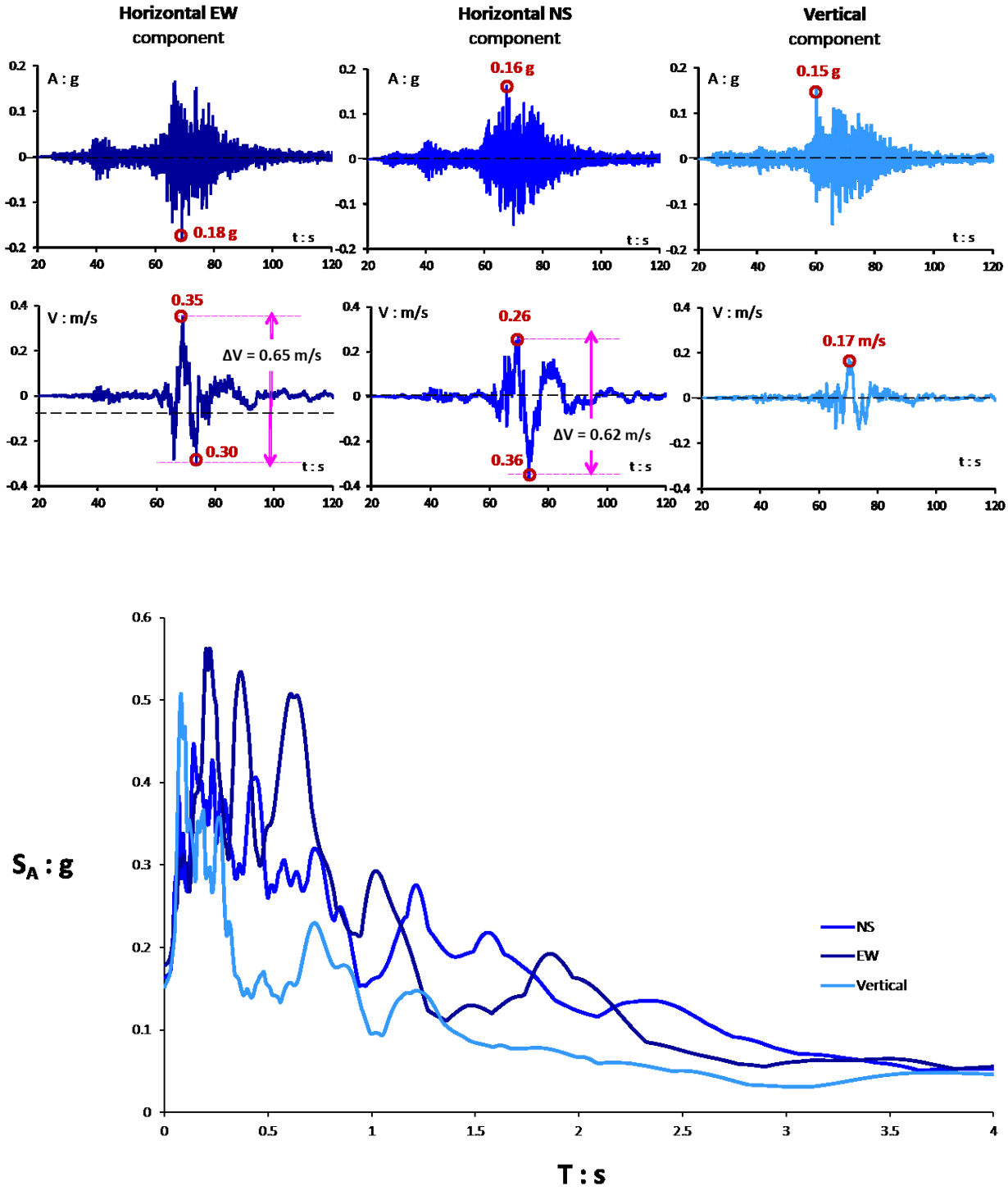

Figure 2.21 Acceleration and velocity timehistories of the two horizontal and one vertical components of station 3116 in Iskenderun, along with their elastic response spectra, as recorded in M_w7.8 Pazarcik earthquake.

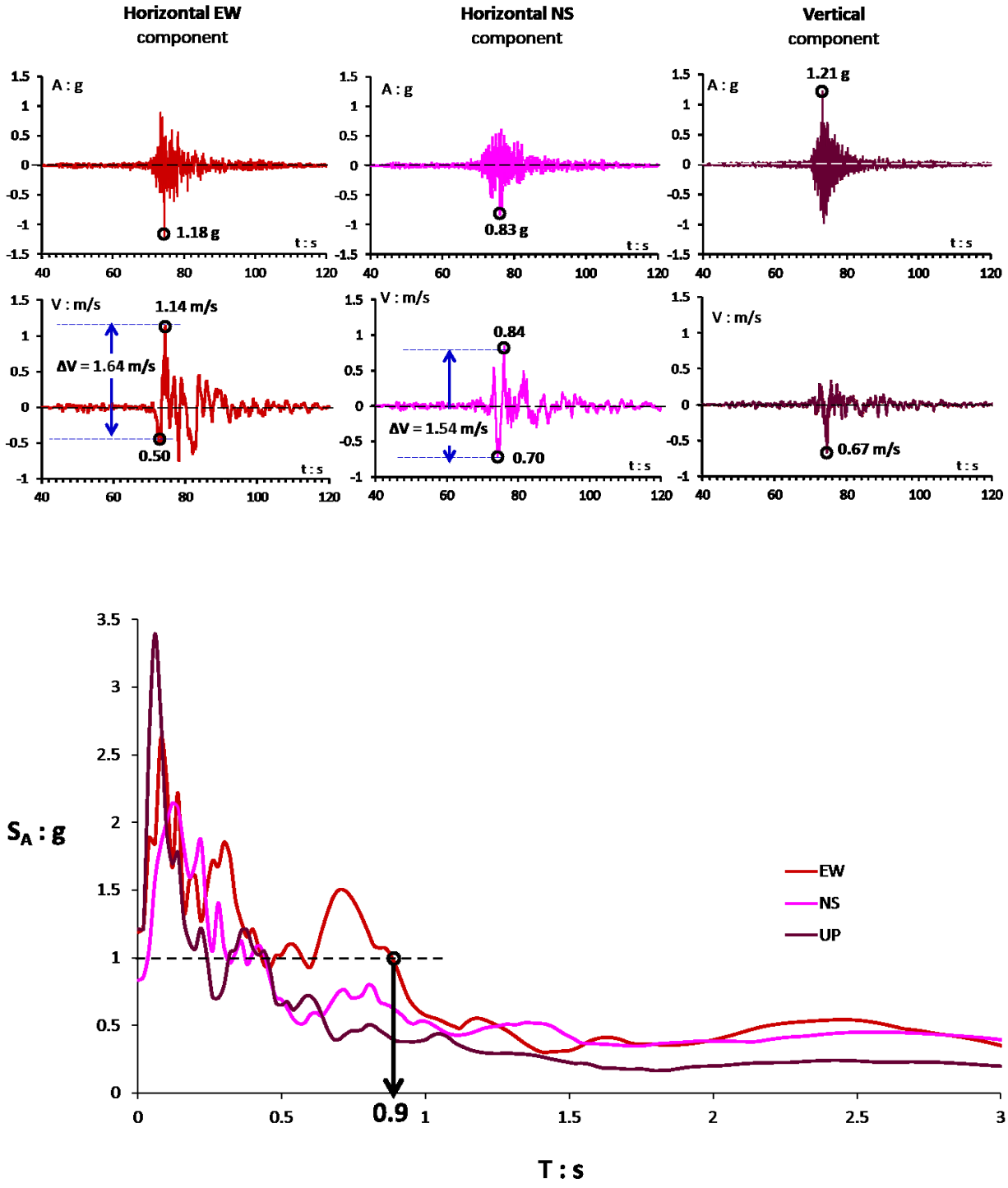

Figure 2.22 Acceleration and velocity timehistories of the two horizontal and one vertical components of station 3125 in Antakya, along with their elastic response spectra, as recorded in M_w7.8 Pazarcik earthquake.

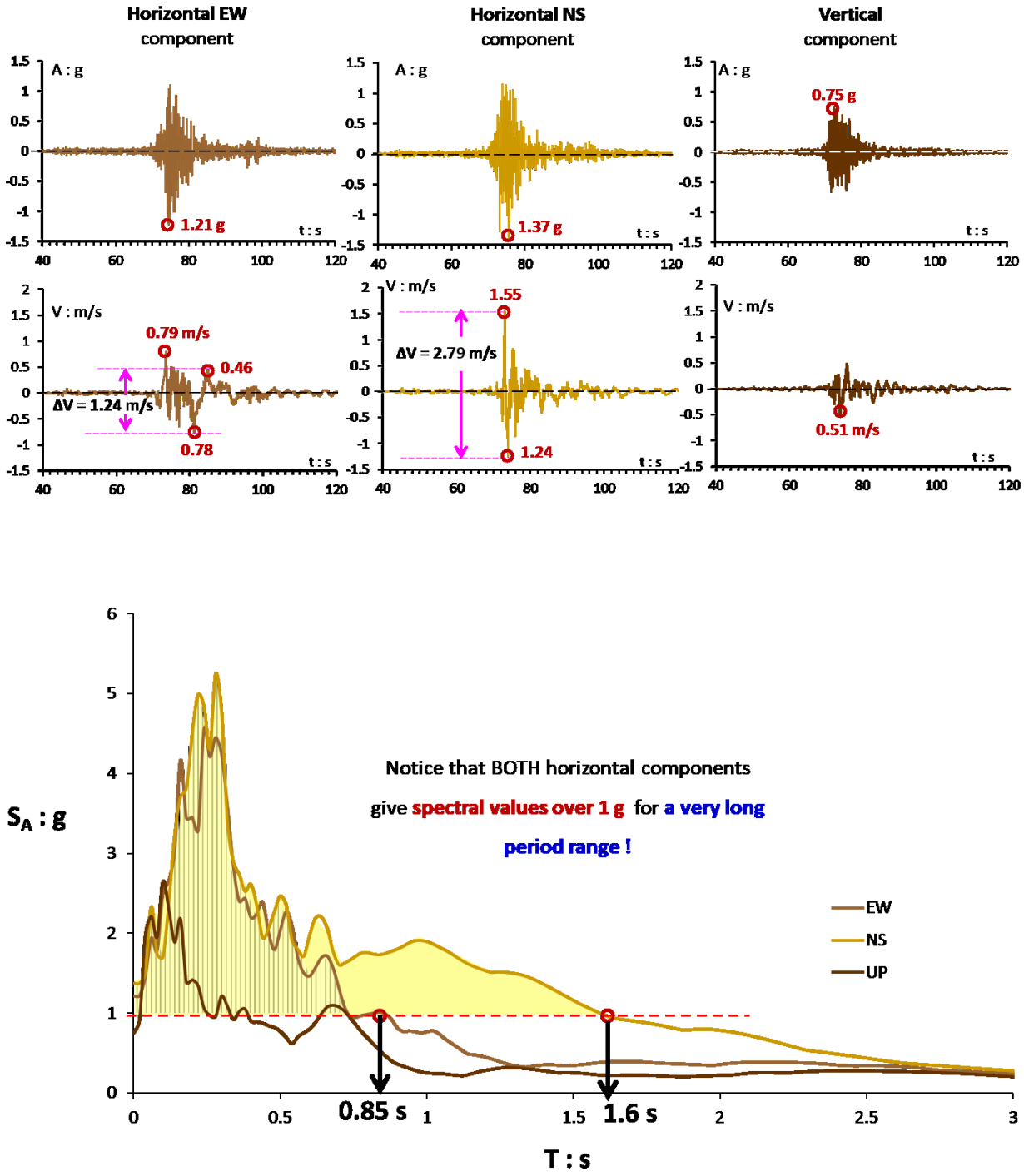

Figure 2.23 Acceleration and velocity timehistories of the two horizontal and one vertical components of station 3129 in Antakya, along with their elastic response spectra, as recorded in M_w7.8 Pazarcik earthquake.

2.2 Recordings from the M_w7.5 Elbistan EQ

On February 6th, 2023, nine hours after the first Pazarcik mainshock of M_w7.8, a second mainshock occurred: the M_w7.5 Elbistan earthquake. As shown in Figure 24, this earthquake took place at a fault zone different than those of the East Anatolian Fault (in which the Pazarcik event was located). The event was also a bilateral rupture, with faulting in three segments. Distribution of PGA and PGV recorded values in AFAD stations are shown in Figures 2.25 and 2.26, respectively.

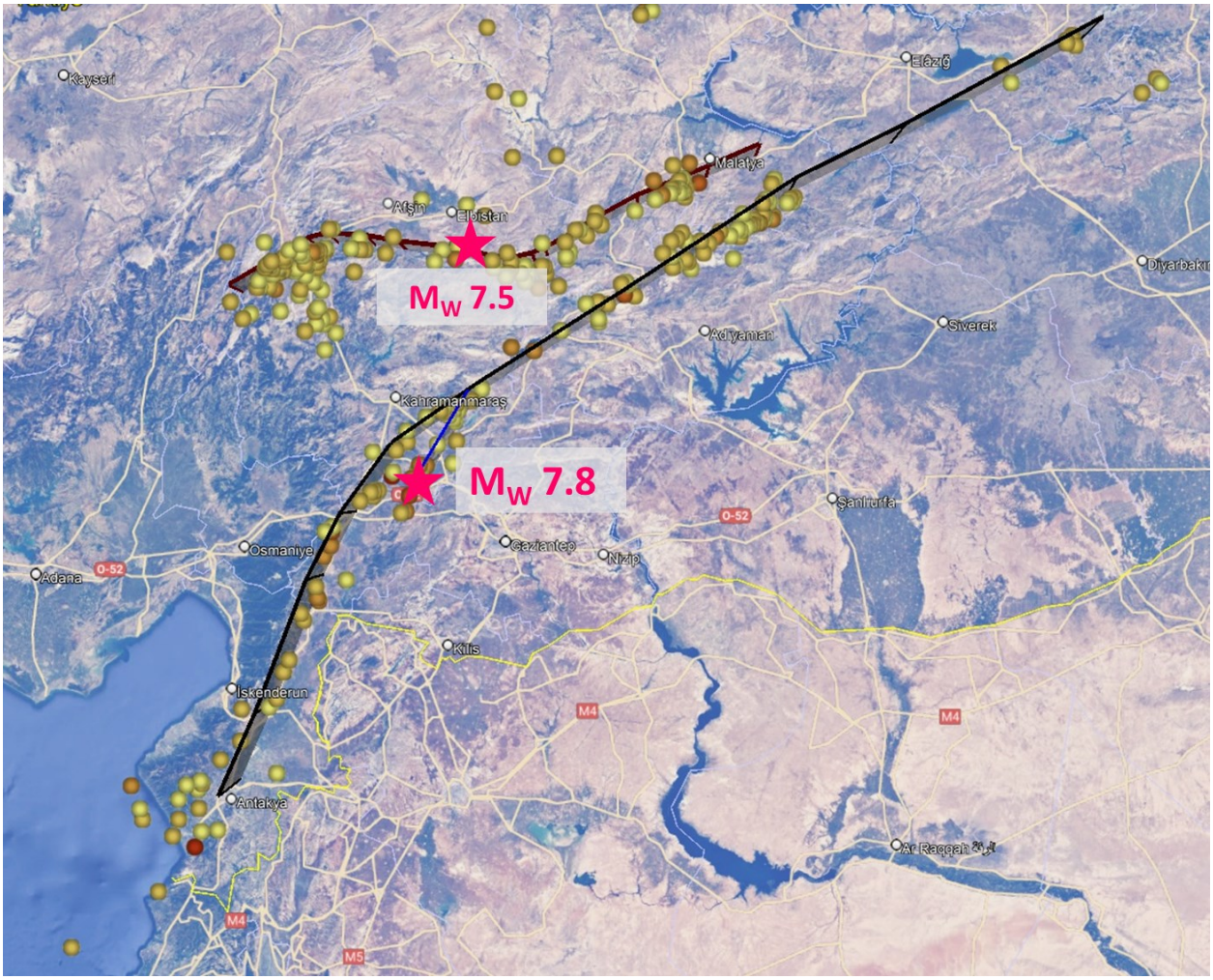

Figure 2.24 Map of aftershock epicenters (yellow and orange circles), mainshock epicenters (red stars), along with the fault segments ruptured during the M_w7.8 Pazarcik and M_w7.5 Elbistan earthquakes.

Table 2.2 lists the peak acceleration values (in all three components) exceeding 0.20 g, of the AFAD stations recorded during the Elbistan earthquake. Notice that the accelerations induced by the Pazarcik mainshock are by far greater than those by Elbistan. Figures 2.27 and 2.28 illustrate

in detail the recorded motions in Antakya stations 3123 and 3124, respectively. Obviously, the effect of this event was insignificant for the southwestern part of the East Anatolian Fault.

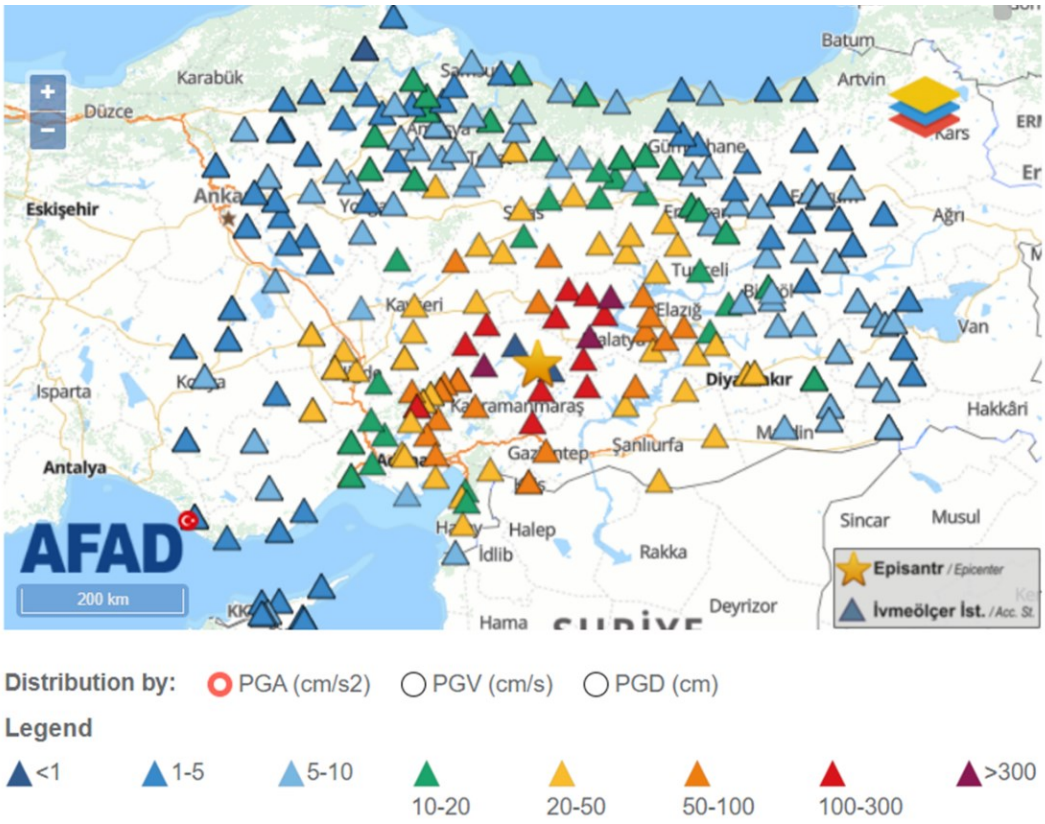

Figure 2.25 Recorded PGAs at the AFAD stations during the M_w7.5 Elbistan seismic event (Source: https://tadas.afad.gov.tr/event-detail/17969).

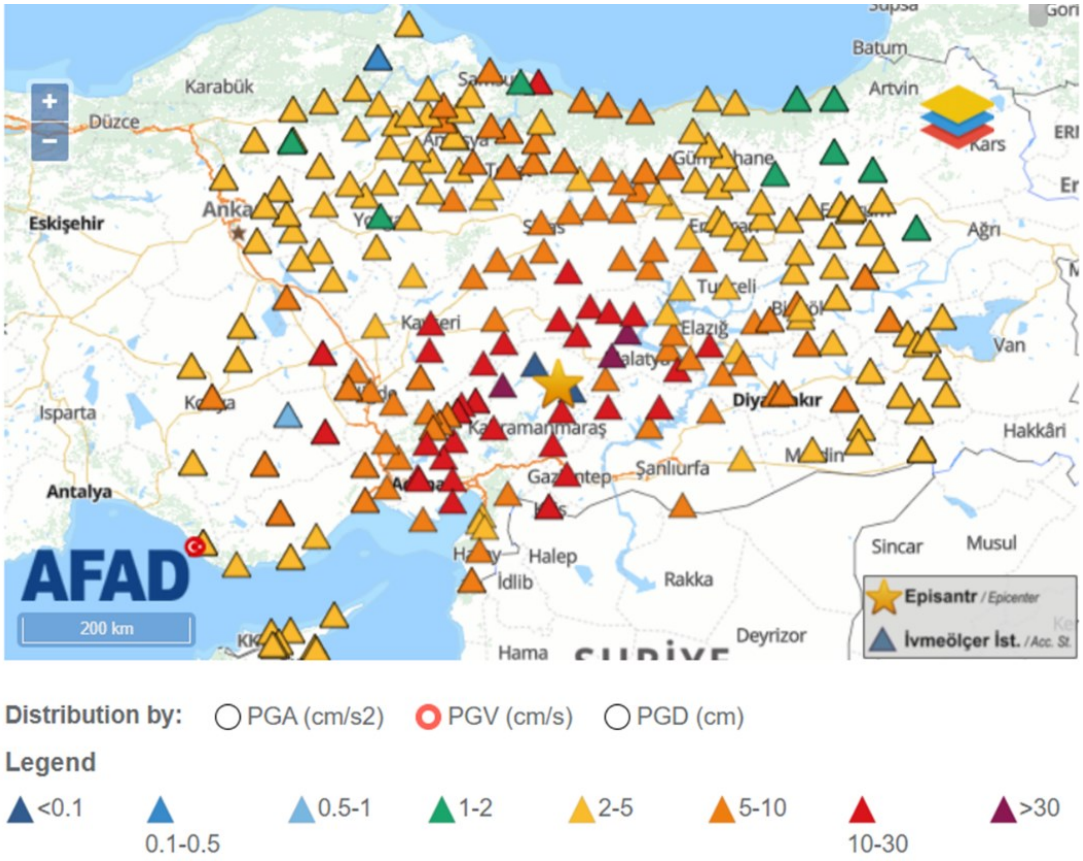

Figure 2.26 Recorded PGVs at the AFAD stations during the M_w7.5 Elbistan seismic event (Source: https://tadas.afad.gov.tr/event-detail/17969).

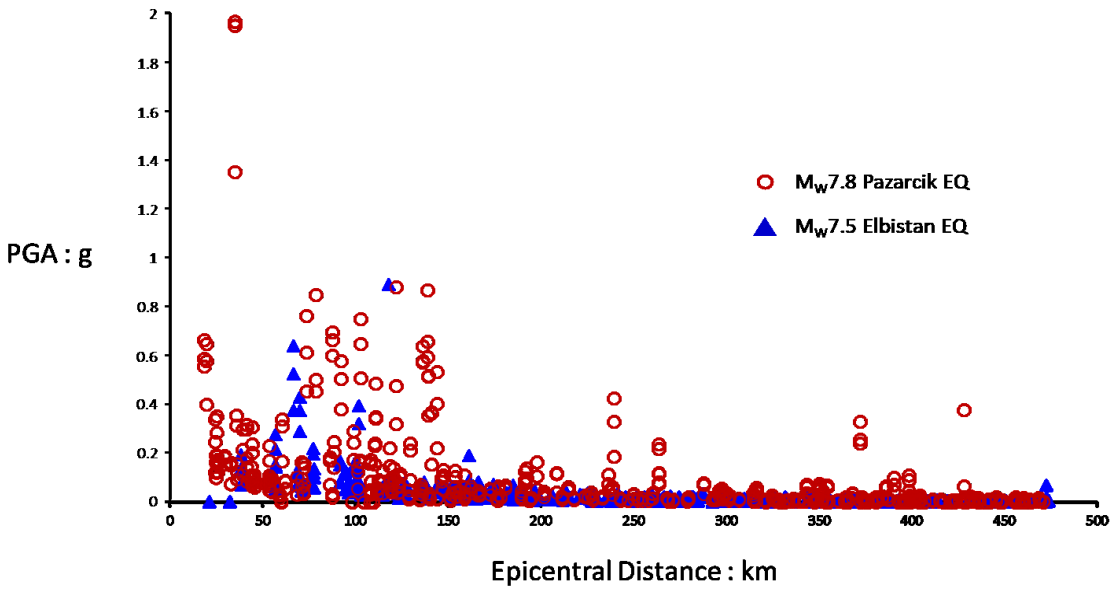

Figure 2.27 Comparison of the recorded PGAs between the M_w7.8 Pazarcik (in red circles) and M_w7.5 Elbistan (blue triangles) earthquakes.

All the recorded PGAs of the M_w7.5 event are plotted in Figure 2.27 with respect to distance, along with the PGA's induced by the M_w7.8 Pazarcik earthquake. Notice that the accelerations induced by the Pazarcik mainshock are by far greater than those by Elbistan. Table 2.2 also lists the peak acceleration values (in all three components) exceeding 0.20 g, of the AFAD stations in the Elbistan earthquake. Figures 2.28 and 2.29 illustrate in detail the recorded motions in Antakya stations 3123 and 3124, respectively. Obviously, the effect of this event was insignificant for the southwestern part of the East Anatolian Fault.

Table 2.2 Stations with recorded PGA over 0.2 g, from the M_w7.5 Elbistan earthquake.

Station Code	PGA_NS (g)	PGA_EW (g)	PGA_UP (g)
4612	0.635	0.523	0.495
4406	0.467	0.409	0.319
4631	0.337	0.389	0.610
0131	0.402	0.332	0.085
3802	0.196	0.221	0.123
4409	0.287	0.218	0.124
4614	0.161	0.206	0.089
0141	0.082	0.204	0.080

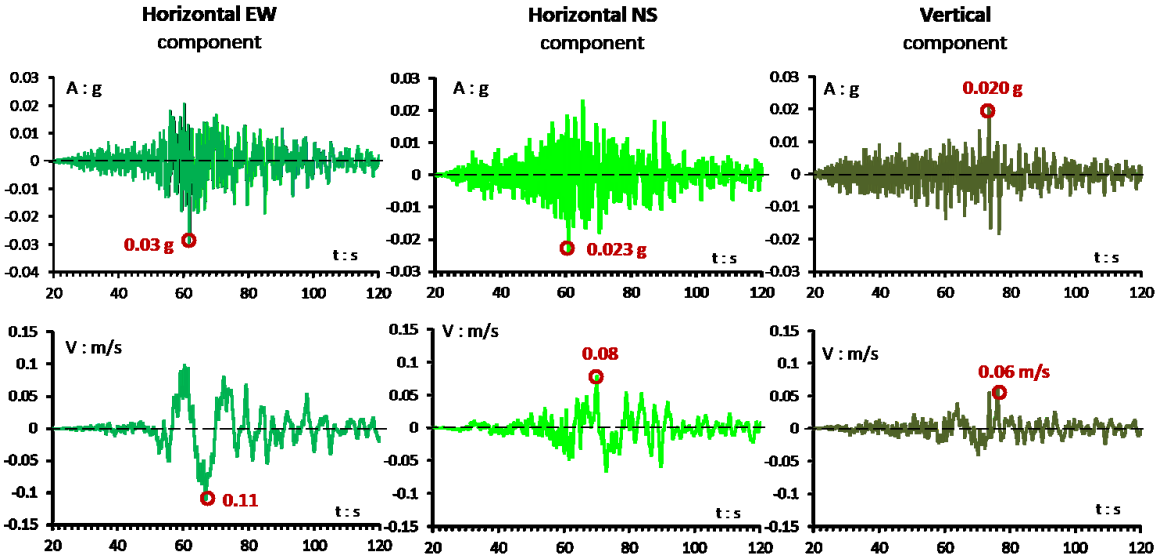

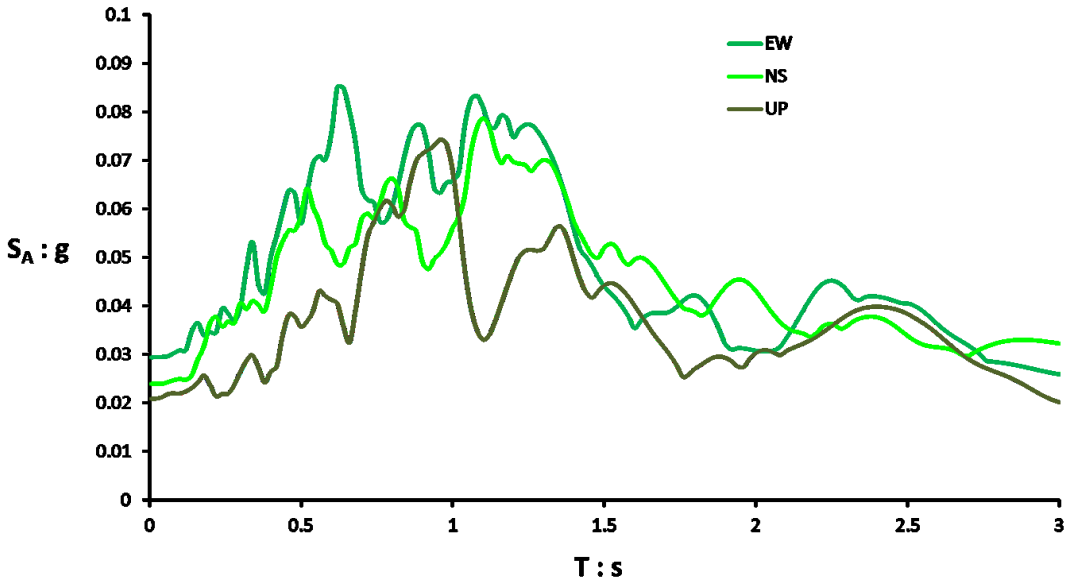

Figure 2.28 Acceleration and velocity timehistories of station 3123 in Antakya, along with their elastic response spectra, as recorded in M_w7.5 Elbistan earthquake.

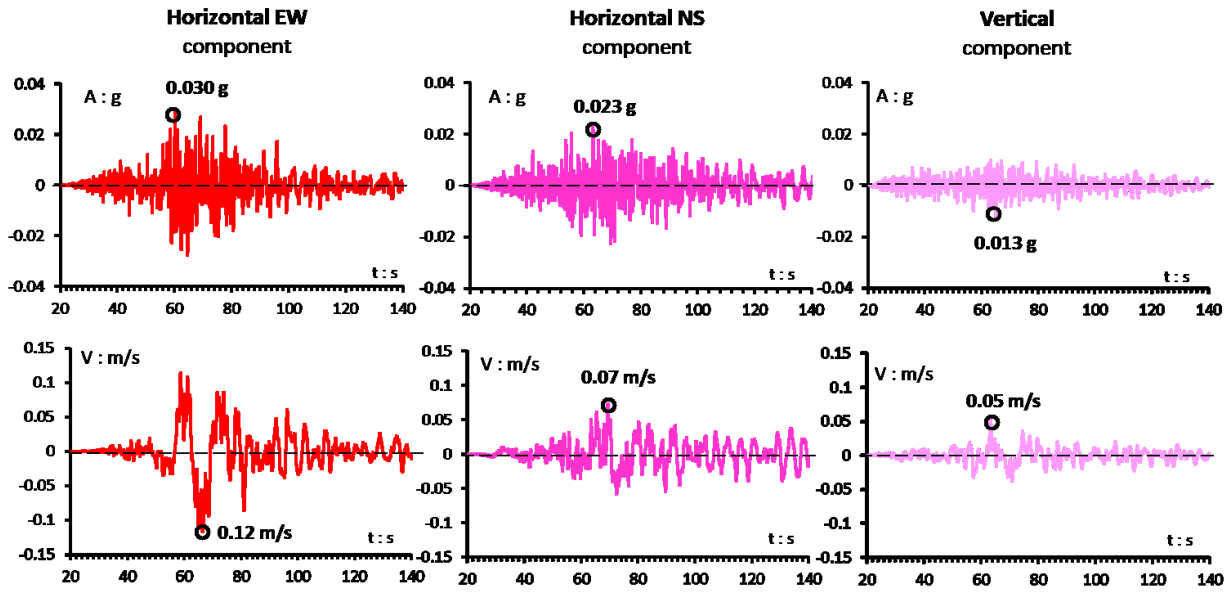

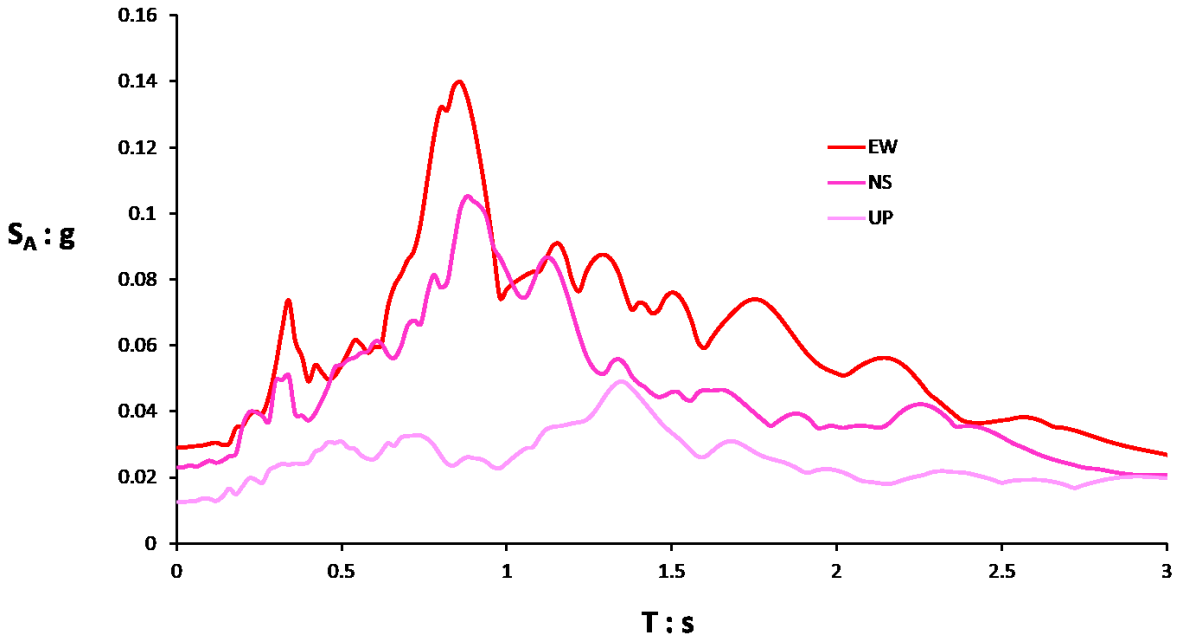

Figure 2.29 Acceleration and velocity timehistories of the two horizontal and one vertical components of station 3124 in Antakya, along with their elastic response spectra, as recorded in M_w7.5 Elbistan earthquake.

References

2.1 AFAD (Disaster and Emergency Management Authority): https://tadas.afad.gov.tr/

2.2 KOERI (Kandilli Observatory and Earthquake Research Institute): http://www.koeri.boun.edu.tr/new/en

2.3 METU Report: MIDDLE EAST TECHNICAL UNIVERSITY : "Preliminary Reconnaissance Report on February 6, 2023, Pazarcik M_w=7.7 and Elbistan M_w=7.6, Kahramanmaraş-Türkiye Earthquakes". Edited by: Kemal Önder Çetin, Makbule Ilgaç, Gizem Can and Elife Çakir, REPORT NO: METU/EERC 2023-01.

2.4 Garini E., Gazetas G. (2023) "Preliminary Report on the M7.8 and M7.5 earthquakes of February 6, 2023 in Turkey-Syria": DOI 10.17605/OSF.IO/V4MSW

2.5 Fliss S., Bhat H.S., Dmowska R., Rice J.R. (2005) "Fault branching and rupture directivity". *Journal of Geophysical Research*, 110 : B06312.

2.6 Rice J.R., Lapusta N., Ranjith K. (2001) "Rate and state dependent friction and the stability of sliding between elastically deformable solids". *Journal of the Mechanics and Physics of Solids*, 49 : 1865–1898.

2.7 Rice J.R., Sammis C.G., Parsons R. (2005) "Off-Fault Secondary Failure Induced by a Dynamic Slip Pulse". *Bulletin of the Seismological Society of America,* 95(**1**): 109–134.

2.8 Wollherr S., Gabriel A-A., Mai P.M. (2019) "Landers 1992 "Reloaded": Integrative Dynamic Earthquake Rupture Modeling". *Journal of Geophysical Research: Solid Earth*, 124: 6666–6702.

2.9 Perfettini H., Avouac J.-P. (2007). "Modeling afterslip and aftershocks following the 1992 Landers Earthquake". *Journal of Geophysical Research*, 112: 07409 (10.1029/2006JB004399).

2.10 Fialko Y. (2004). "Probing the mechanical properties of seismically active crust with space geodesy: Study of the co-seismic deformation due to the 1992 M_w7.3 Landers (southern California) earthquake". *Journal of Geophysical Research: Solid Earth,* 109 (Issue B3): B03307.

2.11 Wang Z., Zhang W., Taymaz T., He Z., Xu T., Zhang Z. (2023). "Dynamic rupture process of the 2023 M_w7.8 Kahramanmaraş earthquake (SE Türkiye): Variable rupture speed and implications for seismic hazard". *Geophysical Research Letters*, 50: e2023GL104787.

2.12 Abdelmeguid M., Zhao C., Yalcinkaya E., Gazetas G., Elbanna A., Rosakis, A. (2023). "Revealing the dynamics of the Feb 6th 2023 M7.8 Kahramanmaracs/Pazarcik Earthquake: Near-field records and dynamic rupture modeling". *EarthArXiv*: https://doi.org/10.31223/X5066R

2.13 Rosakis A., Abdelmeguid M., Elbanna A. (2023). "Evidence of early supershear transition in the Feb 6th 2023 M_w 7.8 Kahramanmaraş Turkey earthquake from near-field records". *EarthArXiv*: https://doi.org/10.31223/X5W95G

3. Geotechnical Seismic Response

*Chapter Authors**: Evangelia GARINI, Vassilis MARINOS, Dimitris PITILAKIS, George GAZETAS***

3.1 Geological conditions

3.1.1 Geotectonic setting of the wider area

The Pazarcık earthquake took place at 4:17 a.m. on February 6, 2023, while the Ekinözü earthquake occurred at 1:24 p.m. on the same day, approximately 9 hours later. Both earthquakes involved rupturing on segments of the East Anatolian Fault and Dead Sea Fault (Figure 3.1).

Turkey, positioned on the Anatolian Block, holds a crucial geographical location where the Eurasian, African, and Arabian plates intersect (refer to Figure 3.1, Figure 3.2). Bounded by the North Anatolian Fault (NAF) to the north, the East Anatolian Fault (EAF) to the east, and the Hellenic and Cyprus subduction zones to the south, with a westward extensional regime, the Anatolian block facilitates the counterclockwise rotation and westward movement between the surrounding plates. Events along the two faults and in relation to the wider geotectonic framework. The seismic events of February 6, 2023, originated on the Narli Fault, a branch of the EAF. Subsequently, they propagated bilaterally along the EAF, emanating from the center towards the NE and SW, resulting in a magnitude of 7.8. Approximately 9 hours later, another event occurred on the Sürgü-Çardak faults, registering a magnitude of 7.7. The smaller fault segments that were activated are illustrated in Figure 3.3.

PAZARCIK EARTHQUAKE: The seismic event occurred at 4:17:35 local time (1:17:35 GMT) along a NE-SW trending fault with a sinistral slip. The Pazarcık earthquake affected the East Anatolian Fault Zone (EAFZ) with two segments and the Dead Sea Fault (DSF) with one segment. The total length of the surface rupture could potentially indicate a Moment Magnitude. Estimates for the magnitude of this earthquake vary among different institutes, ranging between 7.7 and 8.0. Initially, the Pazarcık earthquake spanned a total length of about 210-230 km, later estimated to a final length of 400-450 km (Figure 3.4).

EKİNÖZÜ EARTHQUAKE: This earthquake occurred at 13:24:49 local time (10:24:49 GMT) along an almost E-W trending fault with a sinistral slip. This fault is suspected to be a combined slip involving the Çardak and Sürgü Faults. The Moment Magnitude of this earthquake has been

assessed by various institutes, with estimates ranging from 7.5 to 7.7. As for the Ekinözü earthquake, it affected the east-west trending Çardak and Sürgü faults, covering a total length of 120-130 km (Figure 3.4).

The Pazarcik earthquake caused a slip of about 5-8 m and the distribution has a parabolic shape. The Ekinözü earthquake appears to have the same relative slip. The reconnaissance team identified surface ruptures in several locations (Figure 3.5 and Figure 3.6).

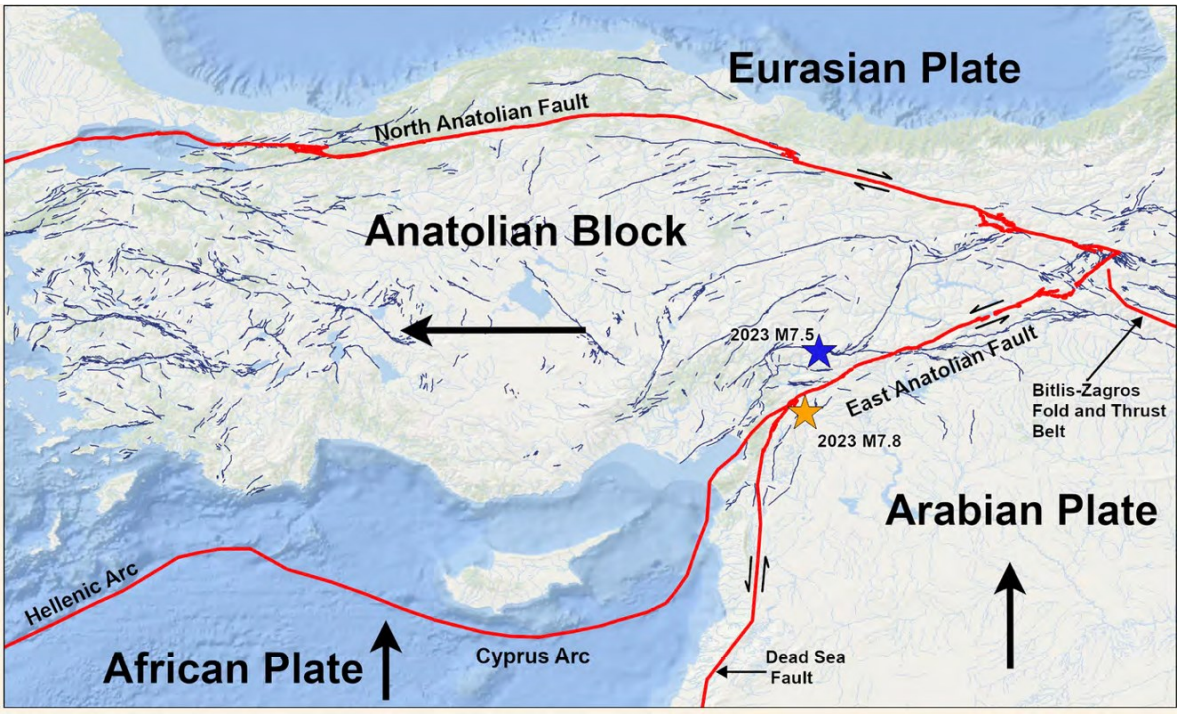

Figure 3.1 Tectonic plate and fault map of the region. Red lines denote faults along the plate boundaries. Gray lines denote other faults (USGS).

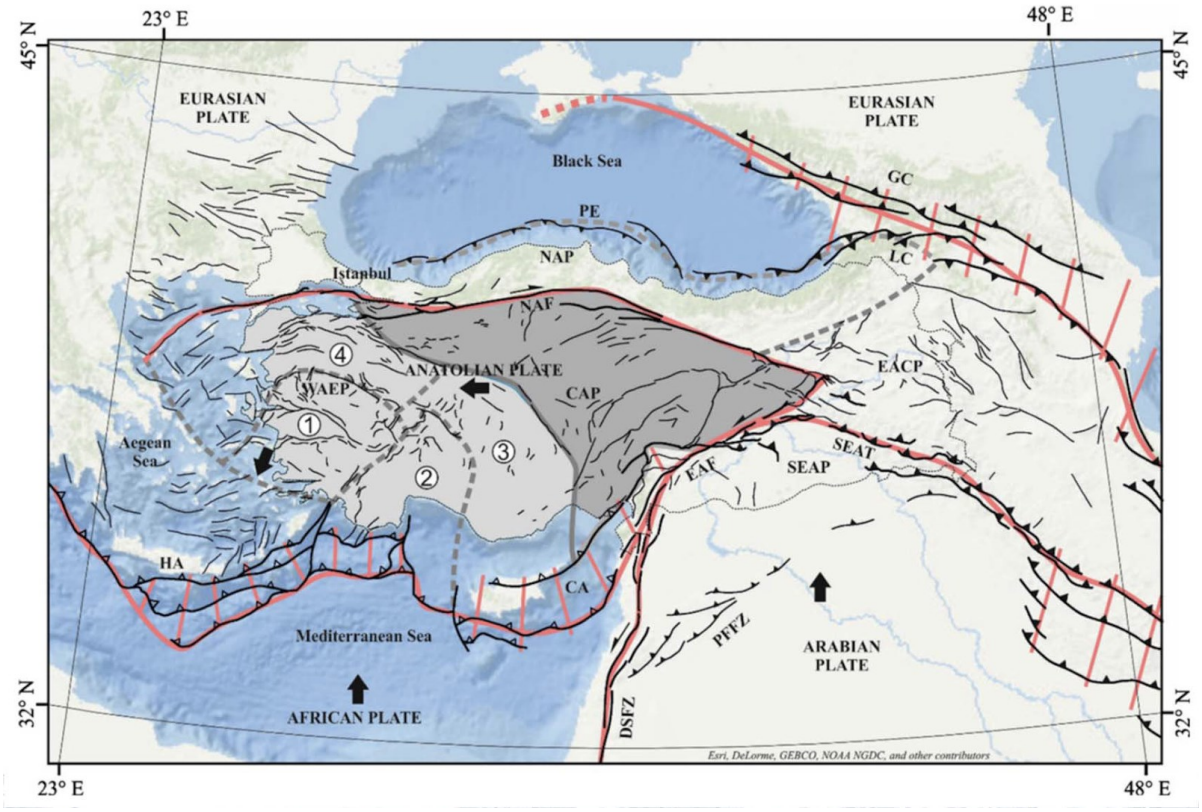

Figure 3.2 Geotectonic map of a wider area (Emre et al., 2018).

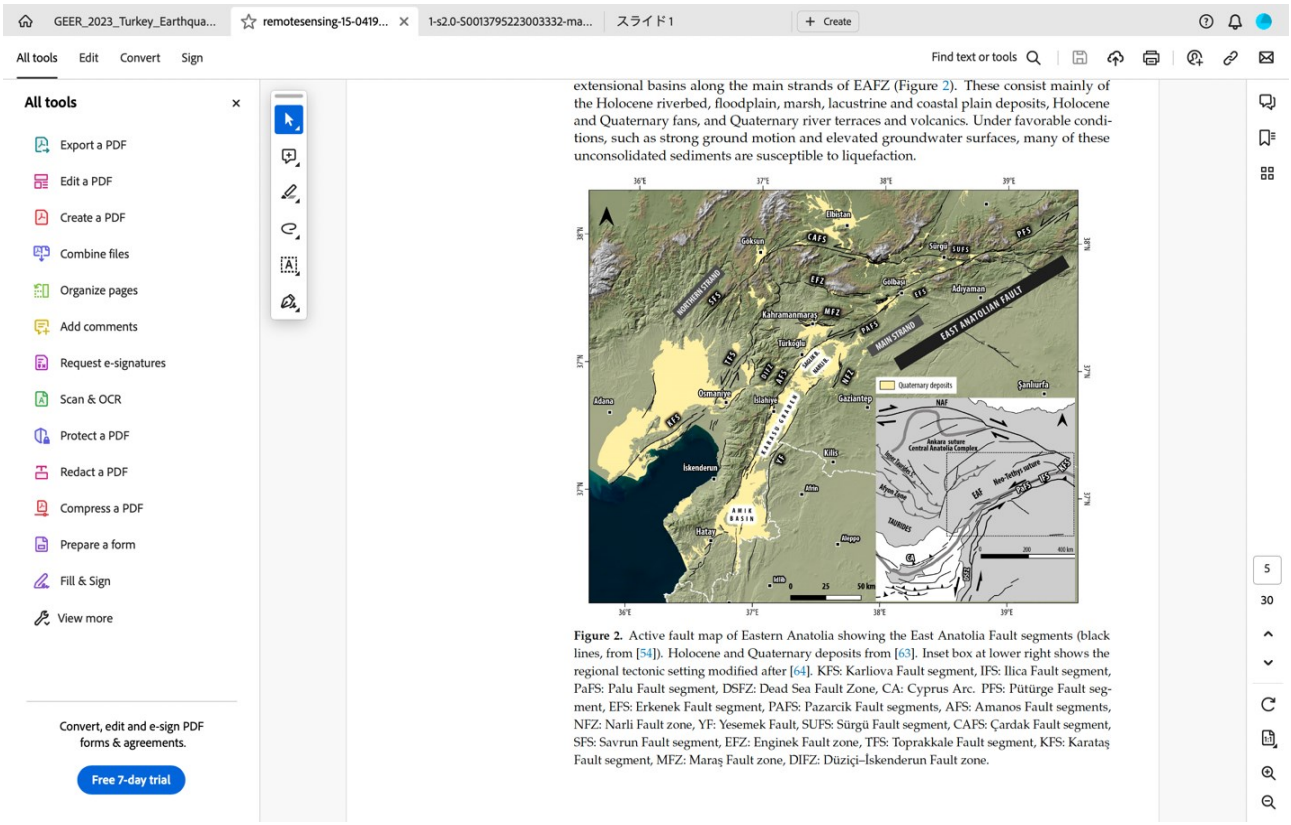

Figure 3.3 Active fault map of Eastern Anatolia showing the East Anatolia Fault segments (black lines, from Duman and Emre, 2013). Holocene and Quaternary deposits from MTA, 2002). The Inset box at the lower right shows the regional tectonic setting modified after [64]. KFS: Karliova Fault segment, IFS: Ilica Fault segment, PaFS: Palu Fault segment, DSFZ: Dead Sea Fault Zone, CA: Cyprus Arc. PFS: Pütürge Fault segment, EFS: Erkenek Fault segment, PAFS: Pazarcik Fault segments, AFS: Amanos Fault segments, NFZ: Narli Fault zone, YF: Yesemek Fault, SUFS: Sürgü Fault segment, CAFS: Çardak Fault segment, SFS: Savrun Fault segment, EFZ: Enginek Fault zone, TFS: Toprakkale Fault segment, KFS: Karata¸.Fault segment, MFZ: Mara¸s Fault zone, DIFZ: Düzi.i–˙Iskenderun Fault zone. The two faults are associated with the movement of large tectonic plates.

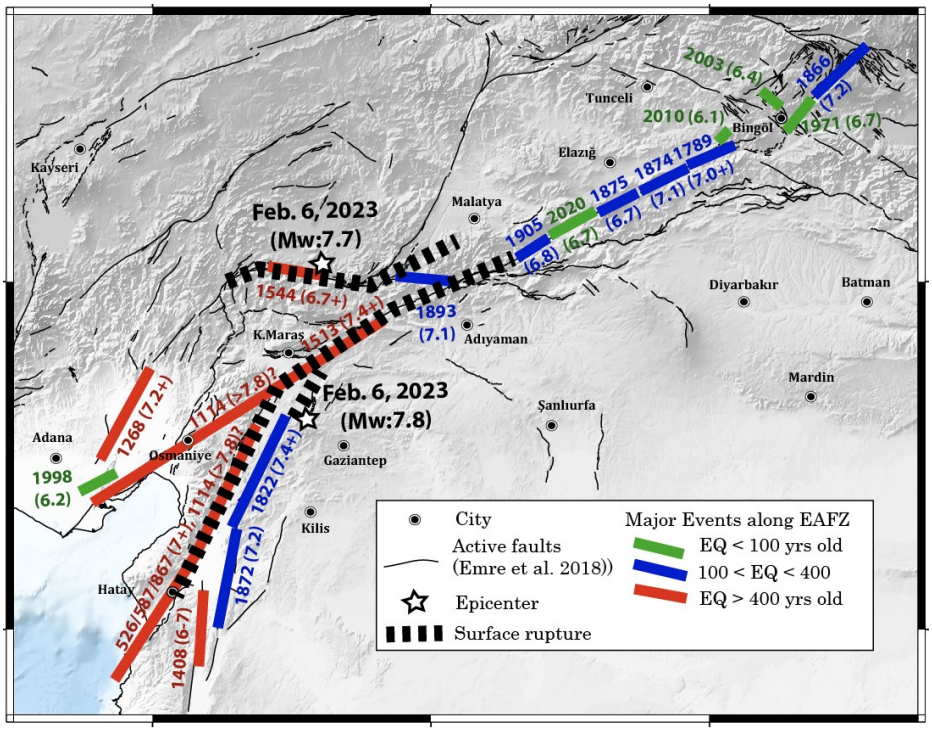

Figure 3.4 Total rupture length: Pazarcik Earthquake 400 km & Ekinözü Earthquake 160 km (Ozacar et al., 2023).

Figure 3.5 Surface ruptures in a) Antioch Airport area, b) Gulbasi c) Osmaniye.

Figure 3.6 Surface ruptures in Turkoglu area.

3.1.2 Ground failure zonation based on the geological conditions

Throughout the reconnaissance, our team observed that many failures strongly correlate to the engineering geological conditions and their variations. Such observations were made in all the urban areas we visited.

In Gulbasi, extended ground failures, as they are more detailed examined in the next paragraphs, were located around the recent lake and river deposits, in a basin formed by two faults. In “Maras”(Kahranmaras), the damages are extensive in very recent loose and soft sediments and reduced in the hilly areas of the consolidated alluvium soils or the bedrock (mainly limestone here). At the same time, a series of faults are located along the foot of the hills. Significant failures are also recorded in a wide zone along the fault in the Turkoglu area, where we also recorded up to 3,5m fault offset. Severe damages occurred in the town of Antakya, in the city center, where recent loose and soft Quaternary deposits are met, and there is a direct proximity to the fault. Here, we could not compare these damages to the hilly parts, where more compacted and sedimented materials of Neogene age are met. Similar observations were made in Adiyaman, where the city is built on recent soil alluvial formations and talus. Part of the fault extends to the outskirts of the city. In Iskenderun, there are numerous phenomena of liquefaction and large settlements that took place along the coastal deposits mainly composed of loose sandy deposits. The coastal zone at the time of our reconnaissance, was still flooded due to significant settlement. Finally, in Islayie, although there is proximity to the fault, the damages are more limited towards the extent of the city due to the outcrops of rocks (mainly basaltic).

Geological and neotectonic maps relating to the areas of interest were collected and geospatially referenced for the execution of the mission. Parts of these maps, for every visited city during the reconnaissance, are illustrated below.

- **Geological conditions in Gulbasi**

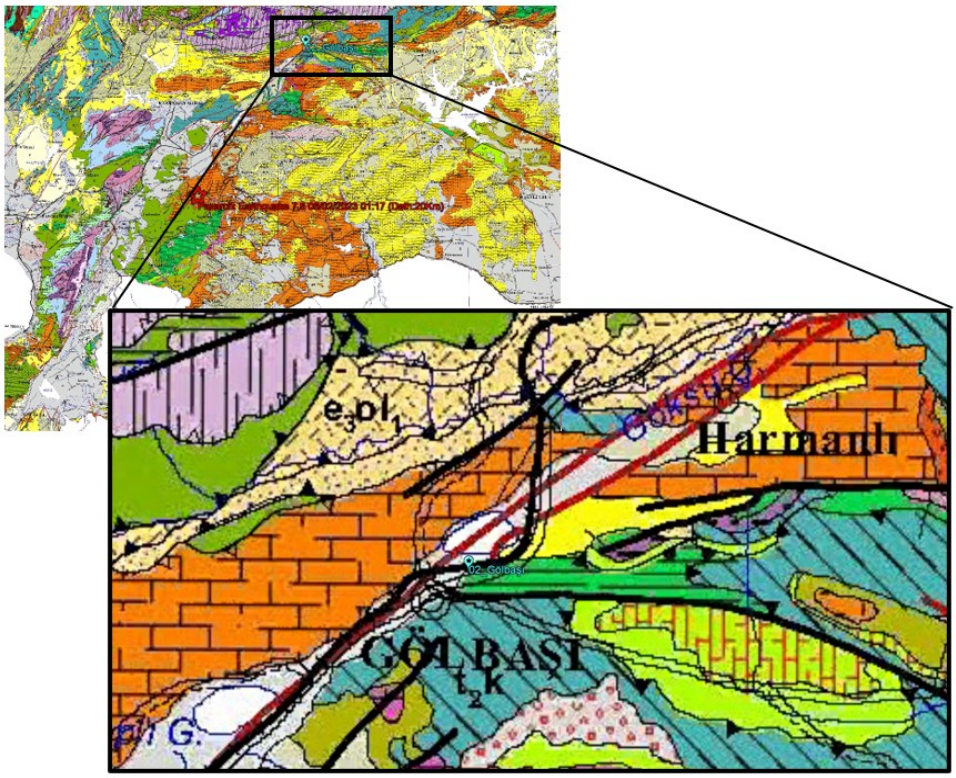

Figure 3.7 Geological conditions in Gulbasi (Geological maps of Turkey No16, Hatay sheet, scale 1:500.000, Editor: M. Senel & Technical Assistant: N. Aydal).

Figure 3.8 Zoning of extensive damage to buildings along and around recent lake and river deposits in a basin formed by two faults in the Gulbasi area.

- **Geological conditions in Kahramanmaras**

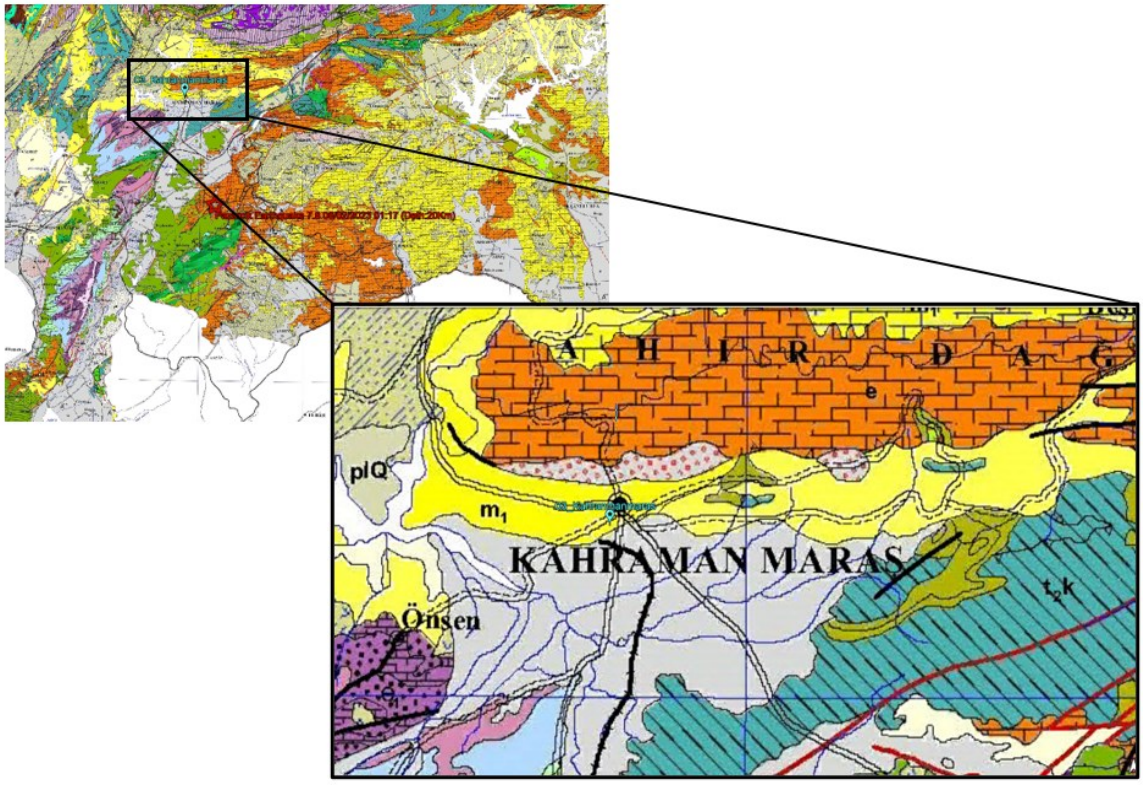

Figure 3.9 Geological conditions in Kahramanmaras (Geological maps of Turkey No16, Hatay sheet, scale 1:500.000, Editor: M. Senel & Technical Assistant: N. Aydal).

Figure 3.10 The damages are extensive in very recent loose and soft sediments and reduced in the hilly areas of the consolidated alluvium-bedrock (mainly limestone here).

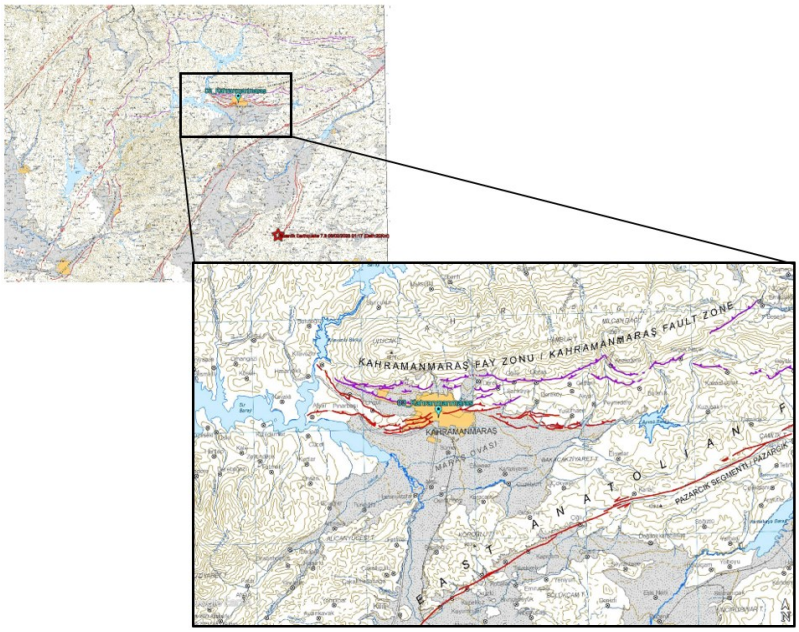

Figure 3.11 Neotectonic conditions in Kahramanmaras. The presence of the East Anatolian Fault is evident very close to the city, while a series of faults run parallel to the base of the cliff (Active fault map series of Turkey, Gazianter (NJ 37-9), Quadrangle, serial No: 38, scale 1:250.000, General Directorate of Mineral Research and Exploration).

- **Geological conditions in Turkoglu**

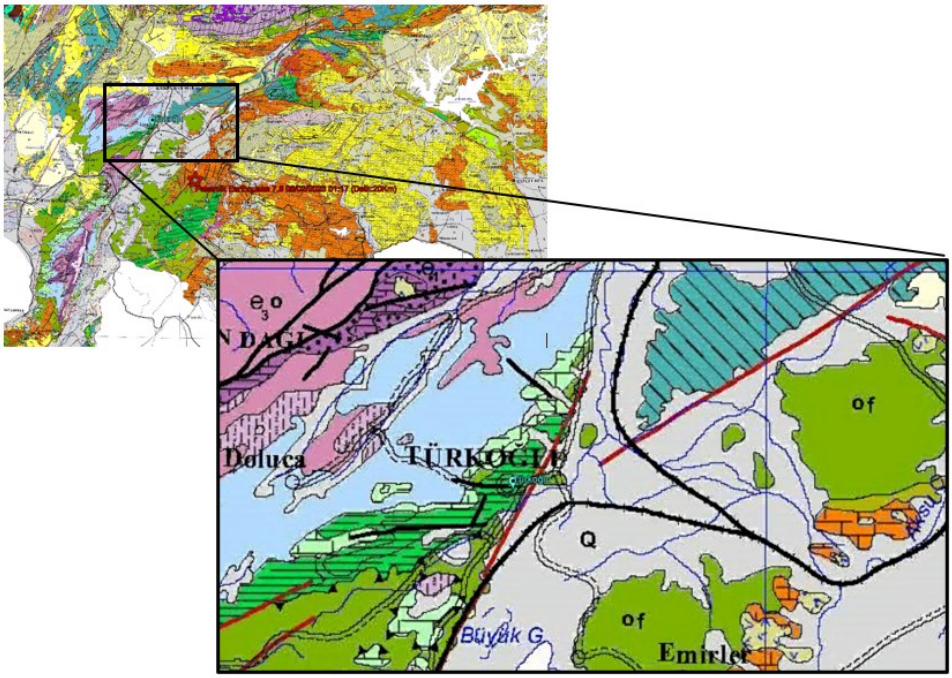

Figure 3.12 Geological conditions in Turkoglu. The fault extends over the area which presents extensive damage (Geological maps of Turkey No16, Hatay sheet, scale 1:500.000, Editor: M. Senel & Technical assistant: N. Aydal).

- **Geological conditions in Antakya**

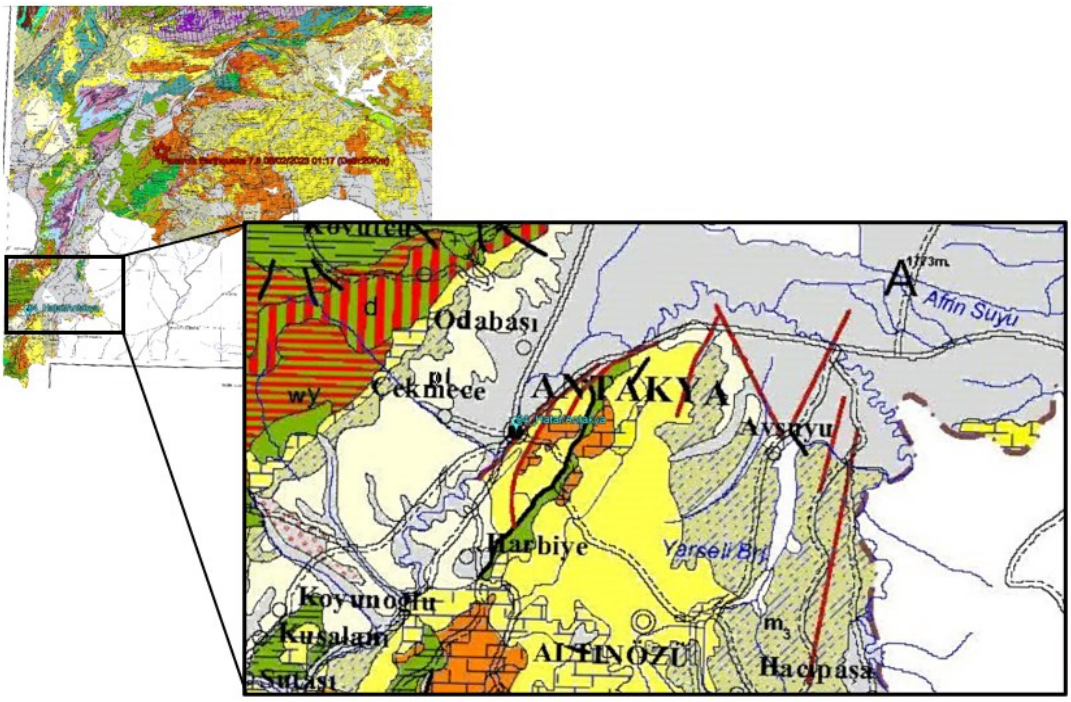

Figure 3.13 Geological conditions in Antakya (Geological maps of Turkey No16, Hatay sheet, scale 1:500.000, Editor: M. Senel & Technical Assistant: N. Aydal).

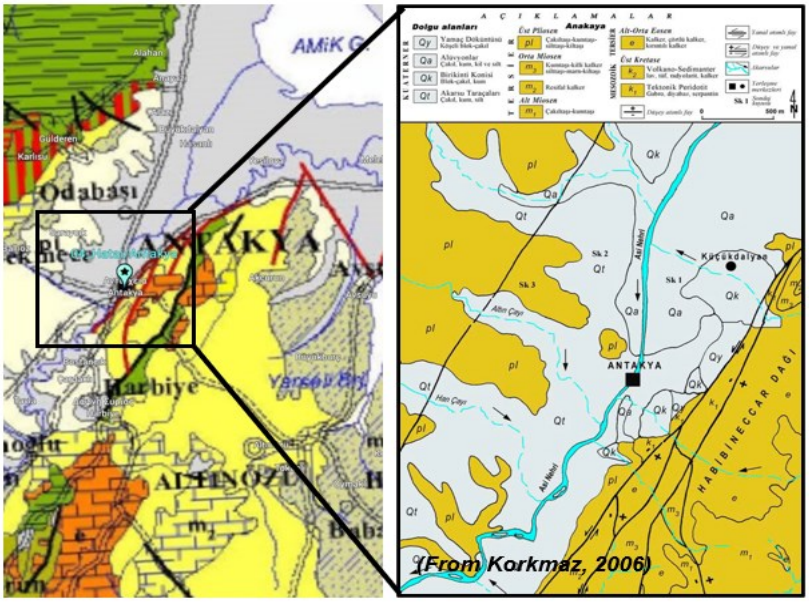

Figure 3.14 The damages are extensive in the city center where recent Quaternary deposits are extended (Geological maps of Turkey No16, Hatay sheet, scale 1:500.000, Editor: M. Senel & Technical assistant: N. Aydal).

Figure 3.15 Quaternary deposits are extended. Direct proximity to the fault.

- **Geological conditions in Adiyaman**

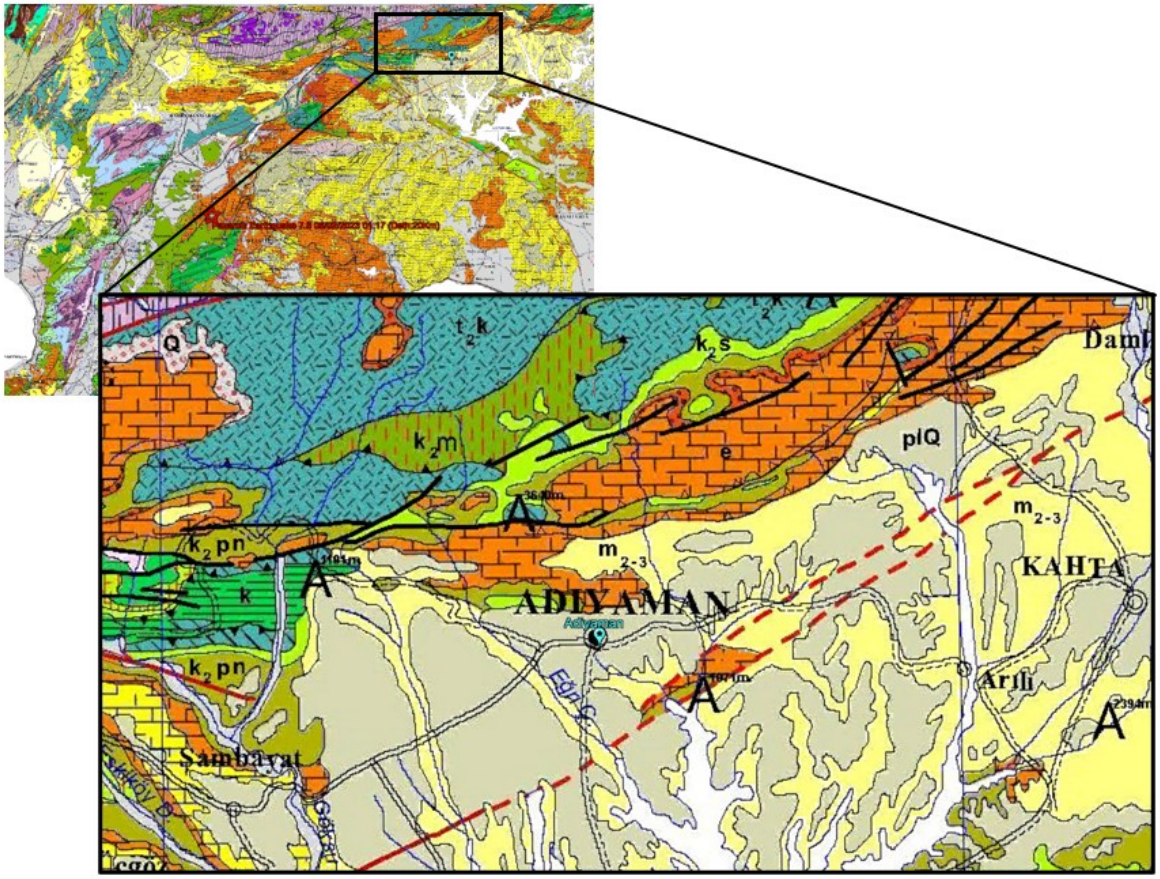

Figure 3.16 Geological conditions in Adiyaman (Geological maps of Turkey No16, Hatay sheet, scale 1:500.000, Editor: M. Senel & Technical assistant: N. Aydal).

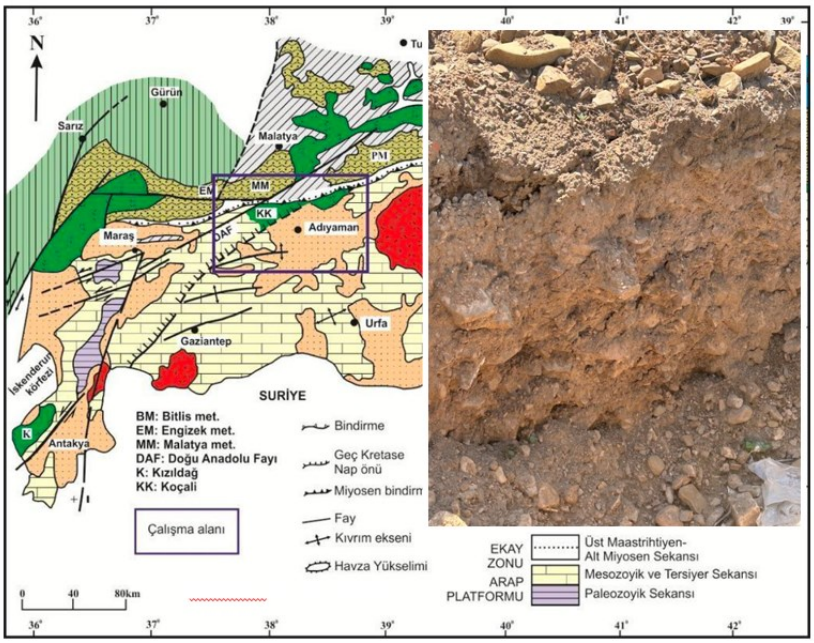

Figure 3.17 The Adiyaman is built on recent soil alluvial formations and talus. Part of the fault extends to the outskirts of the city (Geological maps of Turkey No16, Hatay sheet, scale 1:500.000, Editor: M. Senel & Technical Assistant: N. Aydal).

- **Geological conditions in Iskenderun**

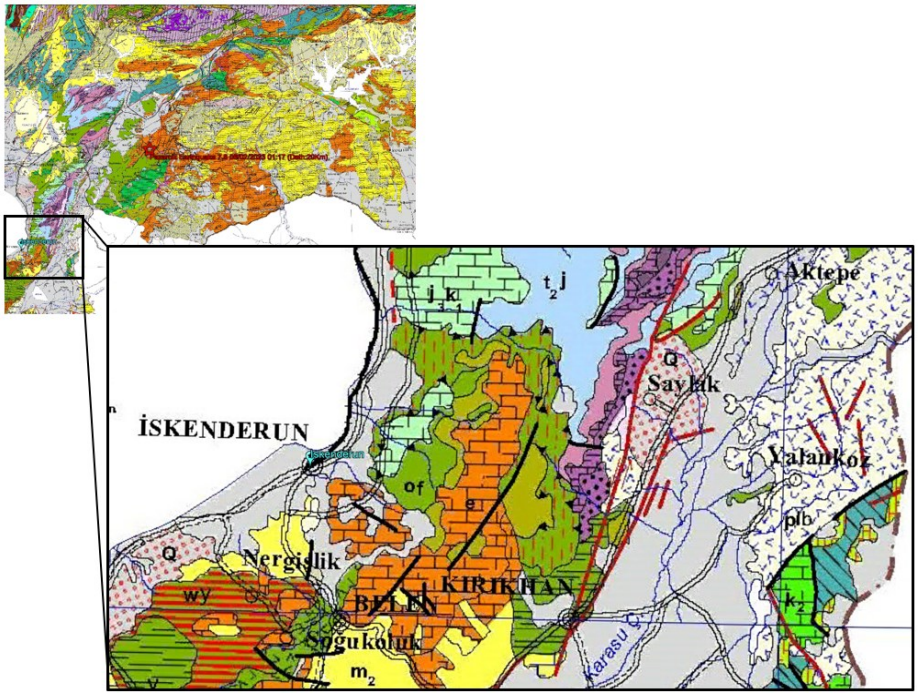

Figure 3.18 Geological conditions in Iskenderun (Geological maps of Turkey No16, Hatay sheet, scale 1:500.000, Editor: M. Senel & Technical assistant: N. Aydal).

Figure 3.19 Coastal deposits from mainly composed of loose sandy deposits. The coastal zone is still flooded due to significant settlement and liquefaction phenomena.

- **Geological conditions in Islayie**

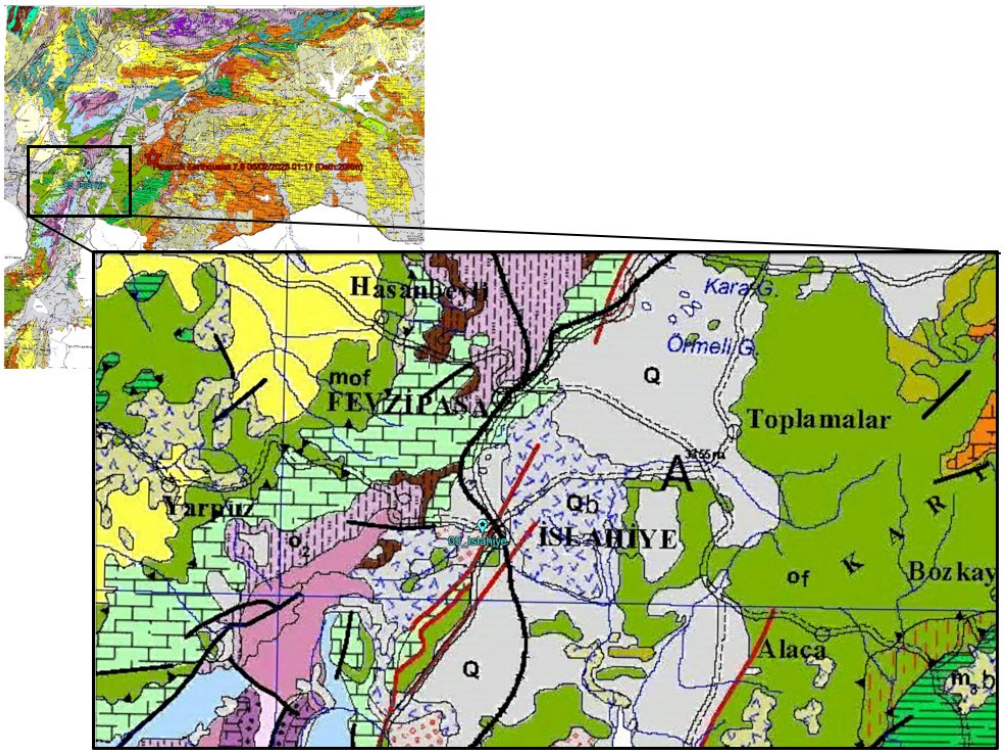

Figure 3.20 Geological conditions in Islayie. Although there is proximity to the fault, the damages here are more limited in extent of the city that are significantly built on rock foundations (mainly basalts) Geological maps of Turkey No16, Hatay sheet, scale 1:500.000, Editor: M. Senel & Technical Assistant: N. Aydal).

3.2 Geotechnical seismic response

Even though the fatal damages from the earthquake sequence of February 6 were of a structural nature, geotechnical failures were also prominent. Because of the great magnitude of the Pazarcik and Elbistan earthquakes (Mw7.8 and 7.5, respectively), the induced damages spread over a wide area covering 13 different prefectures of Turkey. A schematic representation of the geotechnical damage types observed from the seismic events is summarized in Figure 3.21.

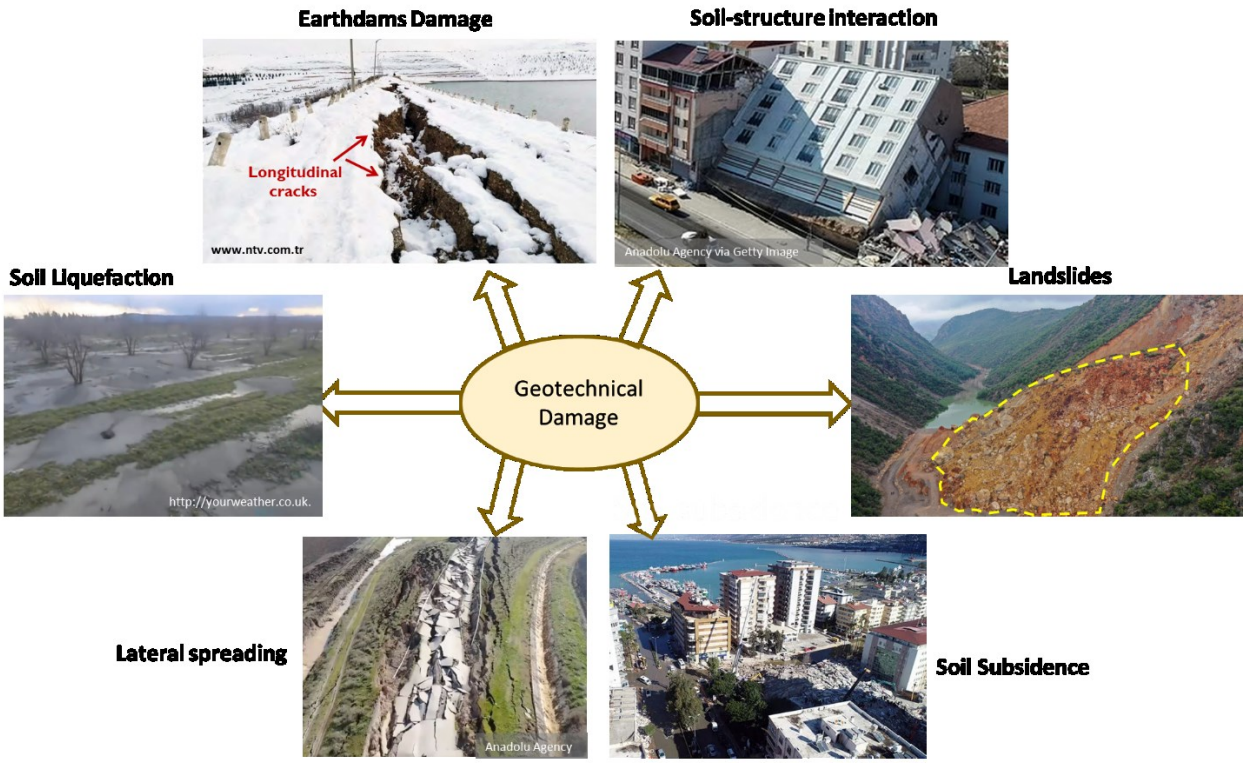

Figure 3.21 Geotechnical failure types observed in the 2023 Kahramanmaraş earthquake sequence.

3.2.1 Soil liquefaction and induced lateral spreading and/or soil subsidence

Seismic liquefaction is the lack of soil strength due to the reduction of effective stresses down to zero values, triggered by the increase of water pore pressures. As a sequence, the soil behaves as a liquid, providing no shear deformation resistance. Saturated non-cohesive soils, especially of low density, are prone to liquefaction.

Observations of soil liquefaction were noticed along the second rupture segment of the M_w 7.8 event, extending from Gölbaşi in the North to Antakya in the South (METU Report; USGS website; Gokceoglu 2023; Garini & Gazetas 2023). Liquefaction and lateral spreading/soil subsidence were also observed:

- at the Hatay Havalimani (airport),
- at the port of Iskenderun in the coastal area,
- at several locations near the Orontes River, north of Antakya, and
- at Lake Gölbaşi, where lateral spreading also occurred at several locations. What is more, total submergence of the lakeshore occurred.

Figure 3.22 to Figure 3.27 depict soil liquefaction in Antakya and Gölbaşi and lateral spreading at Gölbaşi whereabouts. When liquefaction occurs close to waterfronts, usually lateral spreading is caused: the liquefied soil, unable to resist any shear excitation, is deformed laterally, creeping along any stiffer layer sitting above it. This process opens cracks running parallel to the waterway (Youd 1993).

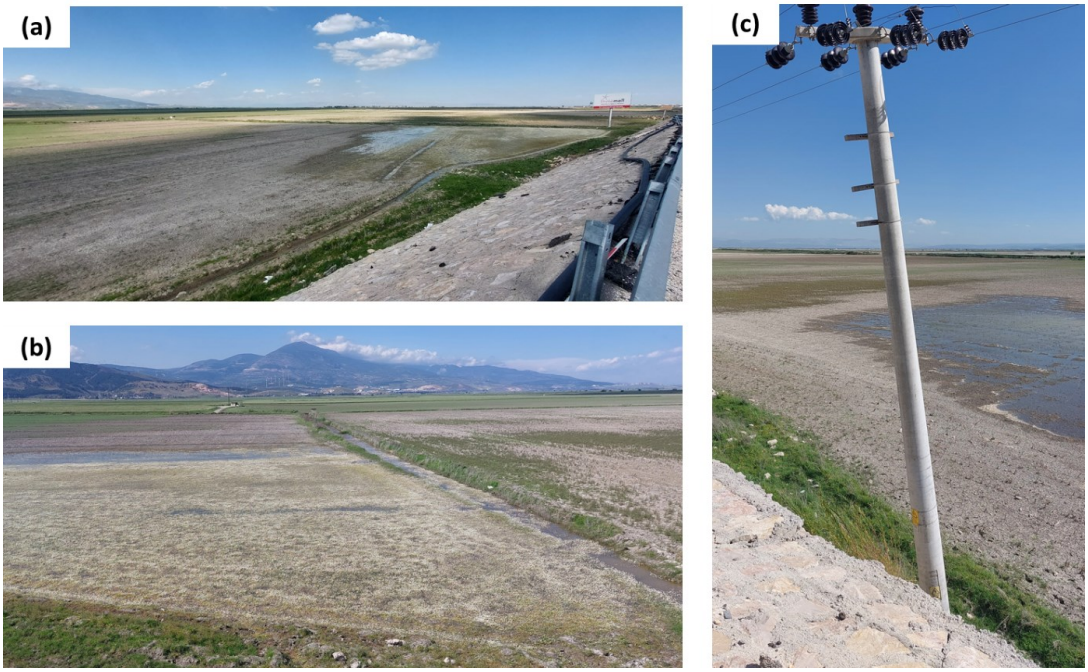

Figure 3.22 (a)-(c): Photos of the widespread liquefaction near Hatay International Airport (36,370148N, 36.260592E).

Figure 3.23 Soil ejecta at the surface, as evidence of seismic liquefaction, occurred in Gölbaşi (37.798553N, 37.662833E).

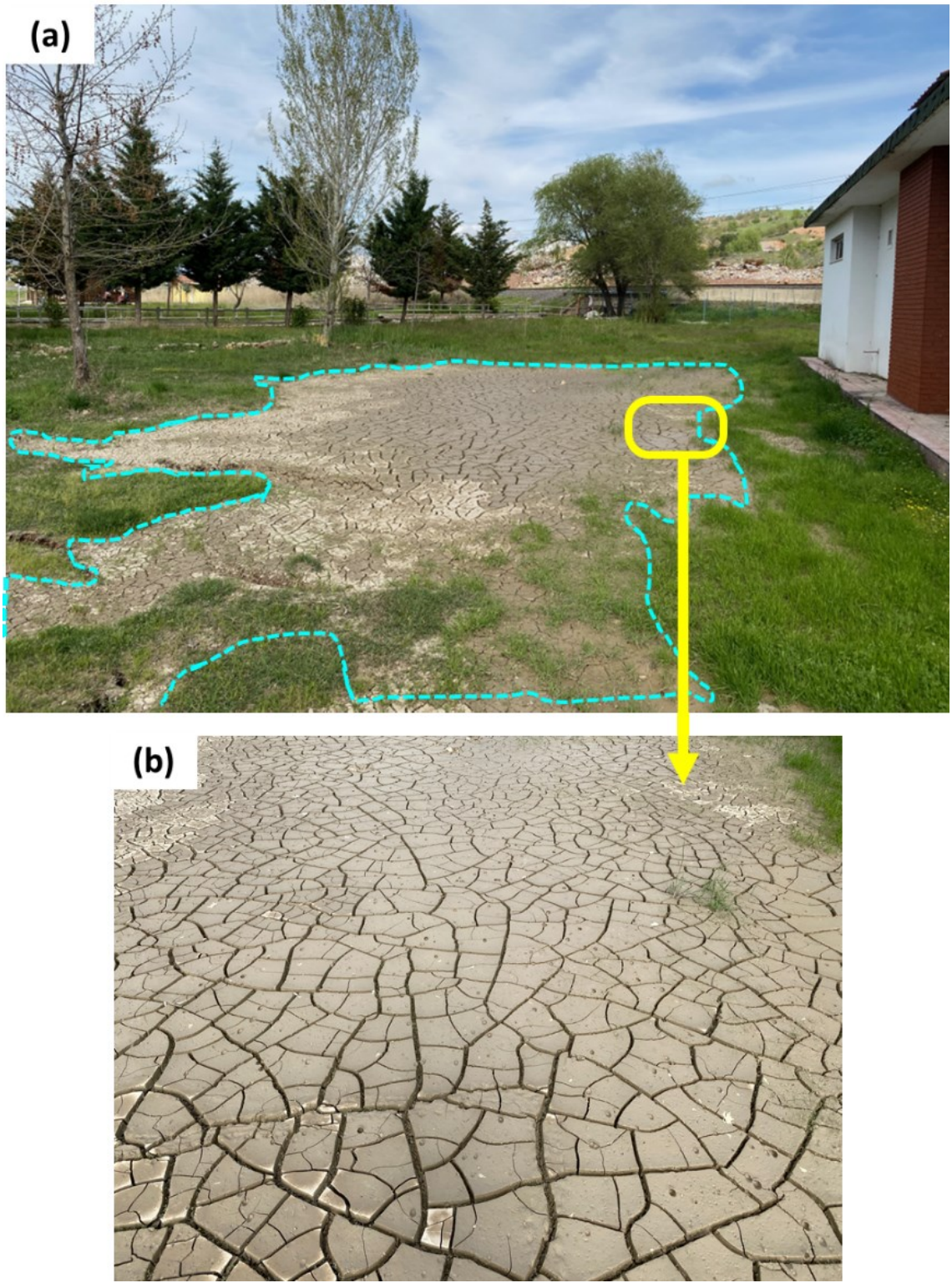

Figure 3.24 Remnants of soil liquefaction at Gölbaşi (a). The drying cracks (b) pattern is a clear manifestation of cohesive material existence in the soil ejecta (37.798553N, 37.662833E)

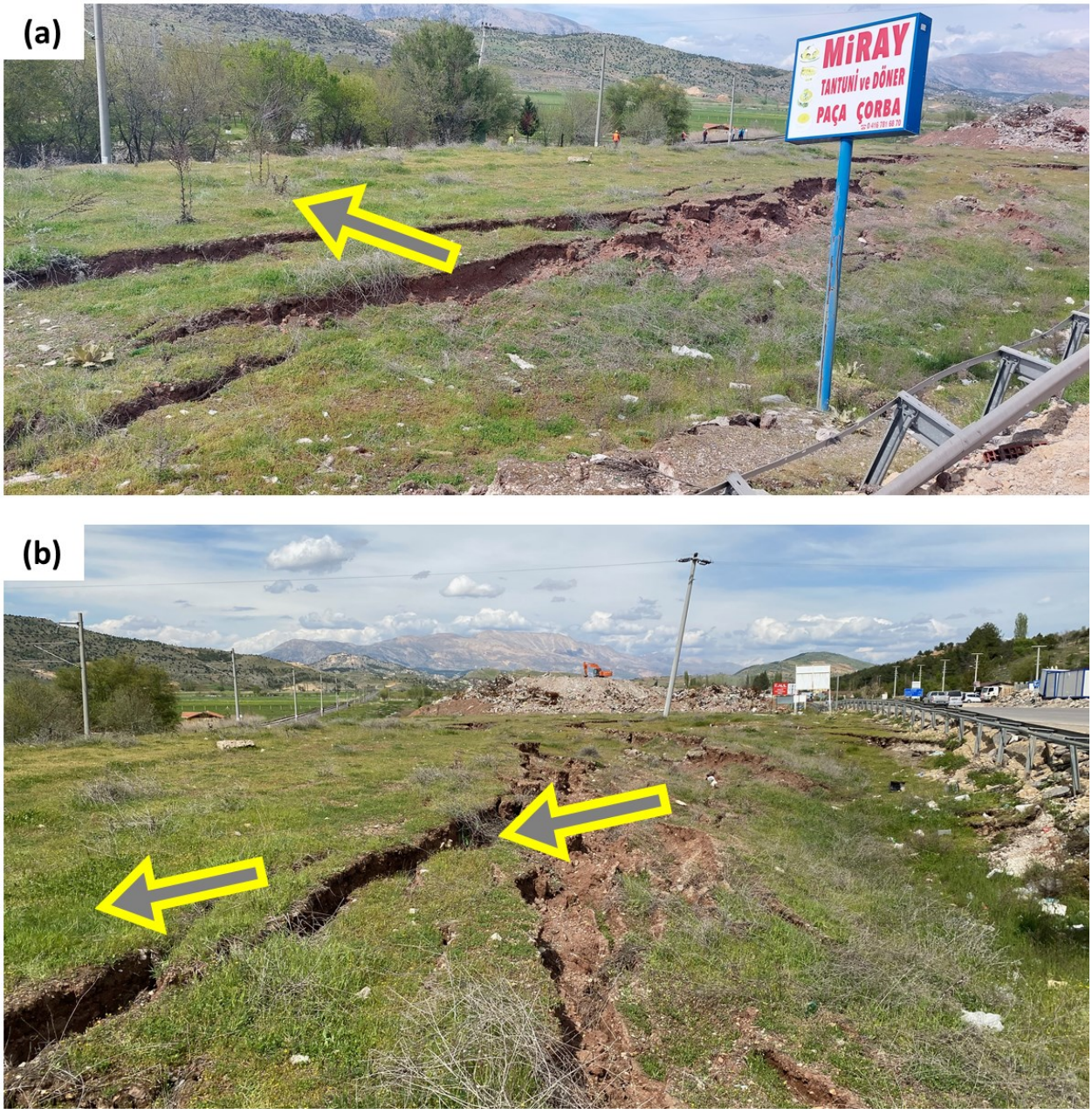

Figure 3.25 (a),(b): Lateral spreading at a slope near the Gölbaşi Lake (37.797857N, 37.6633.7E)

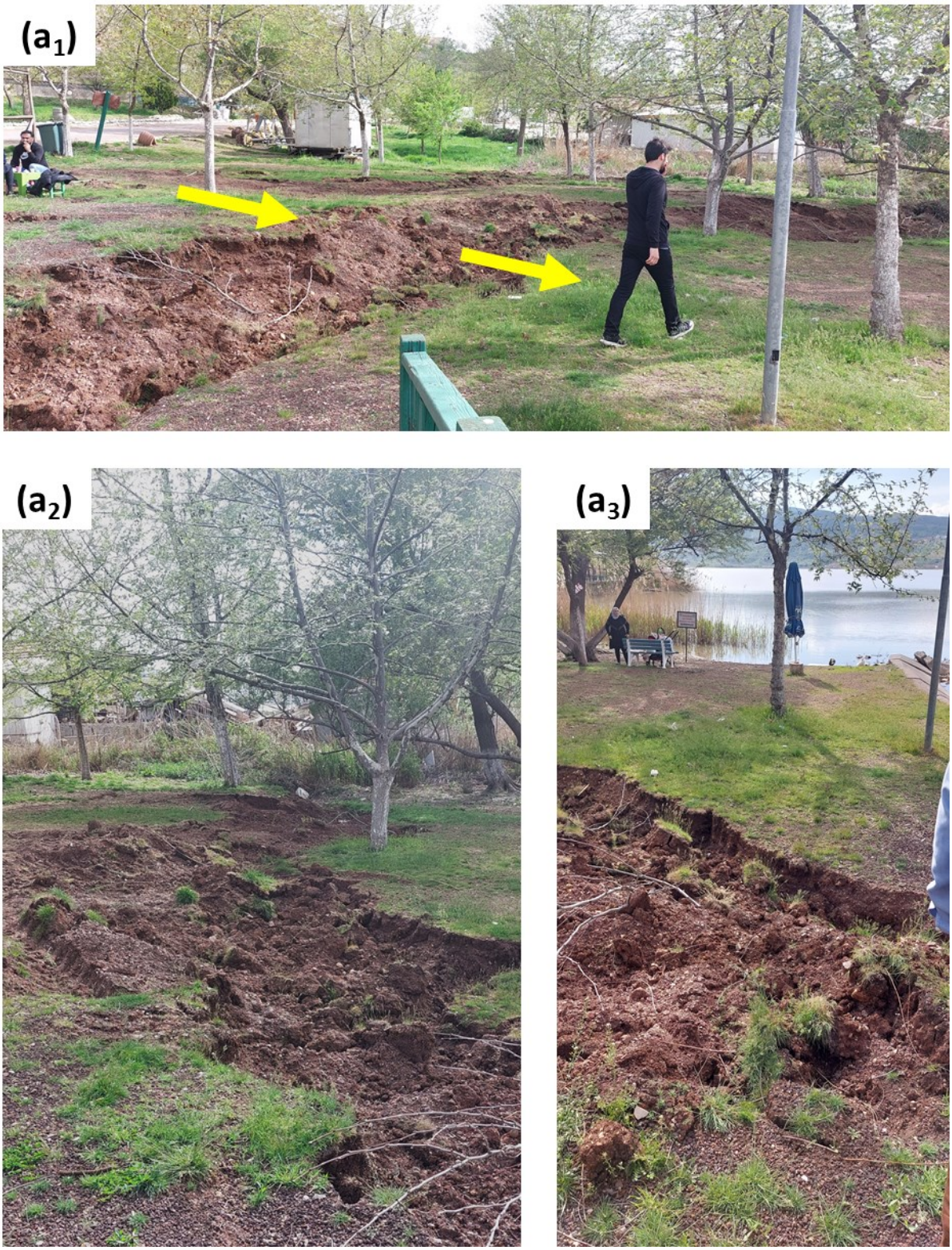

Figure 3.26 (a_1)-(a_3): Cracks induced by the soil's lateral movement towards the Lake Gölbaşi waterfront (37.798226N, 37.662083E)

Figure 3.27 Lateral translation of the pipes at their joints because of lateral spreading close to Lake Gölbaşi (37.798226N, 37.662083E)

Extensive liquefaction and soil subsidence were witnessed in the port area at Iskenderun, close to the waterfront. During our visit, water was still present on the roads and pavements behind the quay wall, but there is no clear explanation why (Figure 3.28).

Figure 3.28 Building and pavement subsidence close to the Iskenderun port (a) (36.590425N, 36.179943E) and (b) (36.590425N, 36.179943E)

Cracking of the road pavement and clayey soil ejecta were also witnessed at a distance of less than 80m from the waterfront (Figure 3.29), because of soil liquefaction and lateral spreading toward the coast (to the north)

Figure 3.29 (a) Cracks on the road pavement (36.591096N, 36.176768E) and (b) soil ejecta (36.591051N, 36.176851E) because of lateral spreading and soil liquefaction

The quay wall at the port of Iskenderun was submerged because of lateral spreading and liquefaction (Figure 3.30).

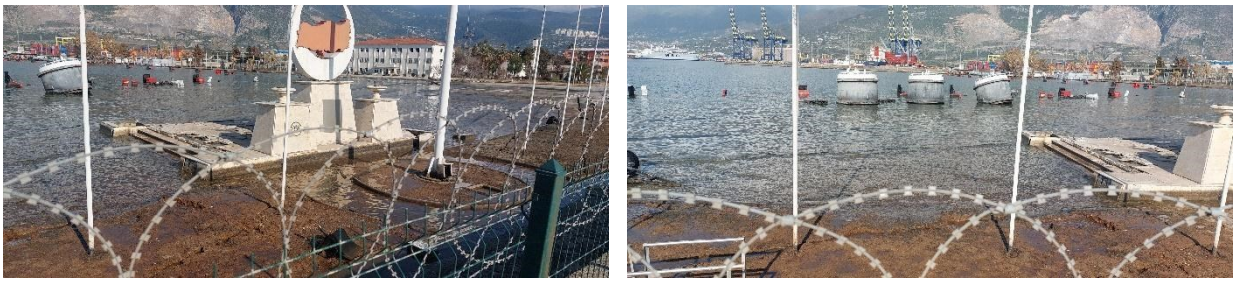

Figure 3.30 Permanent subsidence and tilt of the quay wall at the port of Iskenderun (36.593440N, 36.180389E)

3.2.1.1 Soil-Foundation-Structure Interaction

Seismic settlement (or subsidence) of the ground surface often occurs in earthquakes due to either consolidation, bearing capacity failure under the foundation, or densification of sandy layers due to ground shaking or liquefaction. In the case of seismic liquefaction, settling and rotating buildings founded on mat foundations have been seen in many earthquakes, such as in the notorious examples of Niigata (1964), Dagupan (1990), and Adapazari (1999).

Especially in Turkey, this occurred in the M_w7.6 Kocaeli earthquake of August 17, 1999, in Adapazari, where in some neighborhoods of the city, several buildings had settled (uniformly or differentially), tilted or even toppled (Gazetas 1996). Figure 3.31 shows a few characteristic cases from Adapazari.

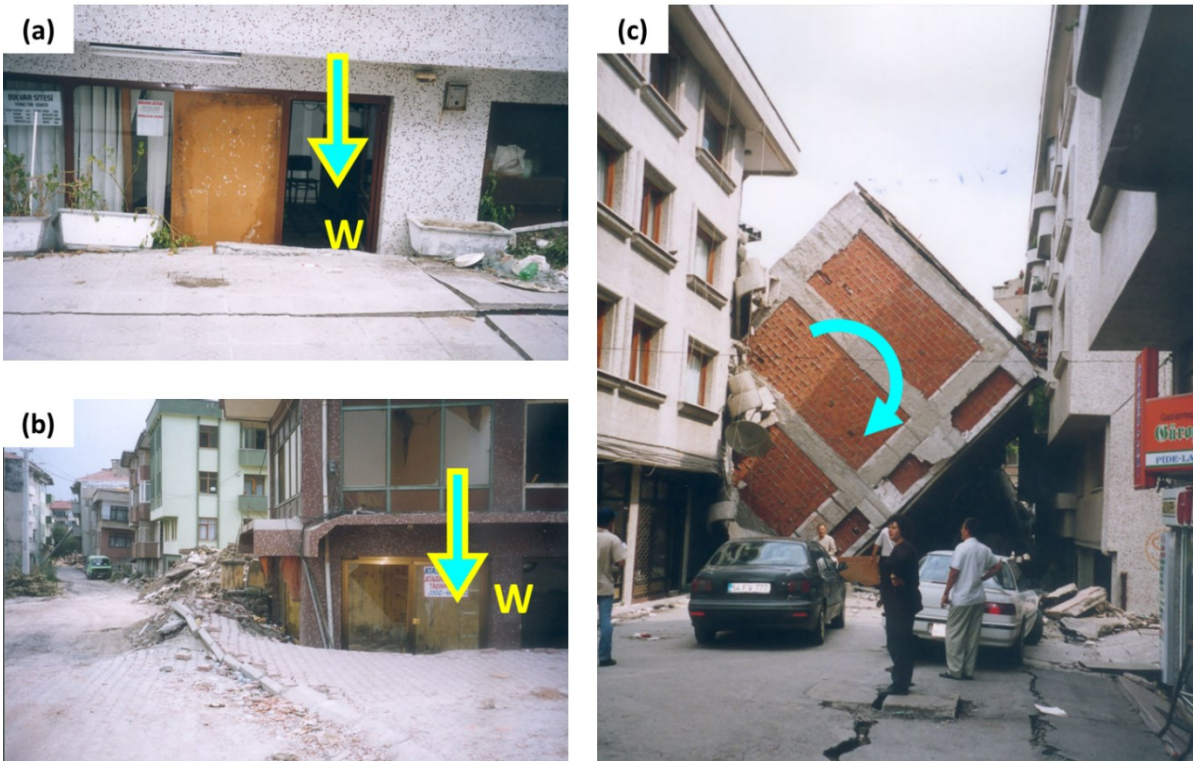

Figure 3.31 Cases from 1999 Adapazari earthquake: (a), (b) seismic subsidence of buildings induced under their static load (their own weight), due to soil liquefaction of an underneath soil layer; (c) toppled of a structure undergone rocking oscillation.

The consequences of seismic liquefaction of a soil layer under the shallow foundation of buildings could be:

- Uniform of differential settlement
- Severe tilting or overturning
- Little or even NO structural distress in buildings
- Sand and water ejection on the surface

Structural performance in Gölbaşi in the 2023 earthquakes is reminiscent of Adapazari during the M_w7.6 Kocaeli earthquake (1999). In a large district of Gölbaşi, most buildings on shallow mat foundations tilted, settled, and a few even toppled. Figure 3.32 to Figure 3.43 illustrate several such cases.

Figure 3.32 a), (b): Cases of permanent tilting of buildings in Gölbaşi city, due to rocking oscillation that results in uplifting displacements in the front side of the structures (37.788762N, 37.649529E).

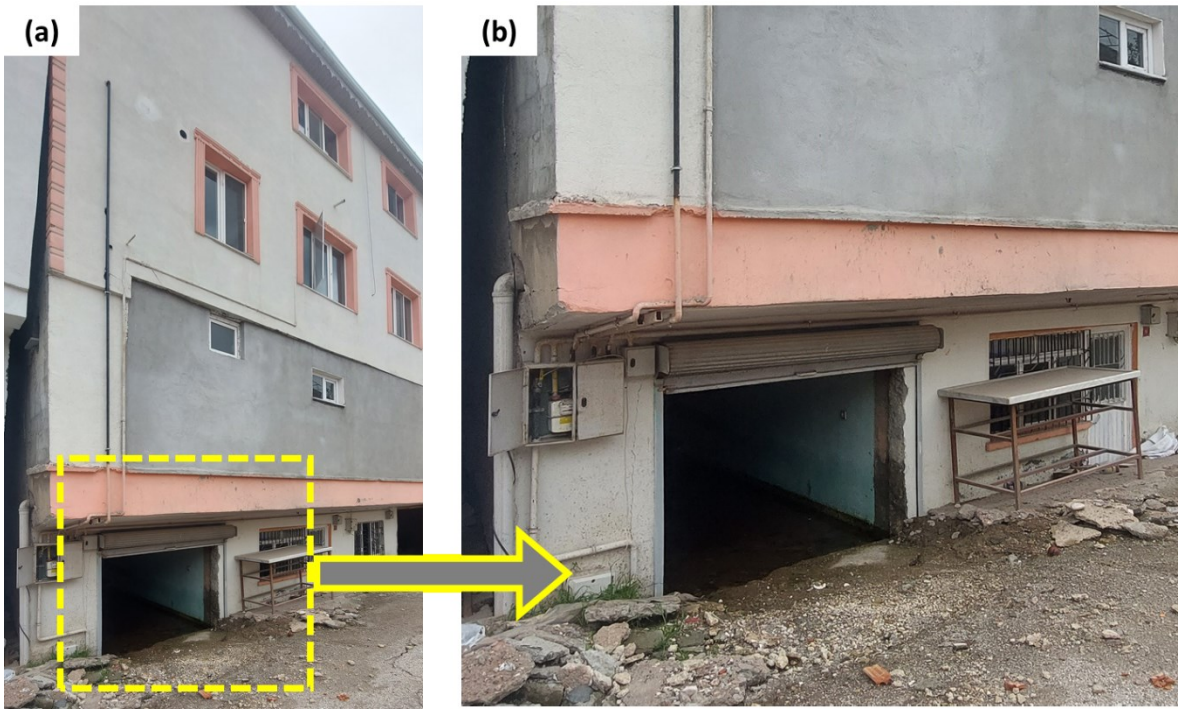

Figure 3.33 (a)-(b): Permanent settlement of a 4-story building in Gölbaşi (37.790248N, 37.650917E)

Figure 3.34 RC building with permanent tilting. Uplifting displacements in the façade (37.790129N, 37.651630E)

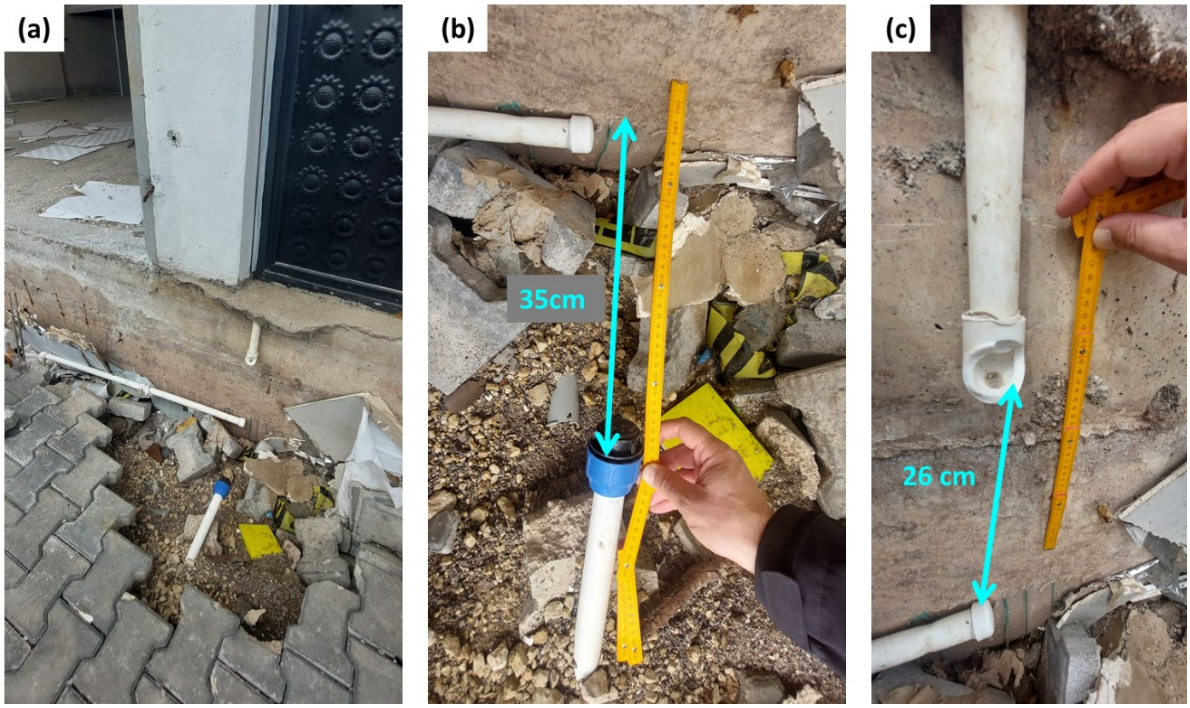

Figure 3.35 (a): Dislodged joint due to permanent uplifting; (b) and (c): measured horizontal and vertical displacement of the joint (37.790129N, 37.651630E)

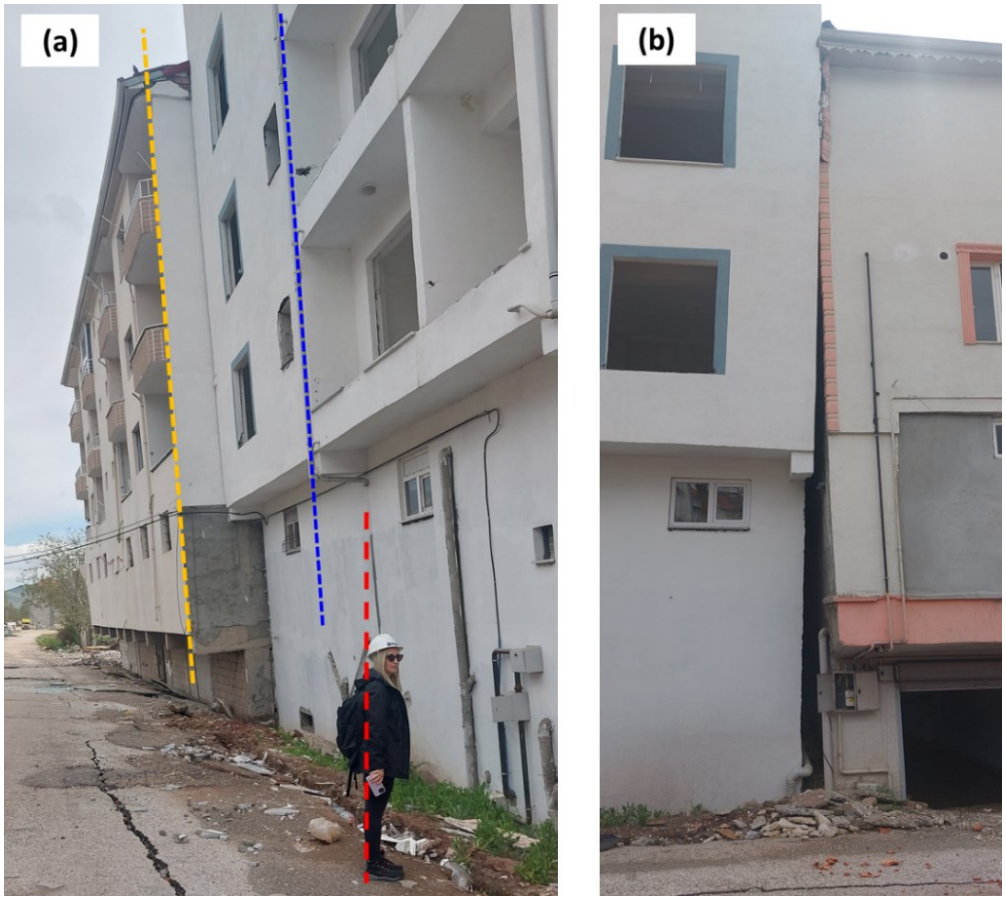

Figure 3.36 Tilted residential buildings in Gölbaşi (37.790134N, 37.650747E)

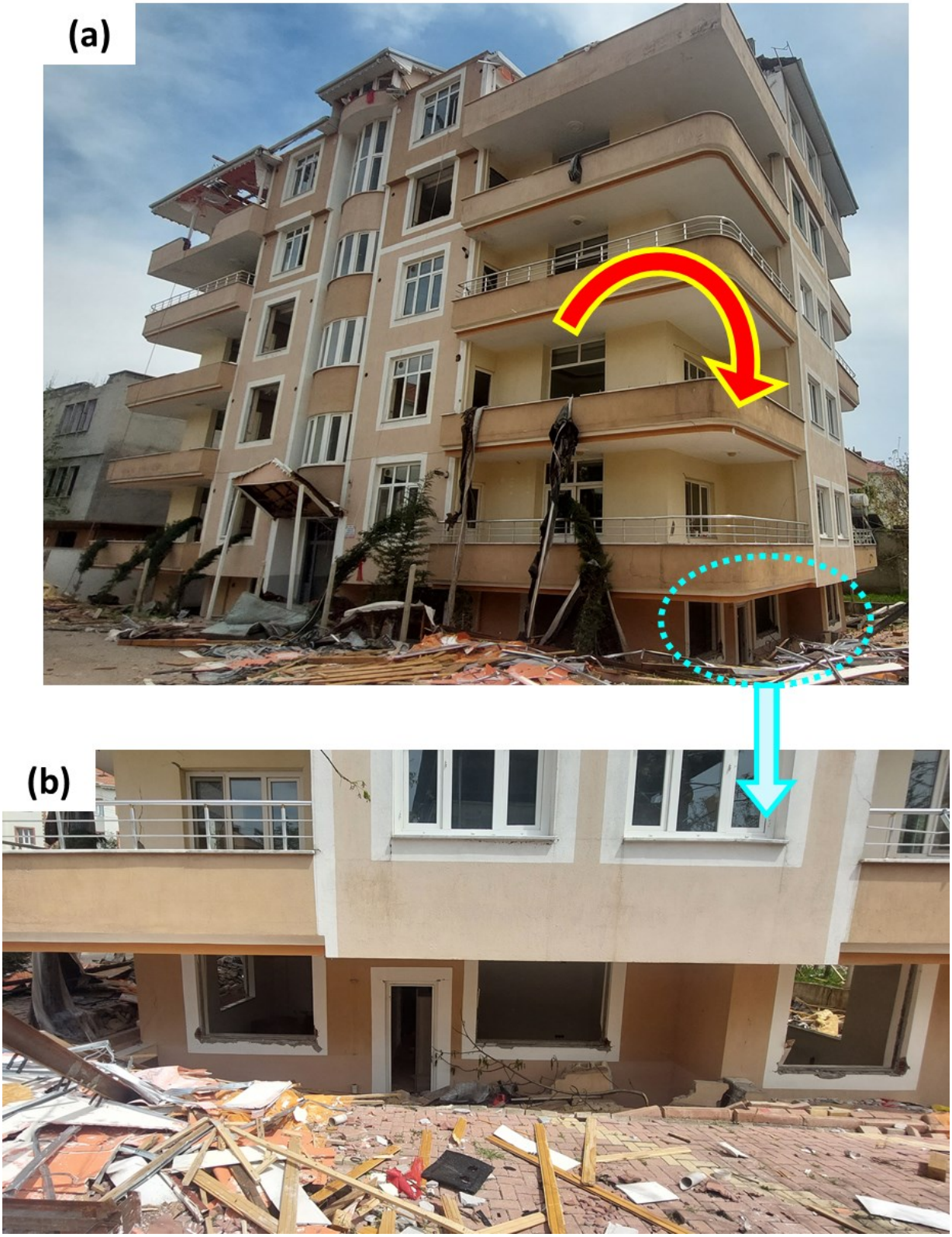

Figure 3.37 (a) Complete and (b) detailed view of a rotated 6-story RC building (37.787913N, 37.646741E)

The cases above of tilted buildings could be modeled as slender blocks on deformable soil excited by earthquake ground motion. A possible mechanism of such behavior is sketched in Figure 3.38 d (see Gazetas 2015, 2019). Cases of severe tilting and overturning are shown in Figure 3.38 to Figure 3.43.

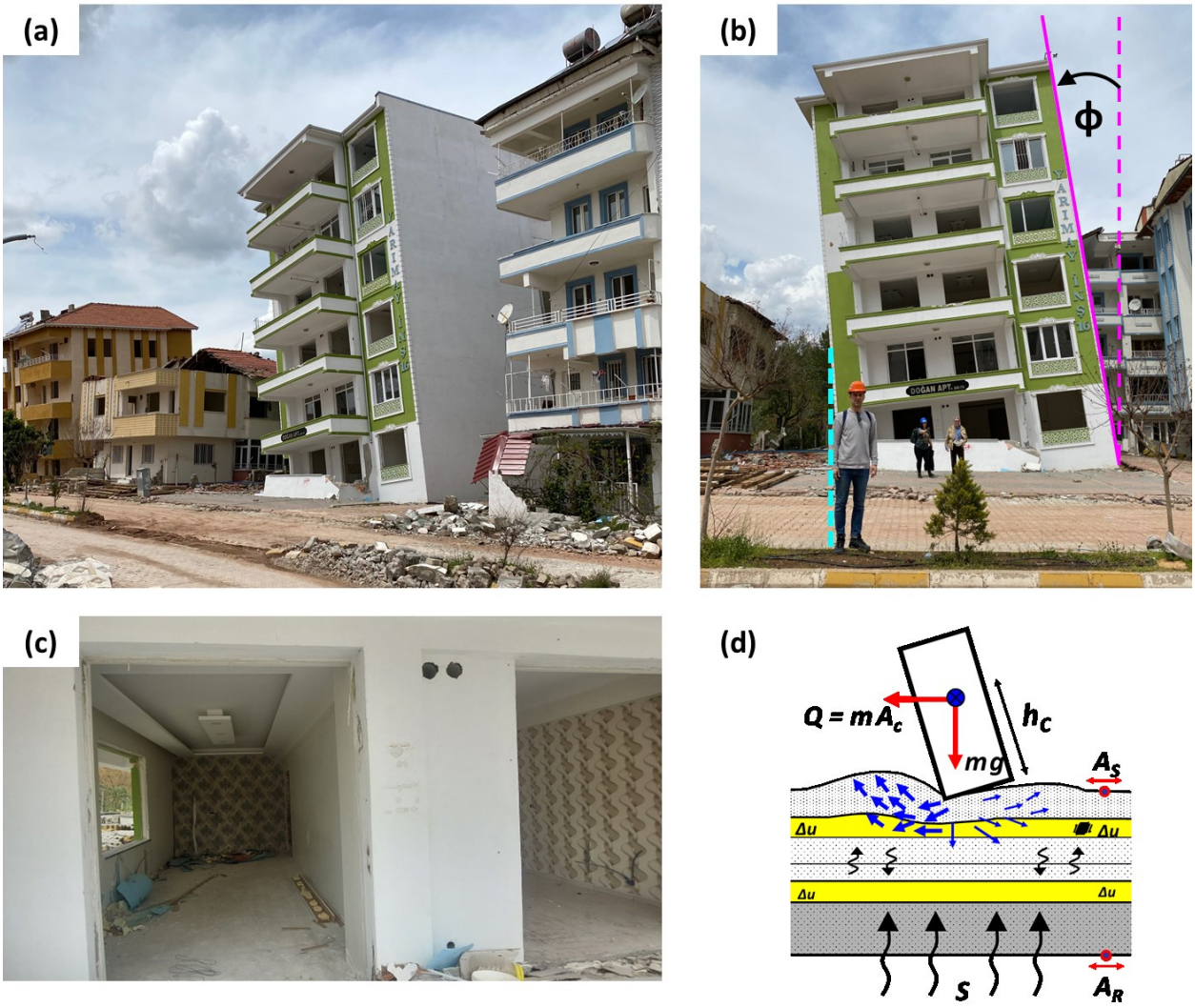

Figure 3.38 (a),(b): 6-story RC building which suffered permanent tilting of approximately 8 degrees to the west; (c): View of the ground-floor interior, revealing no visible signs of structural damage. (d): Sketch of the likely mechanism of foundation bearing-capacity failure leading to the building's permanent tilting (or even toppling) (37.788455N, 37.646016E)

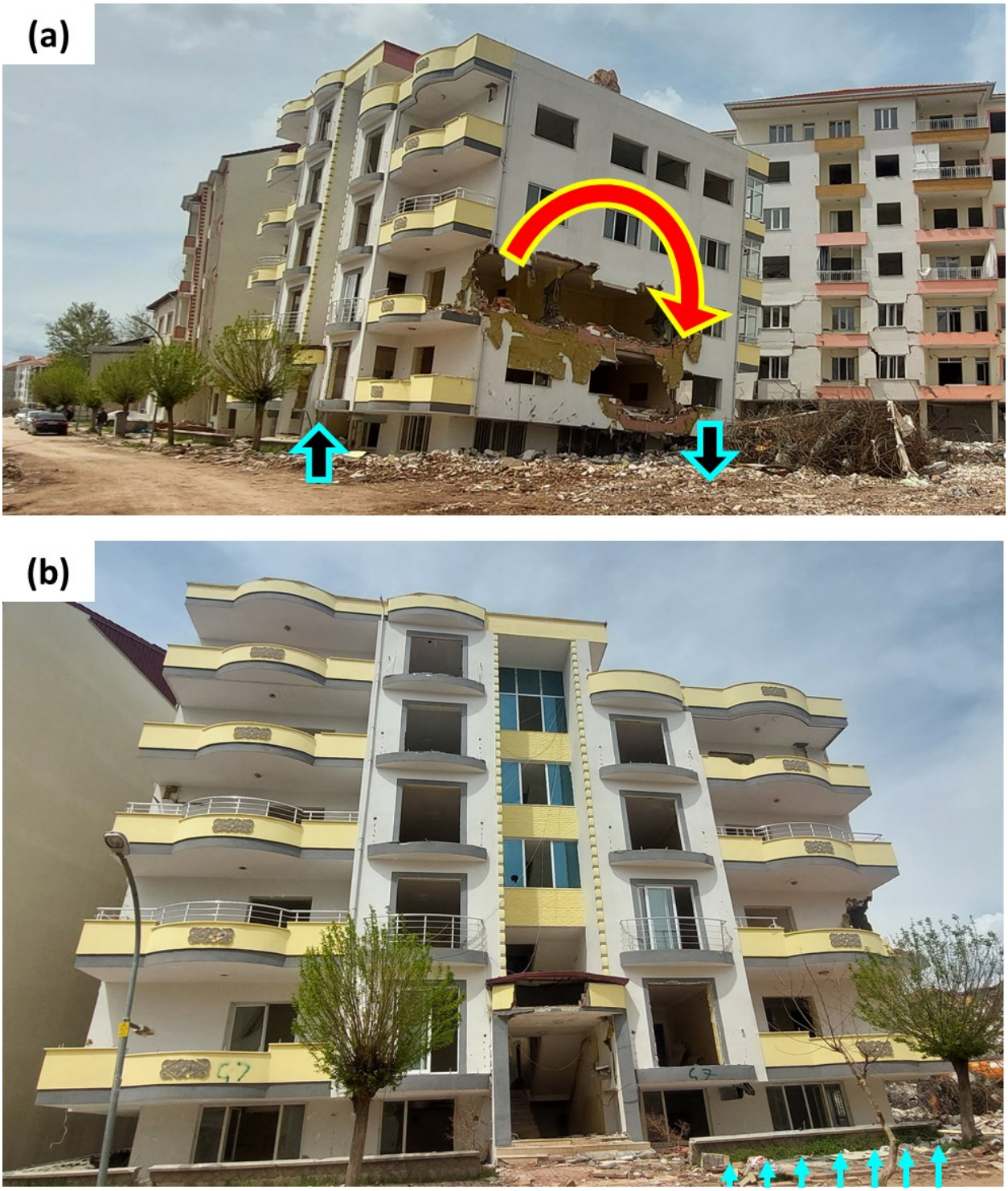

Figure 3.39 (A 6-story residential apartment in No. 92 Gazi Street: (a) The building roof settlement at the southeast corner was estimated as 31 cm and at the southwest corner as 12 cm. The measured tilt at the building's front (south side) was 5 degrees towards the north (37.788007N, 37.643913E)

Figure 3.40 (a)-(d): Views of the essentially toppled to the north (resting at the neighboring building) 6-story RC building in Ada İnşaat, Gölbaşi, likely because of soil bearing capacity fasilure (37.787765N, 37.643365E)

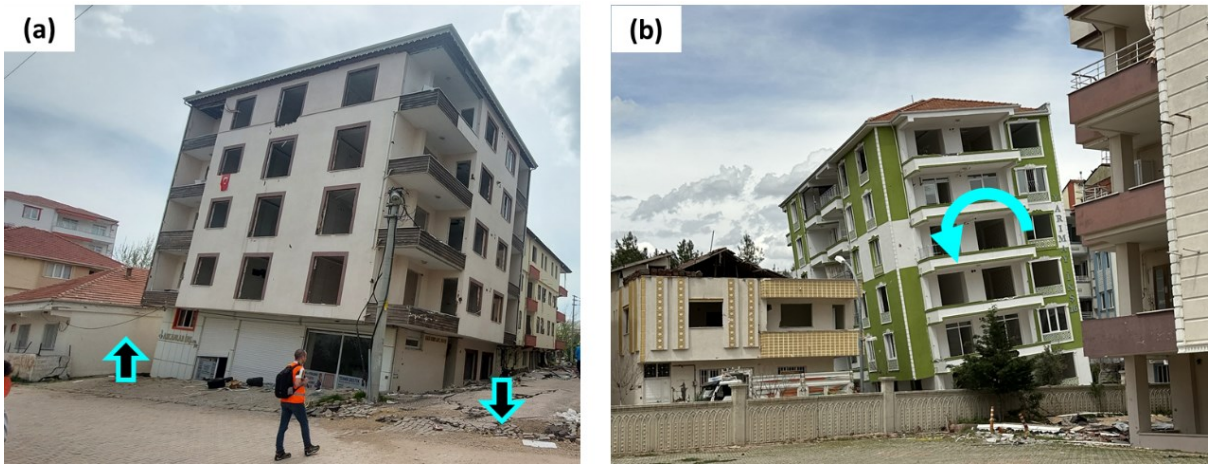

Figure 3.41 Characteristic cases of buildings with permanent rotation in Gölbaşi.

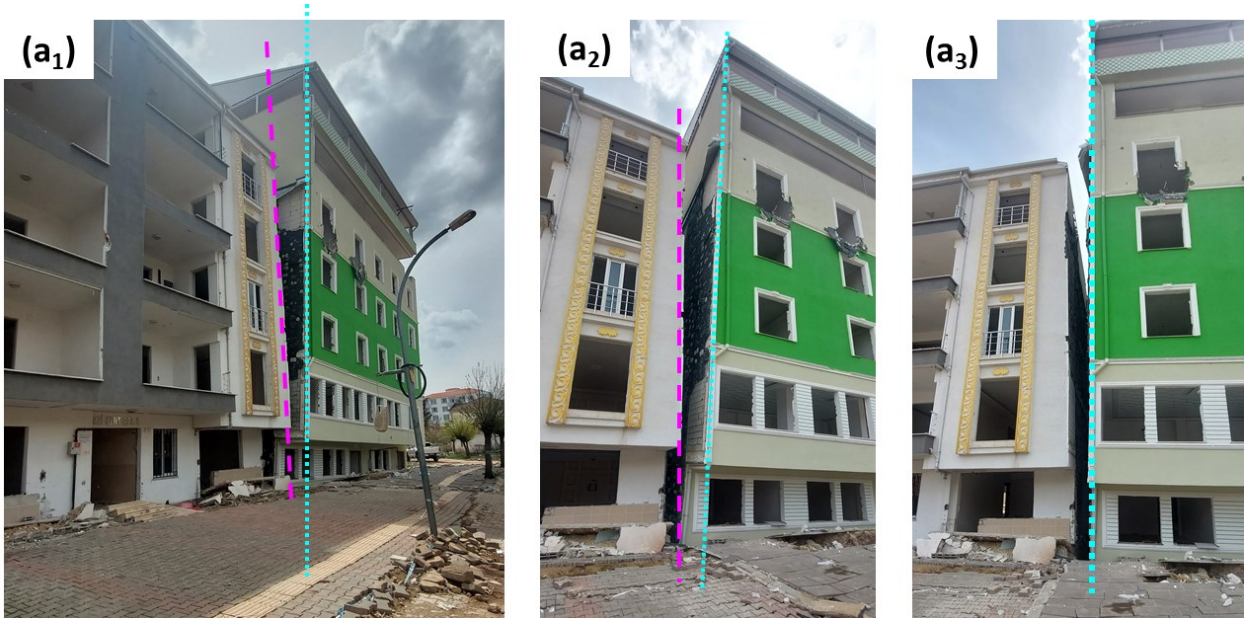

Figure 3.42 (a_1-a_3): Views of two adjacent residential buildings in Gölbaşi. Both are tilted, probably because of soil bearing capacity failure, but with different permanent rotation angles (37.787491N, 37.642797E).

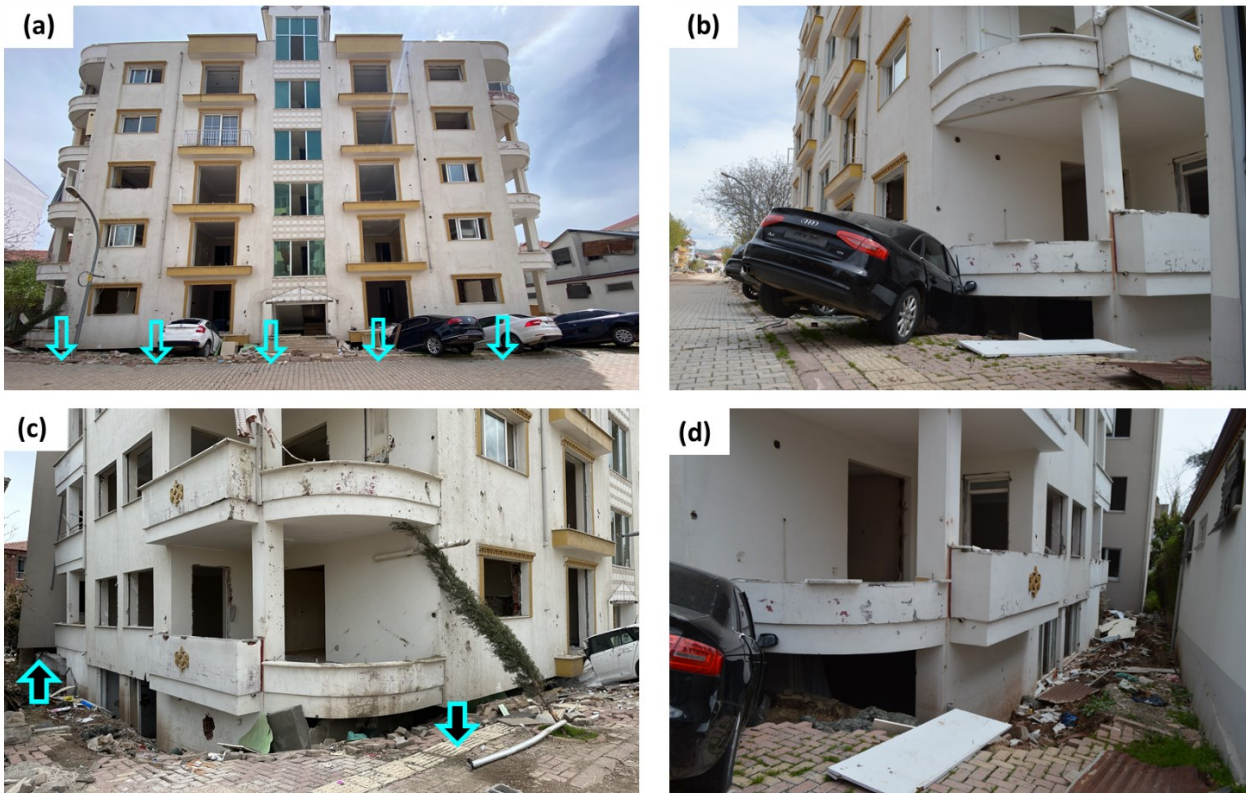

Figure 3.43 Another characteristic case of a tilted residential building in Gölbaşi (37.787491N, 37.642797E).

3.2.2 Landslides

The destructive earthquake series in Kahramanmaraş had impacts on 11 cities in Turkey, affecting a region spanning approximately 90,000 km2 with seismic intensity levels sufficient to trigger landslides (peak ground acceleration > 0.08 g). The undulating terrain, marked by about 15% of the landscape featuring slopes exceeding 20°, enhanced the probability of widespread landslides due to the significant ground shaking (Görüm et al., 2023).

An investigation by Görüm et al. (2023) utilizing high-resolution satellite images, aerial photos, and a field survey confirmed that this earthquake sequence triggered numerous landslides. More than 3,500 landslides that occurred during the earthquake were recorded, with a predominant concentration in the northern region. While rock falls constitute the most prevalent type of landslide, there are also numerous instances of bedrock rotational landslides, translational slides, and lateral spreads. The mountainous terrain experienced surface rupture, leading to the occurrence of several large landslides, some of which were unfortunately fatal. The primary variables influencing the spatial distribution of these coseismic landslides appear to be lithology,

the spatial variability of ground shaking, and topographic relief. Indeed, during our reconnaissance, we had the opportunity to identify a very big dam landslide in the Islahiye area.

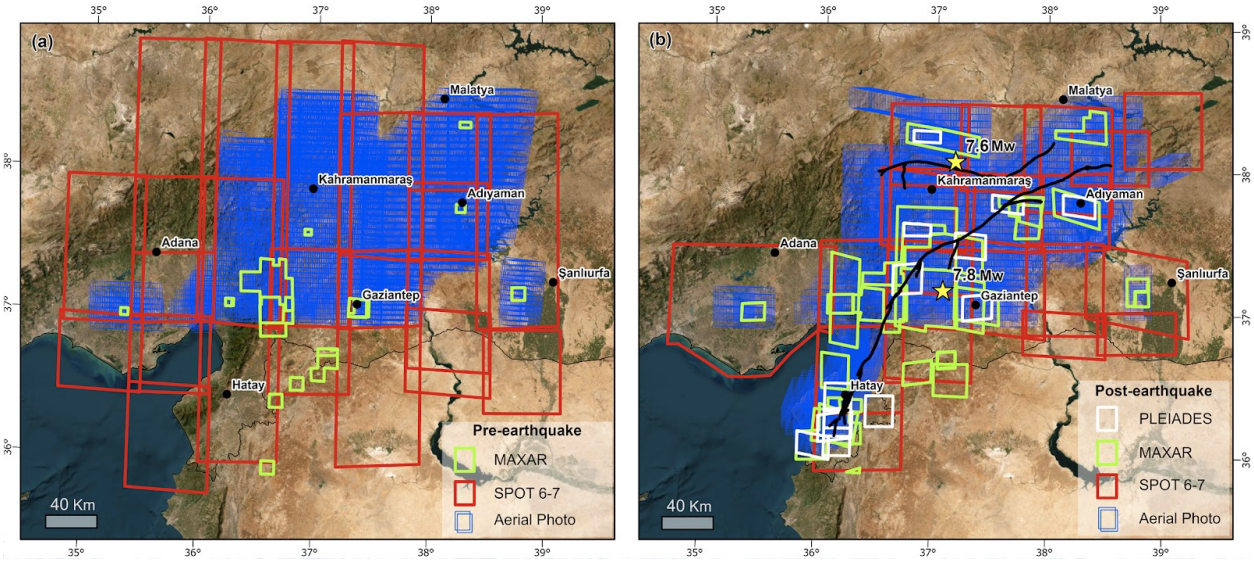

Figure 3.44 Pre- and post-earthquake aerial photo and satellite image coverage (Görüm et al., 2023)

3.2.2.1 Landslide mapping

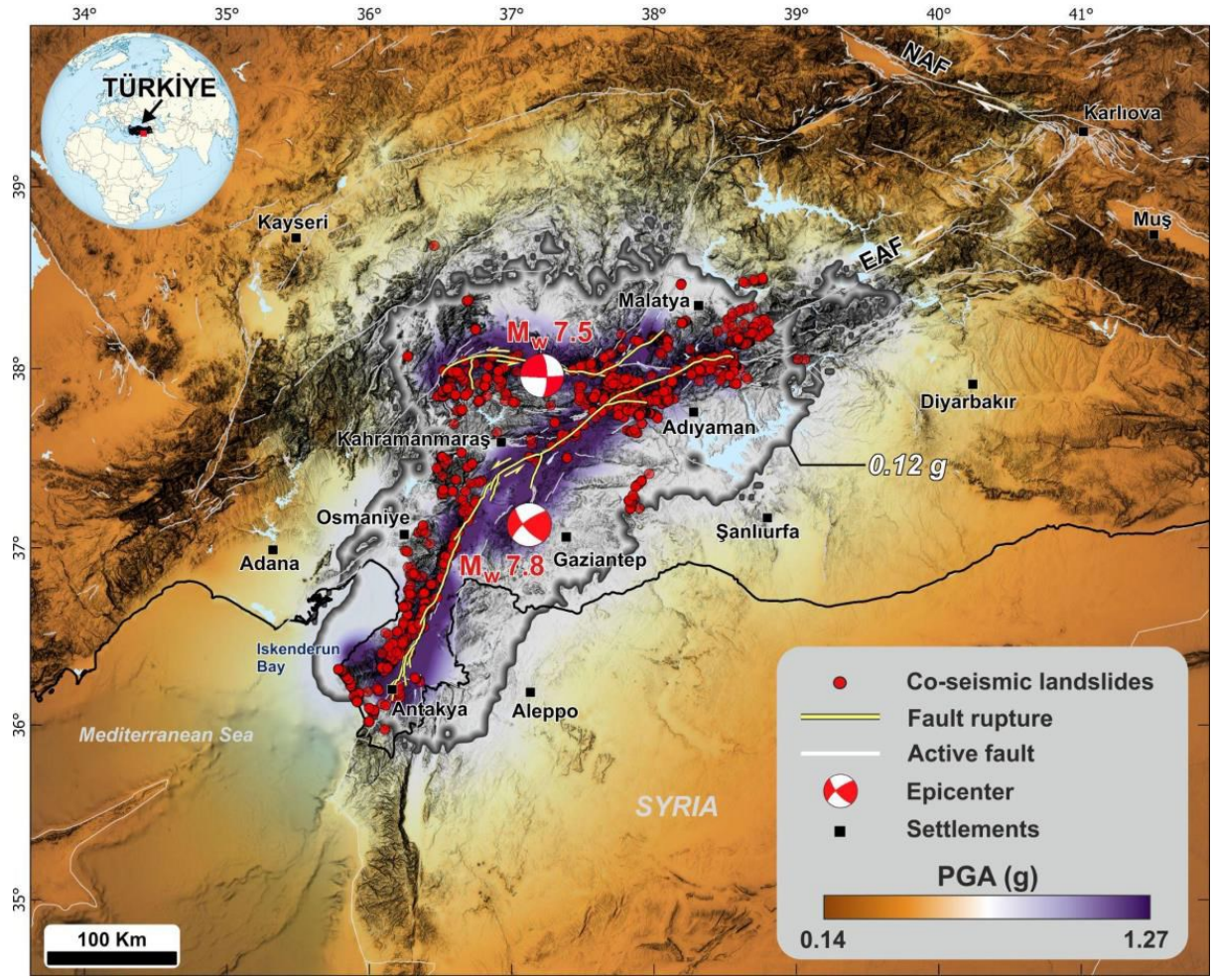

Figure 3.45 Spatial distribution of more than 3500 co-seismic landslides superimposed by the two main earthquake epicenters (USGS, 2023a, 2023b) fault rupture (highlighted yellow, Reitman et al., 2023).

Landslides seem to cluster around the rupture zone, where the estimated probability of landslides is significantly high. Nevertheless, a study of the frequency distribution of landslides indicates that the majority are located on hillslopes, as expected.

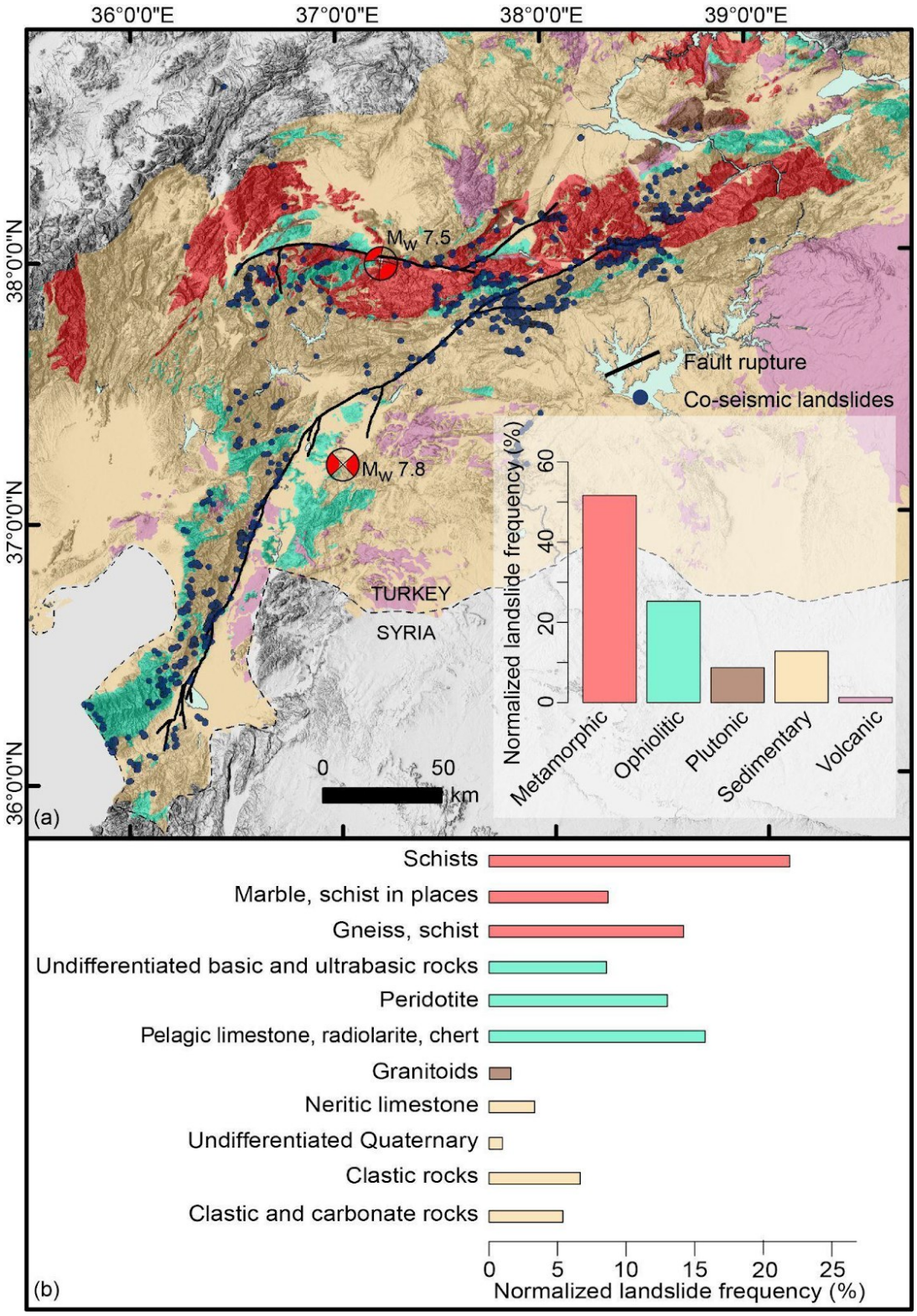

Figure 3.46 Spatial and frequency distribution of landslides over (a) aggregated and (b) specific rock types seen in the study area. Landslide frequencies were normalized for the percentage of the study area covered by each of these rock types (Görüm et al., 2023)

3.2.2.2 Rock falls

The predominant coseismic slope instabilities in the area affected by the earthquake are rock falls. Individual blocks reached sizes of 6-7m3 in certain regions, of limestone nature mainly. Such rock-block falls were identified during our reconnaissance close to Islayie town in limestone steep terrain (Figure 3.47).

Figure 3.47 Rockfall incidents in the Islayie region in limestone steep terrain close to Islahiyi area. Blocks reached up to sizes of 6-7m^3.

3.2.2.3 Bedrock rotational slides

Bedrock rotational slides are common in the study area, especially in the north. They were mainly triggered within pre-existing landslides and on areas, where the rock mass is heavily fractured. A deep-seated landslide was identified in Islahiye region, where millions of m^3 have slid and blocked the river creating a dam behind the fallen mass (Figure 3.48). The rock mass is highly karstified and brecciated with a high presence of clayey infilling material around rock fragments and along fractured certain sub-vertical zones (Figure 3.49).

Figure 3.48 A deep-seated landslide was identified in the Islahiye region, where millions of m3 have slid and blocked the river creating a dam behind the fallen mass.

Figure 3.49 The rock mass is highly karstified and brecciated with high presence of clayey infilling material around rock fragments and along certain fractured sub-vertical zones.

3.2.2.4 Translational slides

Other significant landslides that were triggered by the earthquakes are the translational ones. In Tepehan village near Altınözü, Hatay, there is an illustrative case of a translational landslide. This landslide, covering an area of approximately 1.3 km2, occurred in an area characterized by marl and clay-rich limestone. The landslide resulted in the formation of deep cracks along undulating hillslopes (Figure 3.50). Here, the upper bedding surface of a clay-rich limestone unit slid along the interbedded marl. This unit is intensely weathered in the upper sections and varies in thickness from 10 to 30 meters (Sümer et al., 2023).

Figure 3.50 A rotational landslide in Tepehan village, Altınözü, Hatay (N36 9’39.3”; E36 13’17.9”). A clay-rich weathered limestone mass slide along the interbedded marl

References

3.1 AFAD (Disaster and Emergency Management Authority): https://tadas.afad.gov.tr/

3.2 Aydan O., Ulusay R., 2023. A report Pazarcik and Ekinozu earthquakes (Turkey) of February 6. Prepared for the International Society of Rock Mechanics (ISRM)

3.3 Apostolou M., Gazetas G., Garini E. (2007). "Seismic response of slender rigid structures with foundation uplifting". *Soil Dynamics and Earthquake Engineering* 27: 642–654.

3.4 Duman, T.Y.; Emre, Ö. The East Anatolian Fault: Geometry, segmentation and jog characteristics. Geol. Soc. Lond. Spec. Publ. 2013, 372, 495–529.

3.5 Garini E., Gazetas G. (2023) "Preliminary Report on the M7.8 and M7.5 earthquakes of February 6, 2023 in Turkey-Syria": DOI 10.17605/OSF.IO/V4MSW

3.6 Gazetas G. (2019). The 59th Rankine Lecture: "Benefits of Un-conventional Seismic Foundation Design". British Geotechnical Association, website: https://www.youtube.com/live/pOXzqjTo34o?feature=share

3.7 Gazetas G. (2015). "4th Ishihara Lecture: Soil–foundation–structure systems beyond conventional seismic failure thresholds". *Soil Dynamics and Earthquake Engineering* 68: 23–39.

3.8 Gazetas G. (1996). *Soil dynamics and Earthquake Engineering: Case Histories* (in Greek). Symeon Publishing Co, Athens, Greece.

3.9 Gokceoglu C. (2023). "February 6 2023 Kahramanmaraş-Türkiye Earthquakes: A general overview". 39th International Symposium on Remote Sensing of Environment, 24-28 April, Antalya, Turkey.

3.10 Görüm T., Tanyas H., Karabacak F., et al., Preliminary documentation of coseismic ground failure triggered by the February 6, 2023 Türkiye earthquake sequence, Engineering Geology (2023), https://doi.org/10.1016/j.enggeo.2023.107315

3.11 Konstantinidis D., Makris N. (2007). "The dynamics of a rocking block in three dimensions". Proc. of 8th HSTAM International Congress on Mechanics; Patras, Greece.

3.12 Makris N., Roussos Y. (2000). "Rocking response of rigid blocks under near-source ground motions". *Geotechnique* 50 (**3**):243–62.

3.13 Makris N., Zhang J. (1999). *"Response and Overturning of Anchored Equipment under Seismic Excitation"*. Report No. PEER-98/05. Pacific Earthquake Engineering Research Center: University of California, Berkeley.

3.14 Makris N., Konstantinidis D. (2003). "The Rocking Spectrum and the Limitations of Practical Design Methodologies". *Earthquake Engineering and Structural Dynamics* 32 (**2**):265-289.

3.15 Makris N., Black C.J. (2004). "Dimensional analysis of rigid-plastic and elastoplastic structures under pulse-type excitations". *Journal of Engineering Mechanics* 130 (**9**):1006–1018.

3.16 Vassiliou M.F., Makris N. (2012). "Analysis of the rocking response of rigid blocks standing free on a seismically isolated base". *Earthquake Engineering and Structural Dynamics* 41:177–196.

3.17 Melgar et al.,2023. Sub- and super-shear ruptures during the 2023 Mw 7.8 and Mw 7.6 earthquake doublet in SE Türkiye, Seismica, doi:10.26443/seismica.v2i3.387

3.18 METU Report: MIDDLE EAST TECHNICAL UNIVERSITY : "Preliminary Reconnaissance Report on February 6, 2023, Pazarcik M_w=7.7 and Elbistan M_w=7.6, Kahramanmaraş-Türkiye Earthquakes". Edited by: Kemal Önder Çetin, Makbule Ilgaç, Gizem Can and Elife Çakir, REPORT NO: METU/EERC 2023-01.

3.19 MTA. Geological Map of Turkey in Scale of 1:500,000; Map sheets Adana and Hatay, Gneral Directorate of Mineral Research and Exploration: Ankara, Turkey, 2002.

3.20 USGS website: https://www.usgs.gov/news/featured-story/m78-and-m75-kahramanmaras-earthquake-sequence-near-nurdagi-turkey-turkiye

3.21 Sümer, Ö., Drahor, M.., Ongar, A., Tepe, C., Duman, A., 2023. 2023. 06 SUBAT 2023, Mw=7.7 Pazarcık, Mw=7.6 Elbistan (Kahramanmaraş) ve 20 SUBAT 2023, Mw=6.4 Defne (Hatay) depremleri saha çalişmalari yerbilimsel ön raporu 1. (In Turkish), 66p

3.22 Youd T. (1993). *Liquefaction-Induced Lateral Spread Displacement*. Report N^{o} TN-1862, Naval Civil Engineering Laboratory Port Hueneme California.

4. Evolution of Seismic Design Regulations (Turkey - Greece)

Chapter Author: ***Christos ZERIS***

Due to the increased frequency of damaging large magnitude seismic events that characterize the two major fault systems of Turkey (the Anatolian faults), the evolution of seismic design codes in Turkey followed very closely both in time and in content the evolution of UBC in California and ACI 318 RC design codes; the Turkish design codes and seismic zonation was more frequently revised in between US revisions, after major disastrous earthquakes in the country. Consequently, Turkish seismic regulations adopted US design concepts (namely the R factor, load, resistance, and spectrum amplification factors similar to UBC etc.). Recent Turkish seismic design codes adopt Eurocode 8 requirements (e.g., capacity moment and shear distribution in shear walls (Fig. 4.1 – 4.3) with the normative system switching to the adoption of both EN and ASTM building standards ([4.1] -[4.4]). Compared with the Greek seismic design and practice, the evolution of codes and material grades can be briefly summarized as follows.

Similar to Greece, the Turkish normative system for RC structures comprises two major design codes:

i) TS500, the Requirements for Design (Calculation) and Construction of Reinforced Concrete Structures. Issued as a Turkish Standard, covers all design and detailing requirements for gravity design of RC structures; the norm initially followed allowable stress design per DIN 1045 ([4.5]), and, subsequently, ultimate limit state methods in accordance with ACI 318 ([4.6], [4.7]) evolved.

ii) SBCDA, the Specification for Buildings Constructed in Disaster Areas (later the Building Earthquake Regulation). Issued and maintained by the Ministry of Public Works and Settlement, covers seismic design of buildings, including all modifications to TS500 for the design of structures (including RC) in seismic areas; SBCDA and related seismicity zonation decrees, have been revised with major upgrades in 1968, 1975, 1997, 2007 and 2018 ([4.8] - [4.14]).

Following the post war seismic design codes, SBCDA 1968 [4.8], an allowable stress-based seismic design code, adopted period dependent, triangular inertia load based seismic design and introduced some early dimensioning and minimum critical region detailing provisions for improved seismic performance (Fig. 4.1). The subsequent major revision, SBCDA 1975 [4.9], still allowable stress-based, introduced actual ductility in seismic design following UBC 1971; the introduction of a response reduction coefficient (the K factor), column and beam critical region detailing (12 stirrup diameter spacing), column confinement and a minimum B225 concrete grade; such detailing features were introduced during the Revisions of the Greek 1959 seismic code for RC structures, published in 1985 [4.15].

Following, with the subsequent adoption of ultimate limit state provisions – already introduced in RC design in the TS 500 1985 revision [4.6], SBCDA 1997 ([4.10], was published, following the 1992 Erzincan and 1999 Izmit earthquakes: in line with the seismic design provisions of its contemporary counterparts UBC/ICBO and ACI 318 codes, SBCDA 1997 introduced enhanced spectral analysis and site dependent spectra, improved base shear distribution due to irregularity, compulsory use of ductile design in high seismicity areas and capacity design principles, equivalent to the Greek NEAK Code in effect in 1995 ([4.16]). With the publication of the Compulsory Regulation of Seismic Pre Assessment of buildings in 2001 ([4.13]), additional rules were introduced for the assessment of existing RC buildings in SBCDA 2007 ([4.11]).

The latest revision of the seismic design code SBCDA 2018 ([4.14]) brought an entirely new revision of the existing design philosophy, introducing further, displacement based seismic design, base isolation, additional rules for RC elements (confined columns, flat slabs, shear walls), special requirements for high rise buildings and precast concrete construction; such changes in the Greek normative system are only available through the adoption of Eurocode 8 and its future changes, but not the Greek parallel usage EAK design code [4.16]. It is worth noting that, from this revision onwards, several rules and design formats have been adopted from the published versions of EN 1992 Part 1-1 and EN1998 Parts 1 and 3.

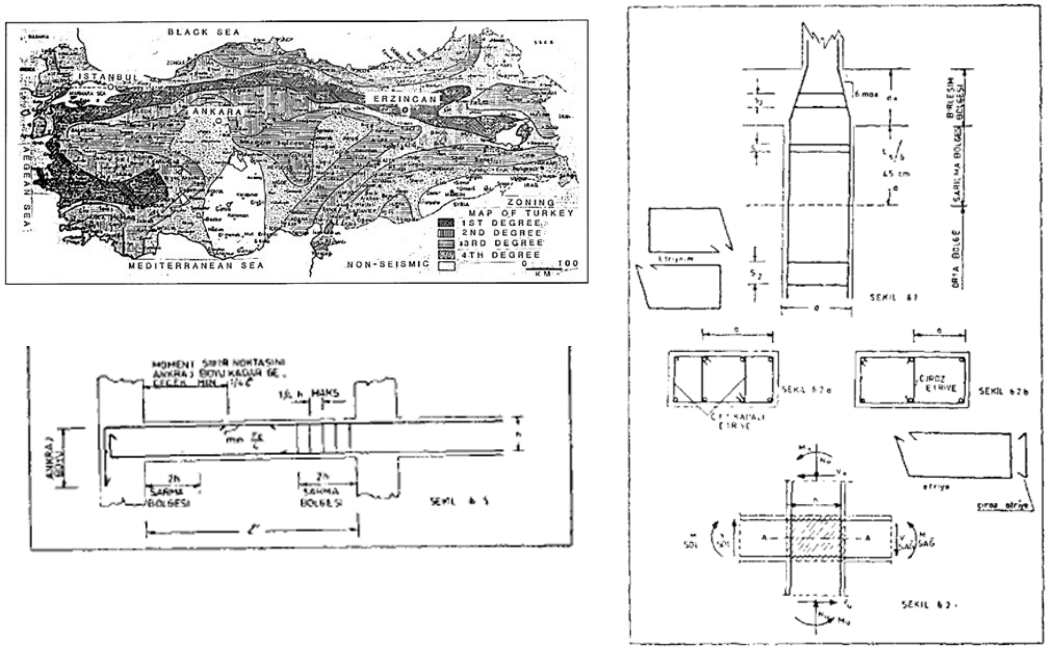

Figure 4.1 Zonation and typical RC frame detailing requirements for ductility, SBCDA 1968 and 1975 ([4.8], [4.9]).

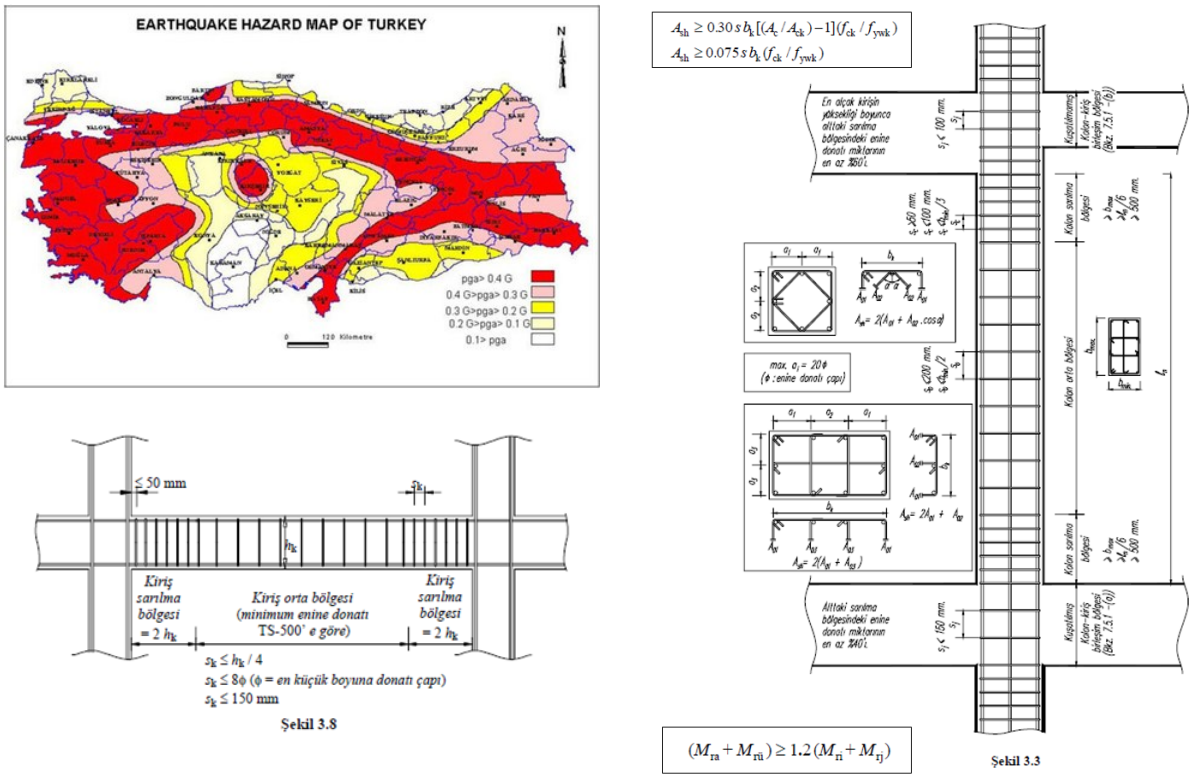

Figure 4.2 Zonation and typical RC frame ductility requirements, SBCDA 1997 and 2007 ([4.10],[4.11]).

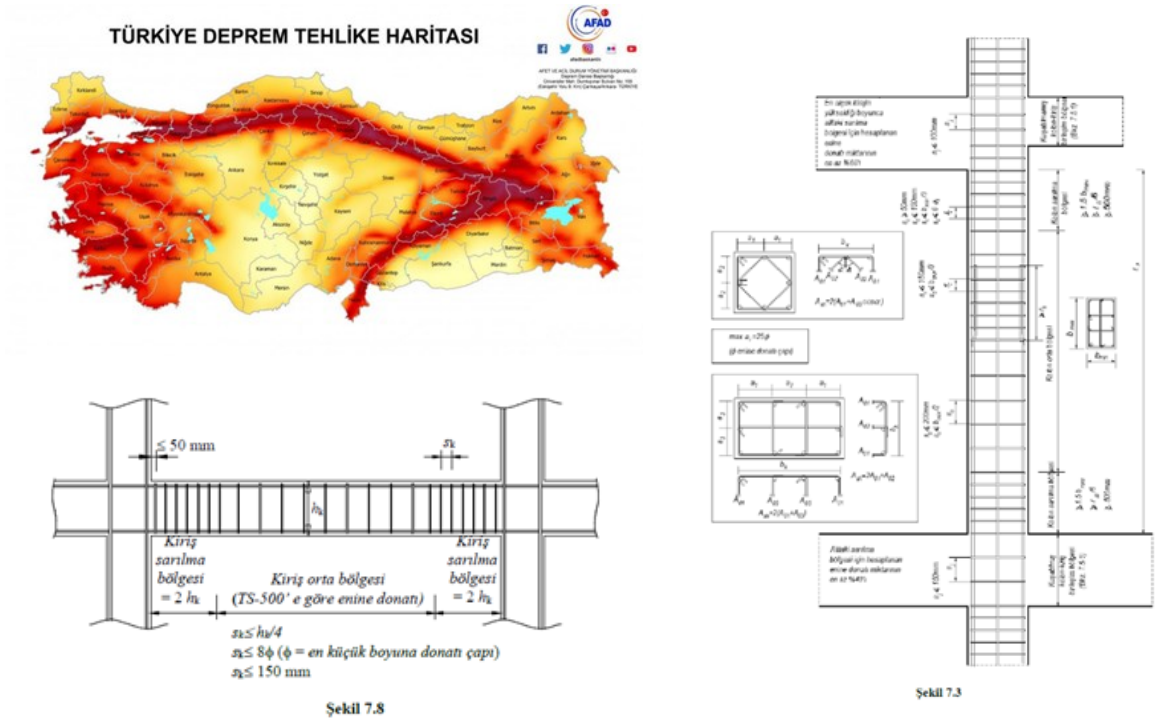

Figure 4.3 Zonation and typical RC frame ductility requirements, TBDY (2018) [4.14] and AFAD [4.12]

It is therefore noted, as a concluding remark, that the seismic design regulations system in Turkey was and still is a modern design system, systematically updated with the State of the Art. One should note, however, that despite this evidenced harmonization of the seismic design codes with contemporary foreign regulations and state of the art technologies, and their rapid synchronization with the accumulated knowledge and field experience obtained from destructive earthquakes in the region, this normative advancement was not immediately followed by the practice: the parallel allowance for non-ductile seismic designs albeit at higher base shear, permitted until the introduction of compulsory ductile seismic design, in 1997, did not enforce the adoption of the introduced ductility requirements, due to higher construction costs. Furthermore, from the point of view of conventional RC design, several reconnaissance reports in subsequent damaging earthquakes have pointed out that concrete quality and details did not, in general, materialize in the field due to poor workmanship and inadequate supervision ([4.17], [4.18]).

Table 4.1 Evolution of structural systems and Seismic Design Regulations for RC Structures

Earthquake event	Year	Seismic Design Regulation	Structural Characteristics
1939 Erzincan (M7.8)	1940 - 1944	*Italian Building Codes in Seismic Regions and Temporary Building Regulations* Allowable stresses, ε = 0,10 throughout	Infilled RC Frames Dense layout of infils Pilotis buildings, mezannines Asmolen slabs > 4 floors Columns reinforced with Φ8/300 St I. No special joint reinforcement Concrete is mostly site mixed (quality control not strictly enforced in practice) Column critical region reinforcement 1980 ready mix concrete
1943 Tosya (M7.2) 1944 Cerede (M7.5)	1949	*Turkish Aseismic Design Regulation* Seismicity Zonation (I, II, III) > Allowable stress design adopted. Design base shear coefficient of ε = 0,10 - 0,05 - 0,0	
	1953	*Regulation for RC Buildings.* Allowable stress design code following ACI 318 requirements.	
1967 Adapazari (M7.1)	1968	*Specification for Buildings Constructed in Disaster Areas (SBCDA 1968)* Response spectrum, triangular lateral load distribution, soil classification. Minimum grade of concrete grades **B160** to **B225**.	
	1972, 1975	*Specification for Buildings Constructed in Disaster Areas (SBCDA 1975):* New seismicity zonation (1-4): Allowable stress design base shear coefficients of ε = 0,10, 0,08, 0,06, 0,03, K factor for frame systems. Design for ductility is introduced. Concrete grade **B225**.	
	1985	*Regulation for RC Buildings (TS 500 1985).* Evolves to ULS Design following ACI 318 requirements.	
1992 Erzincan (M6.9) 1999 Izmit (M7.6), Düzce (M7.2)	1997	*Specification for Buildings Constructed in Disaster Areas (SBCDA 1997):* ULS design. Compulsory requirements for capacity designs, spectral analyses, irregularity rules, ductility introduced, following UBC 1997. Concrete grade **C20**.	2000 RC frames with shear walls Increase in building height: 8-10 floors
	2001	➢ Compulsory Regulation of Seismic Pre Assessment of buildings	
	2007	*Turkish Aseismic Design Building Code (CBCSA 2007)* Included: Assessment and redesign of Existing Buildings. Concrete grade **C20**.	2010 Frames with large Lightly Reinforced Walls (Tunnel Form)
2011 Van (M7.2) 2018 Elaziğ (M7.2) 2023 Kahramanmaraş (M 7.8, 7.6, 6.4)	2018	*Turkish Aseismic Design Building Code (CBCSA 2018)* Included: Tall buildings, Seismic isolation, Wood structures. Concrete grade **C25**.	

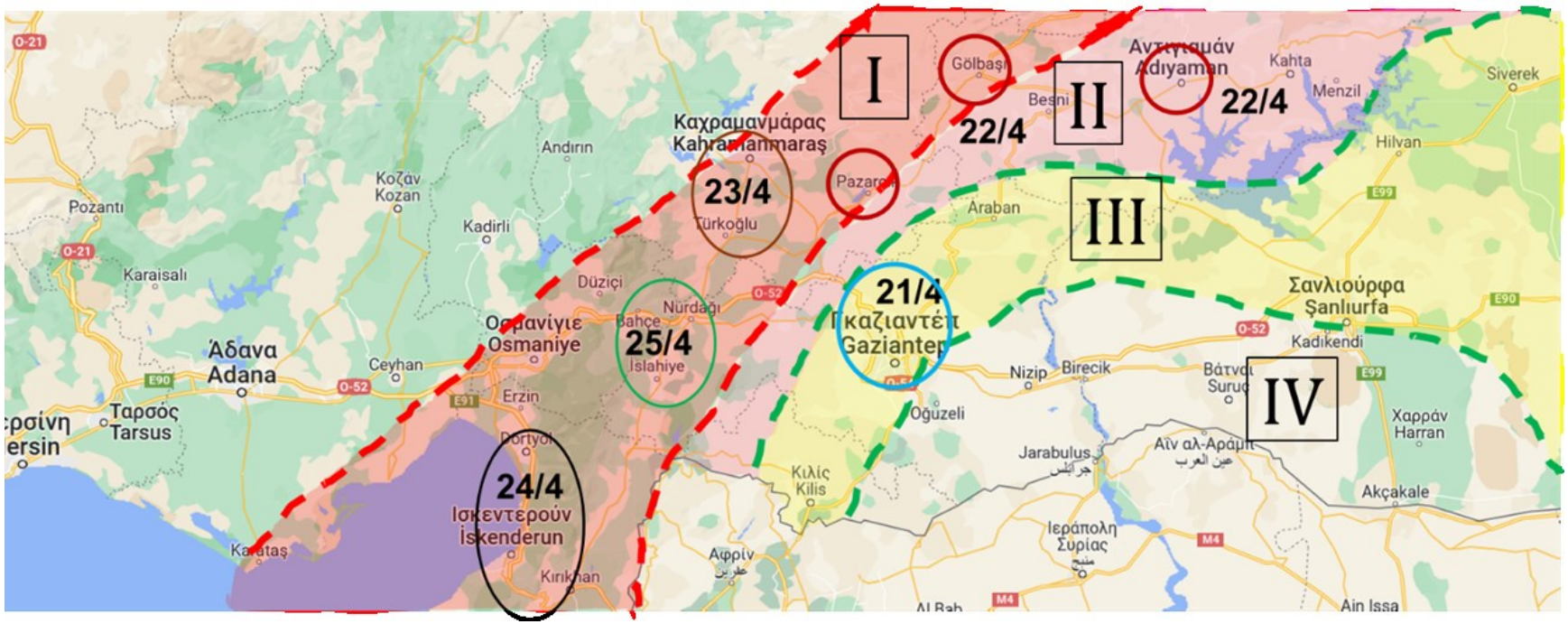

Figure 4.4 Seismic zonation enforced in 1997 in the reconnaissance region following the Kahramanmaraş earthquake sequence. Notice that all affected urban centers were in the highest seismicity Zone I, besides Adiyaman, which was in a lower seismicity Zone II.

References

4.1 Sezen H., Elwood K., Whittaker A., Mosalam K., Wallace J., Stanton J. Structural Engineering Reconnaissance of the August 17, 1999, Kocaeli (Izmit), Turkey, Earthquake. [2000]. PEER 2000/09, Pacific Earthquake Engineering Research Center.

4.2 Celebi M. Earthquake Code for Design and Construction. Earthquake Spectra. [1993]. 9(1_suppl). pp. 43-48.

4.3 Ilki A., Celep A., Earthquakes, Existing Buildings and Seismic Design Codes in Turkey, Arabian Journal for Science and Engineering, Springer, [2012], 37(2), pp. 365-380.

4.4 Soyluk A., Harmankaya Z. Y. The History of Development in Turkish Seismic Design Codes. [2012] International Journal of Civil & Environmental Engineering IJCEE-IJENS, 12(1). pp. 25-29.

4.5 TS 500 (1974) Betonarme Yapilarin Tasarim (Hesap) Ve Yapim Kurallari, Requirements for Design (Calculation) and Construction of Reinforced Concrete Structures. [1974]. TC Resmî Gazete 19054, 21/3/1986, Türk Standardlari Enstitüsü, Ankara, Turkey (in Turkish).

4.6 TS 500 (1985) Betonarme Yapilarin Tasarim (Hesap) Ve Yapim Kurallari, Requirements for Design (Calculation) and Construction of Reinforced Concrete Structures. [1985]. TC Resmî Gazete 19054, 21/3/1986, Türk Standardlari Enstitüsü, Ankara, Turkey (in Turkish).

4.7 TS 500 (2000) Betonarme Yapilarin Tasarim Ve Yapim Kurallari Requirements for Design and Construction of Reinforced Concrete Structures. [2000]. Türk Standardlari Enstitüsü Ankara, Turkey (in Turkish and English).

4.8 SBCDA (1968), Afet Bölgelerinde Yapilacak Yapilar Hakkinda Yönetmelik, Specification for Buildings Constructed in Disaster Areas. TC Resmî Gazete 12801, 16/1/68, [1968]. Ministry of Public Works and Settlement, Turkey (in Turkish).

4.9 SBCDA (1975), Afet Bölgelerinde Yapilacak Yapilar Hakkinda Yönetmelik, Specification for Buildings Constructed in Disaster Areas. TC Resmî Gazete 15260, 9/6/75, [1975]. Ministry of Public Works and Settlement, Turkey (in Turkish).

4.10 SBCDA (1997), Deprem Bölgelerinde Yapilacak Binalar Hakkinda Esaslar, Specification for Buildings Constructed in Disaster Areas (with 1998 amendments), [1997]. Ministry of Public Works and Settlement, Turkey (in Turkish).

4.11 SBCDA (2007), Deprem Bölgelerinde Yapilacak Binalar Hakkinda Esaslar, Specification for Buildings Constructed in Disaster Areas, [2007]. Ministry of Public Works and Settlement, Turkey (in Turkish).

4.12 TDTH 2019, Türkiye Deprem Tehlike Haritaları. [2019]. Ministry of Public Works and Settlement, General Directorate of Disaster Affairs. https://en.afad.gov.tr/turkeys-new-earthquake-hazard-map-is-published

4.13 Yapi Denetimi Hakkinda Kanun, Building Inspection Law 4708, TC Resmî Gazete 24461, 13/7/01 [2001], Ministry of Public Works and Settlement, Turkey (in Turkish).

4.14 TBDY (2018), Türkiye Bina Deprem Yönetmeliği Afet ve Acil Durum Yönetimi Başkanlığı. Turkish Building Earthquake Regulation. TC Resmî Gazete 30364, 18/3/18, [2018]. Ministry of Public Works and Settlement, Turkey (in Turkish).

4.15 MOD84 [1984] Ministry of Public Works, Amendments and Additions to the RD of 26/2/59, G.G., 239 B 6.4.1984 (in Greek), Athens, Greece.

4.16 EAK [2000] Ministry of Environment, Planning and Public Works, Greek Earthquake Resistant Design Code (in Greek), Athens, Greece.

4.17 Bikçe M., Erdem M. [2021]. Investigation of Construction Material Quality and Workmanship Defects of RC Buildings Collapsed and Severely Damaged in the 6.8 Mw Sivrice, Elaziğ, Turkey, Earthquake, January 2020, Bulletin of the New Zealand Society for Earthquake Engineering, 54(3), pp. 184-196.

4.18 Sabahoğlu A., Eryılmaz M.R., Bikçe M., Evaluation of Concrete Compressive Strength of Urban Transformation Buildings in Hatay, [2019], International Conference on Innovation, Sustainability, Technology and Education in Civil Engineering. Iskenderun (in Turkish).

5. Structural Engineering

5.1 Concrete Structures

*Chapter Authors**: Marina MORETTI, Christos ZERIS, Manolis VOUGIOUKAS***

5.1.1 RC Structural systems and materials

Following the second World War, aseismic design in Turkey was quickly established with aseismic design (allowable stress) regulations following the Italian seismic code, which adopted a maximum allowable stress lateral load coefficient of 10% in the highest seismicity zone. According to Table 4.1 depicting the evolution of Turkish seismic design regulations for RC buildings together with the evolution of seismic design methods, structural materials and structural systems, early reinforced concrete (RC) construction in Turkey gradually substituted for bearing masonry construction, comprising medium rise RC framed structures with a relatively dense distribution of masonry infilled bays.

Buildings were mostly regular in plan (as most urban building plots, according to our field observation), with few systematic vertical irregularities, primarily in the form of taller ground storeys for mezzanine space or a taller non infilled softened story at the ground floor for shops. One common form of irregularity in urban block construction, was the adoption of an extended plan above the ground storey, along the facades of the building, that induced systematic damages to the building, as subsequently described. Other types of irregularity, such as recessed top floors or open plan layouts of discontinued beams or columns at the ground floor, equally commonly adopted in Greek RC construction, were not common in Turkey. These RC frame wall masonry infilled structures were mostly gravity load bearing only, with later generations of RC construction gradually substituting RC frames designed for ductility [5.1].

Commonly adopted floor systems included, also depending on the spans, both the use of beams with solid slabs and one way joist slab construction with shallow beams on columns, using brick masonry for casting the joists. Masonry infills were typically either clay brick or lightweight concrete blocks; often, based on our field observation, both types were used in the same building, with concrete units used typically in the lower floors and the basement construction. Concrete materials were initially mixed in situ, with ready mixed concrete production introduced in 1976, although not at the same time in the entire country, with a minimum concrete grade specified in the prevailing design codes.

Following changes in urban design regulations, the conventional residential building height increased in the late 1990s onwards from 5-6 to 8-10 floors or higher, with the use of shear walls

and more ductile frame designs, especially after 1997 when their requirement became compulsory in high seismicity zones. Also, after 2010, with the increasing demand for residential space due to urbanization, large housing development complexes have started being constructed in building blocks often exceeding 15 floors, with the adoption of large lightly reinforced shear wall structural systems, which are often constructed using tunnel forms, with the Turkish government being a particular stakeholder in this endeavor in order to cover the increasing housing demand pressure in urban centers (see Toki [5.2]).

5.1.2 Observed Structural Damages

At the time of the reconnaissance mission, practically all the collapsed buildings as well as most of the debris of the severely damaged buildings in the event of the 6th February earthquake were removed. The inspection of the buildings was usually performed from the outside, and neither plots nor details on the structure, including the period of construction, were readily available. Hence, the observations that follow are subject to those limitations. For clarity and perspective of the structural characteristics background of the buildings under investigation herein, the seismicity zonation enforced in Turkey since the 1990s is superimposed with the urban centers in the area visited, also mostly affected by the earthquake sequence, in Fig. 4.4. It can be observed that all affected urban centers were in the highest seismicity Zone I, besides Adiyaman, which was in a lower seismicity Zone II.

5.1.2.1 Typical RC structural systems observed and characteristic damages

The majority of the reinforced concrete (RC) buildings in the areas visited, with significant damages, were residential, with an average height of 6 to 8 stories above ground level. The ground story of the buildings often had commercial usage, with increased height and less infill walls in respect to the stories above.

In addition, a practice often adopted consists in that the building above the ground floor extrudes in cantilever as may be seen in Figure 5.1.4. This form of plan irregularity, uncommon to Greek modern practice but popular in Turkish urban RC construction, was an extension of the Ottoman şahniş, namely a cantilever overhang over the entire height above the ground story, on the façade or two corner facades, depending on layout. In the absence of shear walls, this infilled overhang resulted in inadequate infill confinement at the facades due to the lack of beams and columns at the cantilever, which, compared with the opposite fully infilled sides of the plan led to plan irregularity, particularly in the building block corners, especially after the failure of the unconfined façade infilled bays.

Frame and frame/wall systems were the prevalent structural type, with wall frame structures being more common in recent construction (see tunnel forms above). Only occasional RC shear walls were observed, especially in buildings constructed later than 2010. Furthermore, in many framed buildings, the use of filler-joist (asmolen) floor system was adopted, often without the

presence of beams, as shown in Figure 5.1.2. The filler material was in all cases cement or clay block

(Photo:) M.Moretti

D.Pitilakis

C. Zeris

C. Zeris

Figure 5.1.1 Typical reinforced concrete buildings in the areas visited, indicating the façade damage in the continuous şahniş, with inadequate infill wall confinement (Adiyaman).

E.Garini C.Giarlelis

Figure 5.1.2 Building with filler-joist (asmolen) floor system (Adiyaman) with filler blocks.

Buildings with inadequate lateral stiffness appear to have been more damaged as compared to similar stiffer buildings. Figure 5.1.3 depicts a commercial / hotel building in Belen-Hatay, near the fault line, in which the ground soft story collapsed.

Figure 5.1.3 Collapse of soft ground story (Belen-Hatay). Photo: M.Moretti.

Figure 5.1.4 depicts a building with flat slabs, with the majority of columns having the same orientation of their cross-section, which collapsed along the weak direction of the columns. The absence of beams contributed in further decrease of the overall lateral stiffness.

Figure 5.1.4 Collapse of RC building with flat slabs along the weak direction of the vertical structural elements (Adiyaman). Photo: E. Vougioukas.

As a rule, less damage was observed in buildings with stiffer vertical structural elements. Buildings using a frame system with irregularity, especially in-height, proved to be more vulnerable, as shown in Figure 5.1.5. The building displayed in Figure 5.1.6 in Nurdagi, with large cross-section columns and several shear walls, despite the moderate irregularity in-height,

suffered damage only in the infills of the lower stories. Incomplete wedge of the outer walls has resulted to the loss of their out-of-plane stability, leading to the reduction of the whole structures' earthquake resistant capacity.

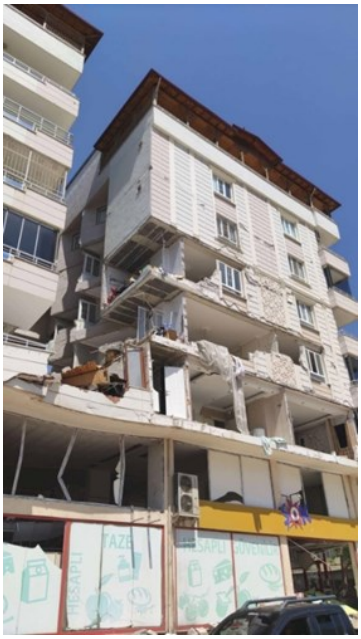

C.Giarlelis (Nurdagi)

A.Papachristidis (Nurdagi)

E.Garini (Kahramanmaraş)

Figure 5.1.5 Irregularities in-height in frame systems proved to increase structural vulnerability.

E.Garini (Nurdagi)

Figure 5.1.6 Buildings with increased structural stiffness showed good to excellent overall seismic performance.

Buildings with more RC shear walls had a better seismic performance and resulted in reduced damage even in respect to the infill walls, as may be observed in Figures 5.1.7 and 5.1.8. It is noted that the building in Islahiye displayed in Figure 5.1.9, which was constructed later than 08/2020 (according to Google Earth), did not show any apparent damage, while many buildings in the close vicinity collapsed or were seriously damaged.

Similarly, the Kahramanmaraş Town Hall, a highly irregular in plan and in elevation RC structure, with large column sections, extensive shear wall elements and of well executed construction quality, suffered only minor damage (hairline flexural cracks at the base and minor joint movement) despite its proximity to the causative fault.

C.Zeris (Golbasi)

P.Thanopoulos (Islahiye)

C.Zeris (the Kahramanmaraş Town Hall)

Figure 5.1.7 Buildings with RC shear walls with no apparent structural damage.

Figure 5.1.8 Building with RC shear walls in Islahiye with no apparent structural damage (constructed later than 08/2020 (source Google Earth) close to seriously damaged buildings. Photo: A.Papachristidis.

Element local damages

5.1.2.2 Columns and beam-column joints

In RC structural elements, damage was observed mainly in the vertical elements, both columns and shear walls, and also in frame joints caused by inappropriate detailing of the shear reinforcement. Sparsely spaced and/or not well closed stirrups resulted in concrete crushing and buckling of the longitudinal reinforcement. Figures 5.1.8 and 5.1.10 display such failures of joints, and columns, respectively.

E.Vintzileou M.Moretti M.Moretti

Figure 5.1.9 Damage in joints of RC frames because of sparsely spaced stirrups and opening of ties, followed by buckling of the longitudinal reinforcement.

E.Garini (Kaharamanmaras)

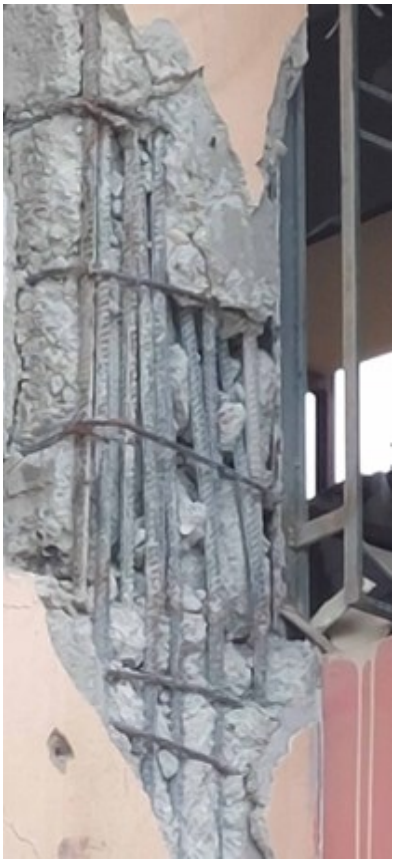

E.Garini (Kaharamanmaras)

M.Moretti (Adiyaman)

Figure 5.1.10 Damage in RC columns because of sparsely spaced stirrups and opening of ties, followed by buckling of the longitudinal reinforcement.

Damage was also observed in columns which behaved as short or captive because of the presence of local restrictions in displacement along only a certain part of the column's height. Figure 5.1.11 displays damage in the free part of columns which had in one or in both sides masonry walls that did not extend to the whole height of the column.

C.Giarlelis (Islahiye)

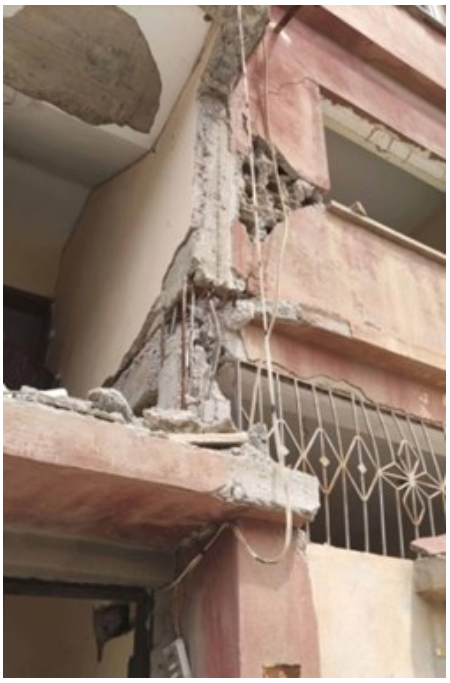

A.Papachristidis (Islahiye)

Figure 5.1.11 Local shear damage in RC columns, because the partial infills did not extend to the whole height of the column, resulting in captive column effect.

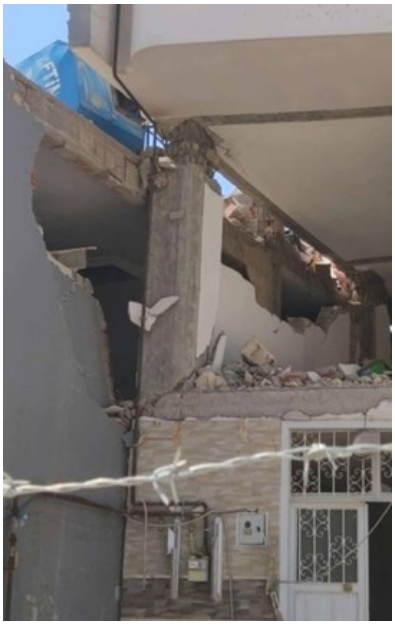

A.Papachristidis (Nurdagi)

C.Zeris (Golbasi)

M.Moretti (Adiyaman)

Figure 5.1.12 Local shear damage in RC columns, because of displacement restrictions in-height, resulting in captive column effect.

C.Zeris (Kahramanmaraş)

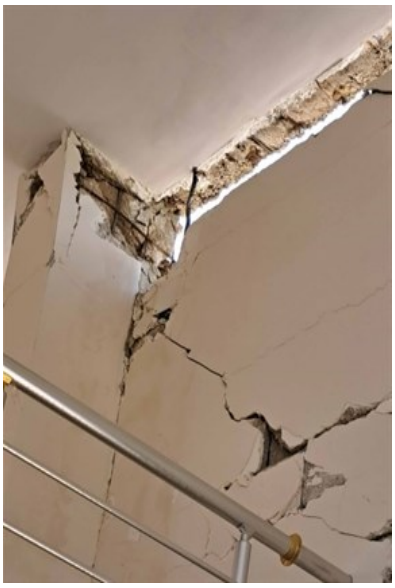

M.Moretti (Nurdagi)

C.Zeris (Pazarçik)

Figure 5.1.13 Local shear damage in RC columns at the critical region below the joint, subsequent to local crushing of adjacent infill walls which resulted in captive column effect.

In the columns shown in Figure 5.1.12 damage occurred because of local restrictions along their height because of, e.g. pounding of an adjacent slab, or the ground level at the external part of the building. Furthermore, local crushing of infill walls in contact to a part of a column may result in subsequent local damage of the column, owing to increased shear force and stress concentration, as shown in Figure 5.1.13. However, when the overall lateral stiffness was sufficient, the existence of short columns per se did not lead to damage of the columns, as may be seen in the building in Kahramanmaraş depicted in Figure 5.1.14.

Figure 5.1.14 Building with short columns in a row which, apparently, did not suffer any damage. Photo: E.Garini.

C.Zeris (Golbasi)

C.Zeris (Nurdagi)

V.Palieraki (Nurdagi)

E.Garini (Golbasi)

C. Zeris (Nurdagi)

C. Zeris (Adiyaman)

Figure 5.1.15 Diagonal and sliding shear failures of RC shear walls.

5.1.2.3 Shear walls

Figure 5.1.15 displays RC walls that have suffered shear damage. In newer structures, the extent of damage in shear walls was, in general, less, as may be seen in Figure 5.1.16.

C. Zeris (Adiyaman)

C. Zeris (Adiyaman)

M.Moretti (Kaharamanmaras)

M.Moretti (Golbasi)

Figure 5.1.16 Damage in RC shear walls in recently constructed structures.

5.1.2.4 Beams

C.Giarlelis (Kahramanmaraş)

C.Giarlelis (Kahramanmaraş)

C.Zeris (Kahramanmaraş)

C.Zeris (Kahramanmaraş)

C.Zeris (Adiyaman)

Figure 5.1.17 Damage of short RC beams (intended or unintentional, due to infill opening

Damage in RC beams was seldom observed, and it was generally attributed to specific structural particularities. Some examples are provided: Figure 5.1.17 depicts the failure of short (coupling) beams either intentional (by geometric dimensions) or unintentional, due to the presence of an infill opening: The low shear span to depth ratio of the beams resulted in increased shear force, and subsequent diagonal shear failure.

i) P.Tsopelas (Golbasi)

ii) Z.Cekinmez (Islahiye)

iii) P.Tsopelas (Islahiye)

iv) Z.Cekinmez (Islahiye)

v) C. Zeris (Kahramanmaraş)

vi) C. Zeris (Adiyaman)

Figure 5.1.18 Damage in beams because of : i) flexural frame action at the beam ends, ii) mid span hinging due to large deflections of slabs, iii) and iv) support failure, v) insufficient end reinforcement anchorage, vi) tensile cracking due to diaphragm load transfer.

Figure 5.1.18 displays beams depicting different modes of local failure due to their function as vertical – seismic load transfer elements: vertical flexural cracks in the bottom, because of large deflections of the slabs caused by a variety of reasons, i.e.: i) settlement of the foundation (in Golbasi); ii) excessive load on the slab owing, among others, to the collapse of the infill wall; iii) and iv) failure and crushing of the top of column that supports the beam, v) collapse from the support due to insufficient end reinforcement anchorage or shear; vi) tensile flexural cracking from transferring diaphragm loads to the vertical elements.

Figure 5.1.19 Inclined cracking in beams caused by non-vertical seismic joint that crosses the beam (Nurdagi). Photo credit: P.Tsopelas

Inclined cracking in the beams depicted in Figure 5.1.19 is caused because the beams were crossed by a non-vertical seismic joint which divides the two parts of the building.

Photo: E.Garini

V. Palieraki

V. Palieraki

Figure 5.1.20 Shear damage in top of columns in the ground story of an RC building with filler-joist (asmolen) floor system (Nurdagi).

Figure 5.1.21 Damage at top of columns in filler-joist floor system in Islahiye. Photo: C.Giarlelis.

Figure 5.1.22 Building with filler-joist (asmolen) floor system without any apparent damage (Golbasi). Photo: C.Zeris

In buildings with filler-joist (asmolen) slabs, which usually do not have any beams, often shear failure at the top of columns was observed, as shown in Figures 5.1.20 and 5.1.21. However, in the building shown in Figure 5.1.22, in which adequate lateral stiffness was provided, no structural damage occurred.

5.1.2.5 Stairways

Figure 5.1.23 Damage to stairways and associated local damage to the vertical framing elements and asmolen slab-stairwell connection . Photo credit: C. Zeris (Adiyaman)

5.1.2.6 Seismic separation joints

In general, seismic joints between neighboring buildings were either insufficient or nonexistent. Two different consequences of adverse interaction between adjacent buildings are discussed: In Figure 5.1.24 the two buildings were in contact with only a small, if any, seismic gap between them, which proved insufficient. Because of the restriction in lateral displacement induced by the low rise building, the 8-story building suffered considerable damage at mid-height between the second and fifth stories, including shear damage in captive columns.

Photo: E.Vintzileou

C. Giarlelis

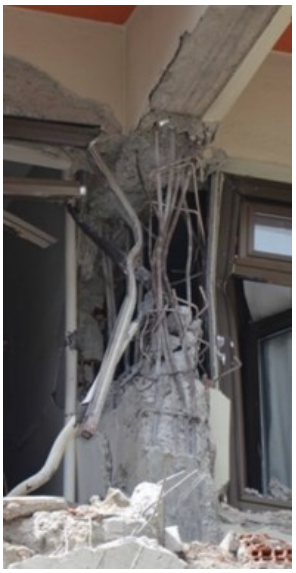

C. Zeris

Figure 5.1.24 Damage at mid-height of an 8-story building in Kahramanmaraş due to pounding of the adjacent structure.

In the case of adjoining buildings which were separated at a certain distance apart, it was observed in certain instances that when a building collapsed, a part of it fell on or collided with the other building, thereby inducing to the latter significant damage. Examples of this type of damage between two buildings may be seen in Figure 5.1.25.

M.Moretti (Kahramanmaraş)

C. Zeris (Kahramanmaraş)

Figure 5.1.25 Damage in buildings caused by the impact at collapse of the adjacent building.

5.1.2.7 Masonry infill construction

E. Vougioukas (Kahramanmaraş)

Figure 5.1.26 Damage of outer walls, due to lack of wedge at the top

One issue that is worth mentioning is that infill walls are built following a practice that results to the reduction of their contribution to the overall seismic capacity of the buildings: common wall construction practice in Turkey is the use of cement blocks, not wedged at the top, as shown in Figure 5.1.26. Also, in case of external walls, built at the end of the cantilever (the continuous sahniş, above), this wall to frame gap might increase several times due to the vertical dynamic response of the cantilever during the earthquake, as shown schematically in Fig.5.1.27. This incomplete wedging of the infill wall (of the order of 1 mm) would significantly reduce its stability to out-of-plane acceleration. Furthermore, for larger gaps, the wall would face an out-of-plane collapse even for medium earthquakes leading to stiffness degradation of the whole structure.

Such premature failure of the external infill walls led to a drastic deterioration of the seismic capacity of the buildings, and, therefore, is an important factor contributing to the increased damage observed.

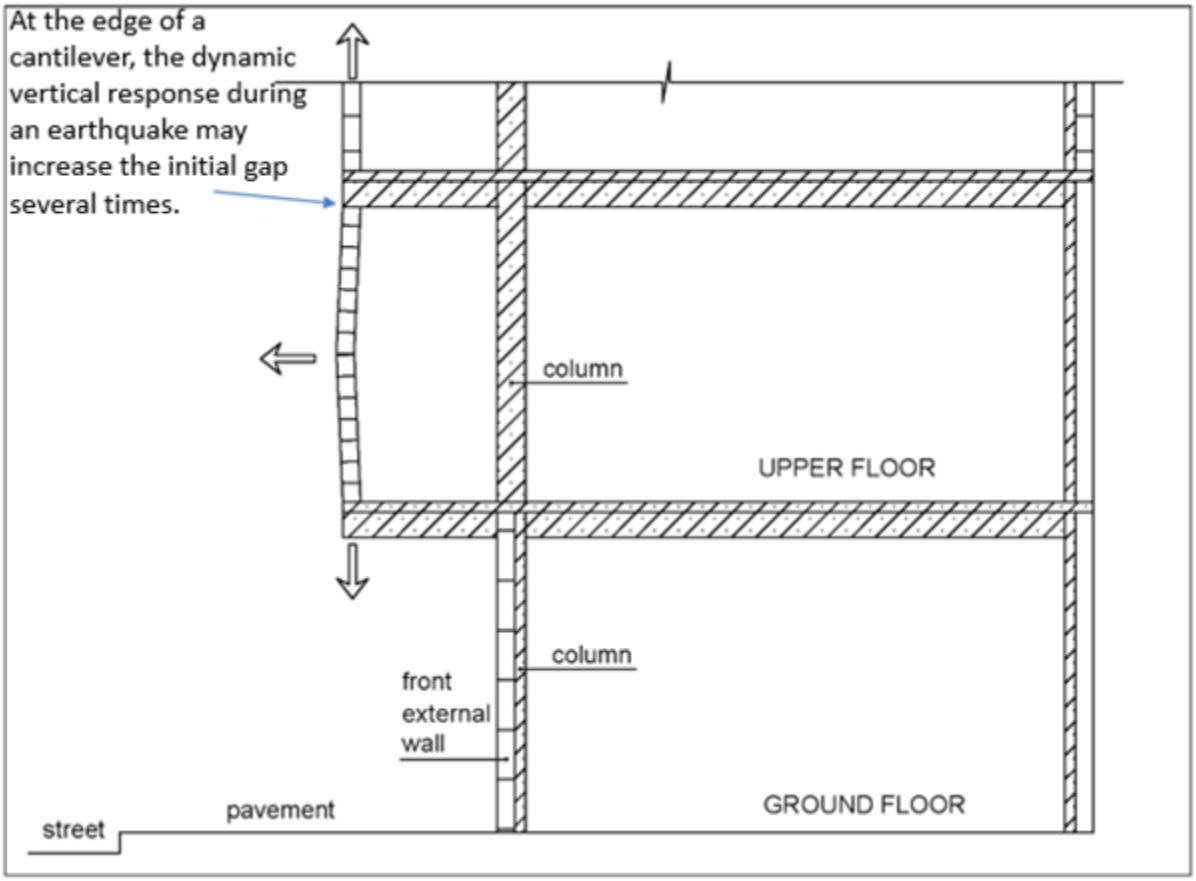

Figure 5.1.27 Outer wall on a cantilever, subjected to combination of horizontal and vertical acceleration

5.1.2.8 Poor workmanship and material quality

As several past earthquake reconnaissance reports that were followed by inspection together with taking material samples (cores and steel coupons) from damaged buildings in the same region (Hatay, Erzincan) have pointed out ([5.3], [5.4]), the material quality was often (especially in older structures) substandard: concrete compressive strength was below the minimum code specified at the time of construction (namely, B225 or C16, and up to C25), and nonductile grades for the reinforcement. This fact, together with the design choice of adopting gravity resisting frame systems without ductility – at higher design load, led to considerable local damage in vertical elements (Fig. 5.1.28).

C. Zeris (Golbash)

C. Zeris (Kahramanmaraş)

Figure 5.1.28 Damages in RC elements related to bad workmanship and supervision: i) Wall edge member lack of compaction and ii) improper diagonal cold joint that led to diagonal shear failure.

5.2 Steel Structures

Chapter Authors: ***Pavlos THANOPOULOS*** *and* ***George TSIATAS***

The structural systems of most residential and non-residential buildings in Turkey are masonry and reinforced concrete. Structural steel systems comprise a negligible ratio of the building stock with a ratio of less than 2% (Gunes 2015, Ay et al. 2016). As a result, there were not any collapses or severe damage to buildings with typical structural steel construction. Nevertheless, several steel structures were inspected during the reconnaissance mission, which performed as expected by design.

Figure 5.2.1 Roof structure of the municipal market in Nurdağı, with structural details showing no significant damage from the earthquake.

Figure 5.2.1 shows the roof structure of the municipal market in the city of Nurdağı. Even though the structure lacks bracing members in the longitudinal direction it behaved exceptionally well, with no visible damage from the earthquake. Small problems observed were probably dated before the event and of reduced structural importance. Due to its structural integrity, the structure was selected to facilitate civil services provided with tents. Similarly, a roof structure used for parking in the city of İslahiye was in excellent condition, continuing to shelter cars and tents after the event.

Figure 5.2.2 Roof structure of outdoor parking in İslahiye, with structural details showing no significant damage from the earthquake other than the ones caused by an adjacent building.

Although not many steel buildings were observed, it was quite common for reinforced concrete or masonry buildings to have steel appendages. Such structures are not critical for the stability of the main building, nevertheless, their failure can cause life safety or serviceability issues. In this case, several failures were observed which are attributed to the failure of the main building or poor detailing of the connections between the two parts (Figures 5.2.3 to 5.2.7)

Figure 5.2.3 Top floor roof on a 10-story building in Adıyaman. Despite the damage to the main building and the increased top-floor acceleration, no significant damage can be observed.

Figure 5.2.4 Top floor roof on a 6-story building in Pazarcık. Total collapse due to poor anchorage.

Figure 5.2.5 Fire escape staircase failure in Gölbaşı due to soil liquefaction and extreme settlement of the main building.

Figure 5.2.6 Failure of a slender roof structure adjacent to a heavily damaged concrete building (Nurdağı).

Figure 5.2.7 Top floor steel roof of a heavily damaged concrete building mainly due to pounding of the adjacent collapsed building (Antakya).

A special type of building was observed along Kurtuluş Avenue in Antakya. Although there were various typologies, probably depending on the era of construction of each building, their common characteristic was the projection of the first floor over the ground floor towards the avenue. The buildings consist of masonry or brick outer walls with or without timber elements. Most of the slabs were reinforced concrete, supported by steel I-beams which also supported the cantilever. The damage to the buildings varied from negligible to total collapse (Figure 5.2.8). At the time of the reconnaissance mission, it was not easy to identify clear causes for this versatile behaviour, other than the possible difference in the quality of construction and the unfavourable response of the corner buildings.

As far as concrete buildings strengthened with steel elements are concerned, only a single building was recorded, in the city of Antakya. The building had heavy structural steel frames integrated with the concrete frame and lighter steel members which facilitated the placement of the façade. Severe damage was observed in the second story where the system was placed with the non-structural elements destroyed. Even though the building did not collapse, repairing seems difficult due to the significant permanent lateral deformation.

A different case was recorded in Kahramanmaraş where a building, which probably suffered damages due to pounding from an adjacent building that collapsed, was repaired with the use of steel elements. Part of the building was demolished, and composite slabs and steel frames were placed to return the building to its initial status.

Figure 5.2.8 Various 2-story buildings along Kurtuluş Avenue in Antakya.

Figure 5.2.9 Concrete building was retrofitted with steel elements before the event (Antakya).

Figure 5.2.10 Restoration of concrete buildings with steel frames (Kahramanmaraş).

Although bridges were not the main focus of the Greek reconnaissance mission, no significant problems were detected other than small permanent deformations of the bearings and activation of the seismic stoppers. This was more the case for steel bridges which were in service without visible problems (Figures 5.2.11 to 5.2.15).

Figure 5.2.11 Pedestrian bridge with non-structural damage (Antakya).

Figure 5.2.12 Road bridge with steel tower (Antakya).

Figure 5.2.13 Steel truss pedestrian bridge with non-structural damage (Antakya).

Figure 5.2.14 Pedestrian steel arch bridges in normal service, Iskenderun (left) and Adıyaman (right).

Figure 5.2.15 Railway steel bridge in normal service (Adana).

5.3 Prefab/Precast concrete construction - Industrial Buildings/facilities

*Chapter Authors**: Pavlos THANOPOULOS** and **George TSIATAS***

As in all types of buildings, industrial buildings in Turkey primarily consist of prefabricated/prestressed reinforced concrete members (Figure 5.3.1). The stability of this type of structure mainly depends on the stiffness of the foundation and the connection between the column and the beam. As it was observed, the latter connection was realized through two rebars extruding from the bracket, which were inserted in two holes at the edge of the beam. These holes were left void, as no mortar was observed, which allowed significant movements of the beams and led to the total collapse of entire bays (Figure 5.3.2). This can be also attributed to the significant vertical component of the earthquake which significantly decreased or even eliminated the friction force at the beam-bracket interface. Several additional types of failure were recorded in other buildings of the same area both on structural and non-structural elements (Figure 5.3.3).

Figure 5.3.1 Typical reinforced concrete industrial building (Kahramanmaraş).

Figure 5.3.2 Total collapse of the middle bay of a reinforced concrete industrial building and details of the prestressed beam end (Kahramanmaraş).

Figure 5.3.3 Various types of failures of reinforced concrete industrial buildings and their structural steel appendages (Kahramanmaraş).

Several steel industrial buildings were observed with no significant structural damage, especially if they were not built with an unconventional structural system. Nevertheless, many of them had significant damage to their panels (Figure 5.3.4). The same observation applies to the steel silos and tanks that were observed along the way. Although some collapses were recorded, most of the structures seemed intact (Figure 5.3.5).

Figure 5.3.4 Structural steel industrial buildings in Adıyaman (top left) and Kahramanmaraş.

Figure 5.3.5 Storage facilities in Kahramanmaraş.

5.4 Infill Walls

Chapter Author: ***Vasiliki PALIERAKI***

In the cities visited during the Reconnaissance Mission and affected by the earthquakes, reinforced concrete buildings with masonry infill walls are identified.

In the current paragraph, the typology of the infill walls, their construction type and materials, as well as their damage and typical failures are described.

5.4.1 Typology- Construction Materials of Infill Walls

The infill walls are, in most cases, non-load bearing masonry enclosures in RC frames. In the buildings with severe damages, different construction types and materials of the infill walls have been recognized.

The infill walls are constructed with clay bricks, of different sizes and percentages of voids (Figure 5.4.1), or with concrete units (Figure 5.4.2). In some cases, the infill walls of the ground floor are constructed with concrete units, while the upper floors are constructed with clay units (Figure 5.4.3).

As already mentioned, the clay bricks have different sizes. In many cases, the construction type adopted for enclosures in the '70s can be seen, namely cavity brick masonry walls (Palieraki et al., 2018). The typical thickness of each leaf (made, typically, of horizontally perforated clay bricks) is smaller than 100 mm. The space between the two (unconnected) leaves is used to accommodate insulation or sliding doors and windows (Figure 5.4.4).

It is noted that the infill walls are not in all cases constructed with attention to details: The connection of the infill to the surrounding frame, and mainly in the upper part of the infill leads to the formation of gaps, while the construction of RC tie beams in the mid-height of the walls are not common (Figure 5.4.5). On the other hand, also local carving of the masonry has been located, serving the need of installing the plumbing and electrical features (Figure 5.4.6).

Additionally, it is common to see that the plan of the upper floors is larger than the plan of the ground floor. Overhangs, constructed upon cantilever slabs, are made of non-load bearing masonry (Figure 5.4.7). This masonry is very vulnerable when subjected to earthquake loading.

Figure 5.4.1 Infill walls made of clay bricks, of different sizes.

Figure 5.4.2 Infill walls made of concrete units.

Figure 5.4.3 Infill walls made of concrete units in the ground floor, and clay brick units in the upper floors.

Figure 5.4.4 Infill walls made of two independent masonry leafs.

Figure 5.4.5 Walls constructed with the use of RC tie beams.

Figure 5.4.6 Carving of the infill walls for installation of electrical and plumbing fixtures.

Figure 5.4.7 Overhangs, constructed upon cantilever slabs.

5.4.2 Pathology of Infill Walls

The most common types of damage observed was:

(a) separation of the infill wall from the concrete frame and in some cases overturning (Figure 5.4.8),
(b) in-plane diagonal or in most cases bi-diagonal cracking (Figure 5.4.9),
(c) out-of-plane movement and cracking or overturning due to out-of-plane bending (Figure 5.4.10).

In some cases, the cracking of the infill walls was indicative of the main direction of the earthquake (Figure 5.4.11).

Figure 5.4.9 and Figure 5.4.10 show wall cracking, and severe damage at the corners of heavy overhangs.

The structural benefits and weaknesses of the infill walls were similar to those observed in previous earthquakes in Turkiye, such as Kocaeli 1999, Bingöl 2002, Van 2011, Izmir-Samos 2020 (Cetin et al., 2021). In some buildings, the infill walls appeared to stiffen the building and reduce the lateral deformation demands.

In other buildings, the damage of the infill walls was very extensive. Even though the damage of the bearing elements was not so extensive, the buildings will be demolished, given that the cost for the reconstruction is increased.

Figure 5.4.8 Separation of the infill wall from the frame and (partial) overturning.

Figure 5.4.9 Extensive bi-diagonal cracking.

Figure 5.4.10 Overturning of infill walls, because of out-of-plane loading.

Figure 5.4.11 Infill walls with diagonal cracking, along the direction of the earthquake and failing to out-of-plane loading, perpendicular to the main direction of the earthquake.

5.5 Performance of Seismic Isolated Buildings

Chapter Authors: ***Christos GIARLELIS*** *and* ***Panos TSOPELAS***

In Turkey since 2012, all new medical facilities with a minimum size of 100 beds are required to be seismic isolated. During the past decade a relatively large number of hospitals in the affected area (Fig. 5.5.1, Table 5.5.1), were built following this regulation. These buildings (with one exception attributed to construction mistakes) demonstrated an excellent seismic behavior, with no damage on structural or non-structural elements. Furthermore, they remained fully operational during and after the earthquake sequence at the time they were needed the most, treating the injured.

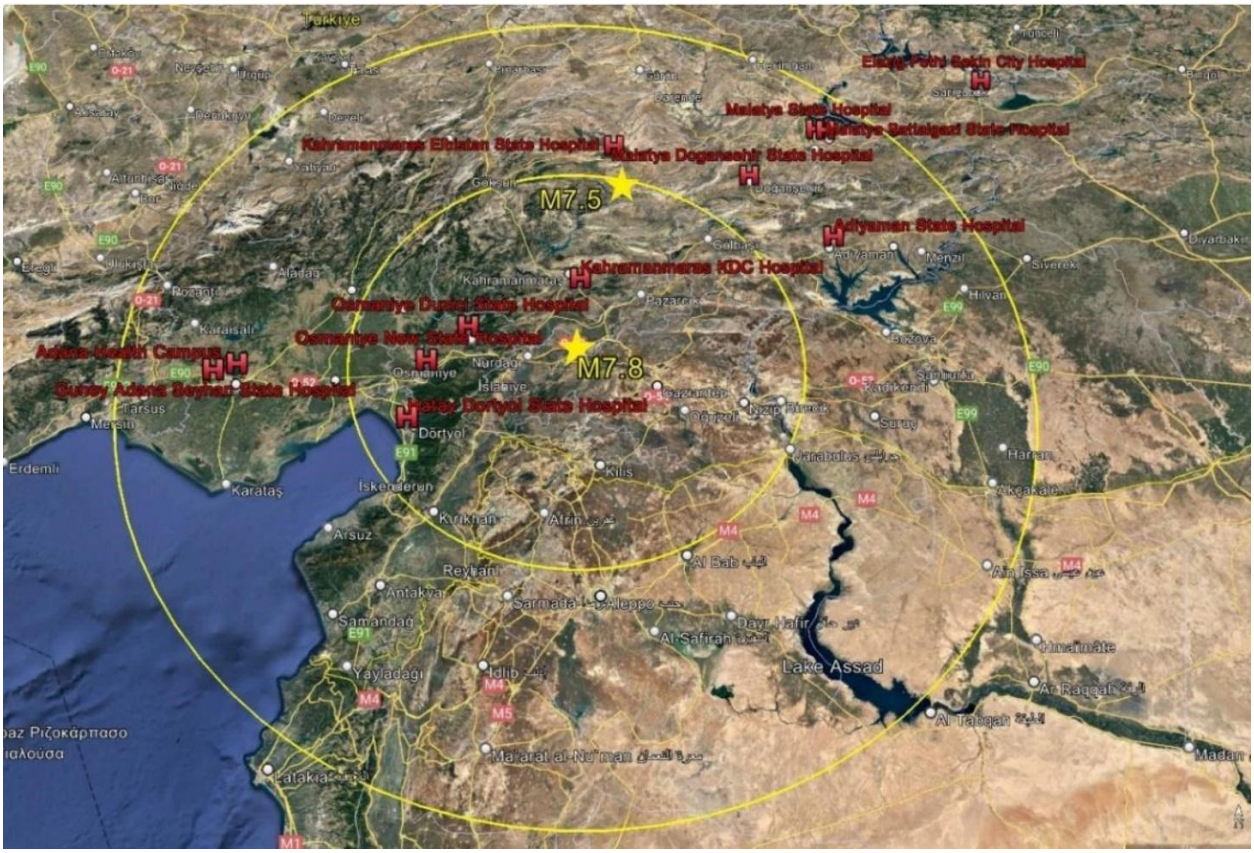

Figure 5.5.1 Location of the seismic isolated facilities (credits: Seismic Isolation Engineering Inc.)

Table 5.5.1 List of seismic isolated hospitals in the earthquake-affected area (credits: Seismic Isolation Engineering Inc)

Facility	Type of Isolators	Number of isolators
Kahramanmaras KDC Hospital	DP or CSS	361
Osmaniye Duzici State Hospital	DP or CSS	200
Osmaniye New State Hospital	DP or CSS	541
Hatay Dortyol State Hospital	DP or CSS	340
Kahramanmaras Elbistan State Hospital	DP or CSS	455
Malatya Dogansehir State Hospital	DP or CSS	122
Adiyaman State Hospital	DP or CSS	264
Adana Health Campus	TFP	1,552
Guney Adana Seyhan State Hospital	DP or CSS	251
Malatya State Hospital	DP or CSS	264
Malatya Battalgazi State Hospital	DP or CSS	222
Elazig Fethi Sekin City Hospital	TFP	878

DP: Double Pendulum / CSS: Curved Surface Sliders
TFP: Triple Friction Pendulum

The new wings of the Kahramanmaraş KDC (Maternity) Hospital (Fig 5.5.2a) were under construction, next to the existing ones (Fig 5.5.2b), at the time of the earthquake sequence. For one of the wings (right part in Fig 5.5.2a) the construction of the structural system was almost finished while for the other (left part in Fig 5.5.2a) only the substructure had been completed. The total number of bearing is 361 (TIS). The isolators were locked (Fig 5.5.3), following the construction practice, in order to avoid any involuntary displacement during the building process. At the almost-completed building, the isolator locks broke during the first earthquake and the structure responded very well (however, it should be mentioned that it was not fully loaded). On the other hand, the existing, non-isolated wing of the hospital (Fig 5.5.2b), which was built in 2010, experienced damage to the infill walls, the suspended ceilings and the EM equipment that rendered the facility non-functional.

Figure 5.5.2 Kahramanmaraş KDC Hospital (a) the under construction new wings (b) the existing wings

Figure 5.5.3 Kahramanmaraş KDC Hospital (a), (b) bearings layout at the new wings

Figure 5.5.4 Kahramanmaraş KDC Hospital (a), (b) broken isolator locks, showing that the isolation system was activated during the earthquake sequence.

Hatay Dörtyol State Hospital (Fig 5.5.5) is another seismic isolated facility that has been constructed in 2019. It has a total number of 340 double pendulum bearings (Fig 5.5.6) (TIS). The facility has demonstrated an excellent performance during the earthquake sequence, remaining operational. The only signs of the earthquakes were a limited number of tiles that came off or had crushed edges at the seismic joint and a residual displacement (Fig 5.5.7). The latter has been estimated at 30-40mm (Fig 5.5.8).

Figure 5.5.5 Dörtyol State Hospital

Figure 5.5.6 Dörtyol State Hospital l (a), (b) isolators layout at the basement level

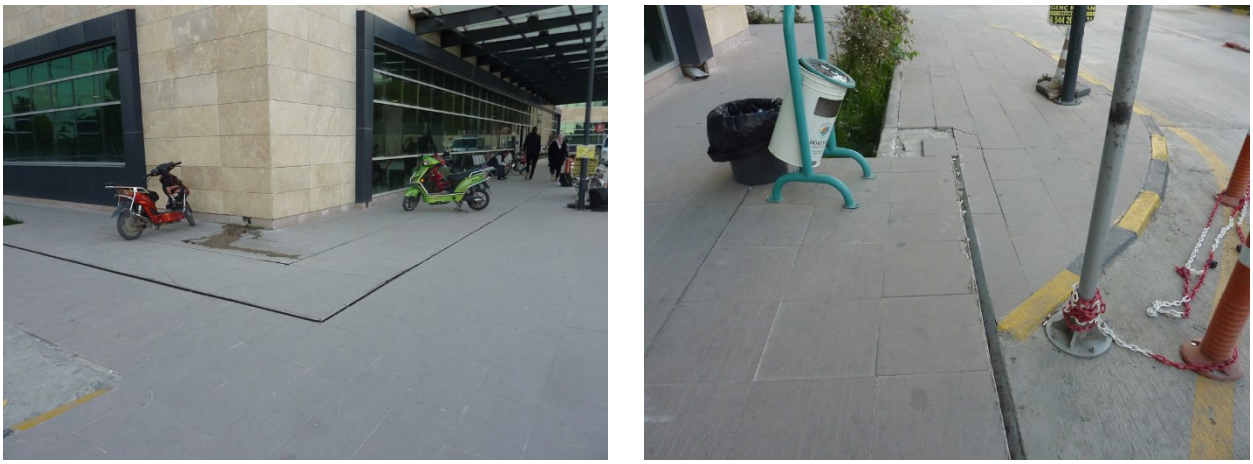

Figure 5.5.7 Dörtyol State Hospital (a) seismic joint, (b) slightly damaged tiles at the seismic joint

Figure 5.5.8 Dörtyol State Hospital (a), (b) permanent displacement and damaged tiles at the seismic joint

There is one reported case (Qu et al.) of a seismic isolated medical facility that did not perform well: a 6-story hospital building of the Doğanşehir State Hospital. The building experienced non-structural damage to the suspended ceilings and the masonry infill walls of the superstructure as well as structural and non-structural damage at the isolation level. Early investigations show that seismic joints at the isolation level had been compromised (blocked) as result of poor construction therefore the structure could not move freely as it was supposed to.

Unlike seismic isolated hospitals, most of the conventionally designed medical facilities, faced structural or non-structural damage that made them non-operational. A large number collapsed or had been demolished due to the extensive damage. Characteristic are the cases of the collapse of the Iskenderun State Hospital (Fig 5.5.9a) and the partial collapse of a private hospital in Antakya (Fig 5.5.9b).

Figure 5.5.9 (a) Collapse of the Iskenderun State Hospital (credits: REUTERS/Tessier) (b) partial collapse of a private hospital in Antakya (Credits: Sumer et al.)

However, if heavy structural damage could have been prevented by better design and construction this is not the case for non-structural damage. Medical facilities that performed well from a structural point of view were rendered non-functional due to damage to infill walls, suspended ceilings and EM equipment. Characteristic examples of non-structural damage that prevented the function of a medical facility are the Pazarcık State Hospital (Figs 5.5.10-5.5.11) and the Nurdağı State Hospital (Fig 5.5.12).

Figure 5.5.10 The conventional (non-seismic isolated) Pazarcık State Hospital (photo credits: google maps)

Figure 5.5.11 Pazarcık State Hospital (a), (b) heavy damage to the infill walls, suspended ceiling and EM equipment (photo credits: Sumer et al.)

Figure 5.5.12 Nonstructural damage to the fixed-base building F2 of the Nurdağı State Hospital (a) Façade (b) damaged suspended ceiling (Credits: Qu et al.)

5.6 Historical Constructions and Monuments

*Chapter Authors**: Elizabeth VITZILEOU** and **Vasiliki PALIERAKI***

The area that was affected by the earthquakes is rich in urban nuclei, as well as in individual cultural heritage structures (castles, mosques, churches, bridges, etc.).

This Report focuses on the damage observed in Antakya and in Gaziantep, two cities representative of high and moderate intensity respectively. Before presenting typical construction systems, and their behaviour, it is appropriate to mention a significant parameter, related to the seismic behaviour of the buildings and affecting the protection of the population. The urban nuclei are characterized by narrow picturesque streets (Figure 5.6.1 and Figure 5.6.2), which in numerous cases were blocked with rubble (Figure 5.6.1 and Figure 5.6.2), thus making hard - if not impossible - the escape of inhabitants of damaged or collapsed buildings. This aspect of protecting the built cultural heritage, with the aim of protecting the population immediately after a strong earthquake is not always given the necessary attention.

(a)

(b)

(c)

Figure 5.6.1 The narrow streets of the old part of Antakya, before (google maps, street view, November 2022) and after the February 2023 earthquakes**.**

Figure 5.6.2 A street in the old part of Gaziantep, before (source: Google maps, street view, October 2022) and after the February 2023 earthquakes.

5.6.1 Structural Systems of buildings in historical centres

The masonry buildings in the historical centres of Gaziantep and Antakya are typically 2-storey or maximum 3-storey buildings. In Gaziantep, most of the buildings are unplastered (Figure 5.6.3), in contrast to Antakya, where plastering is a rule (Figure 5.6.4). As presented in detail in the following paragraph, this is a characteristic that affects the construction typology of masonry.

Figure 5.6.3 Historical buildings, Gaziantep

Figure 5.6.4 Historical building, Antakya

Floors and roofs are made of timber, although in a number of cases the roof is substituted by a reinforced concrete slab, as described in detail in Section 5.6.3.4.

Another structural system is quite frequently met in Antakya. Two-storey buildings (Figure 5.6.5, Figure 5.6.6) are made of stone masonry at the ground floor, whereas the upper storey is made of timber-framed masonry. The floor and the roof are made of timber, while the upper storey is protruding either over the entire perimeter of the ground floor or over two or three faces of the buildings (depending on whether the building is isolated or in a continuous system with other buildings. The protruding part of the upper storey is supported by timber beams (cantilevers). The same system is found in Gaziantep, as well, where the upper storey is made of stone masonry, while its protruding part is completely made of timber (Figure 5.6.3).

(a) (b)

Figure 5.6.5 Mixed, stone masonry and timber-framed masonry buildings in Antakya

Figure 5.6.6 Closed balcony, Gaziantep

In a number of cases, there are balconies, covered and closed (Figure 5.6.6), made of timber.

Finally, there are few buildings (Antakya and Islahiye) made of non-fired bricks (adobe), as shown in Figure 5.6.7 and Figure 5.6.8.

Figure 5.6.7 Antakya, collapsed building, partly made of adobe containing straw.

Figure 5.6.8 Islahiye, adobe building**.**

5.6.2 Construction Typology of Masonry

The damage that numerous masonry buildings have suffered has revealed the construction typology, not only of the faces of masonry elements, but within their thickness as well.

Figure 5.6.9 Gaziantep, Şirvani Camii

Figure 5.6.10 Gaziantep, masonry typology of a historical building

As shown in Figures 5.6.9 to 5.6.12, masonry is typically three-leaf. The exterior leaves are made either of cut stone masonry (with very thin mortar joints, Figures 5.6.9, 5.6.10 and 5.6.12e) or of rubble stone masonry (e.g., Figure 5.6.11, Figure 5.6.12a and 5.6.12b). The interior leaf is typically

made of rubble stone masonry, although there are exceptions (Figure 5.6.10) where both outer leaves are made of cut stones. The space between the exterior leaves is filled with a mix of small rubble stones and rather poor- quality mortar, either lime mortar (see e.g., photos in Figure 5.6.12) or earthen mortar (Figure 5.6.10). The collapsed outer leaf shows that there are no header stones connecting the exterior leaves in the transverse direction (e.g., Figure 5.6.12c).
It is noted that this construction typology is quite typical for historical masonry buildings around the Mediterranean, and it is a very vulnerable type of masonry, as numerous earthquakes have proven (Figure 5.6.13).

Figure 5.6.11 Antakya, stone masonry (ground floor) and adobe (first storey)

(a) (b)

(c) (d)

(e)

Figure 5.6.12 Antakya, stone masonry in buildings of the historical centre

Figure 5.6.13 Samos island, typical masonry typology (2020, Samos earthquake)

Figure 5.6.14 Antakya, three-leaf masonry with the interior leaf made of timber-framed masonry

In few buildings, in Antakya, a different construction typology was identified, as shown in Figure 5.6.14. The exterior leaf is made of rubble stone masonry, while the interior leaf is made of timber-framed masonry. Similar construction type is identified (Figure 5.6.15 and Figure 5.6.16) in the island of Lesvos (Greece), both in Plomari and Vrissa (severely damaged due to the June 12th, 2017 earthquake).

(a) (b)

(c)

Figure 5.6.15 Plomari, Lesvos: The interior leaf of masonry (a) in a residential building (NTUA Report) and (b) in a factory, (c) The exterior leaf has collapsed, and the interior leaf is visible.

Figure 5.6.16 Vrissa, Lesvos Island, after the 2017 earthquake. The collapse of the exterior leaf of masonry revealed the interior timber-framed masonry (NTUA Report)

5.6.3 The vulnerability of masonry buildings

Unreinforced masonry buildings constitute a significant portion of the building stock in many earthquake-prone areas in the globe, while most of them are part of the built cultural heritage. Unreinforced masonry buildings are characterized by enhanced vulnerability against earthquakes, compared to RC or steel buildings:

(a) They are massive structures, made (frequently) of a material of rather poor mechanical properties. Masonry is an anisotropic and brittle material, unable to withstand large imposed deformations without pronounced disintegration. The historical masonry typologies, namely, two- and three-leaf masonry without transverse connection of the leaves, are vulnerable both to in- and to out-of-plane actions.

(b) Typically, masonry buildings are provided with rather flexible in their plane timber floors and roofs, sitting on the walls and allowing for significantly different deformations of the vertical walls during an earthquake. Thus, the box-action of the buildings is inadequate.

Those characteristics of unreinforced masonry buildings are responsible for typical damage patterns, identified in countries with similar construction traditions, after the occurrence of moderate and strong earthquakes. All those typical damage patterns were observed in the regions affected by the February 6th, 2023, earthquakes, as shown in the following Figures.

5.6.3.1 Diagonal or bi-diagonal cracks in walls due to in-plane shear

This typical damage, consisting of diagonal or bi-diagonal cracks in the walls, appears in varying degree, ranging from simple diagonal cracks of rather limited width (e.g., Figure 5.6.17c and 5.6.17d) to the occurrence of large cracks and disintegration of the walls or piers (e.g., Figure 5.6.17b and 5.6.17g). It is also observed that the oblique cracks may extend to the floor (e.g., Figure 5.6.17b and 5.6.17g).

(a)

(b)

(c)

(d)

(e)

(f)

(g)

Figure 5.6.17 Typical damage due to in-plane shear cyclic deformation of walls.

5.6.3.2 Damage due to out-of-plane actions

It is noted that in many buildings, there were combined in-plane and out-of-plane failures of walls. This was the case, mainly, in the historical centre of Antakya. The damage due to out-of-plane actions presents various degrees of severity, as shown in the photographs of Figure 5.6.18. It should also be noted that out-of-plane collapse of walls is frequently the cause of collapse of the roof and, hence, of injuries and/or casualties.

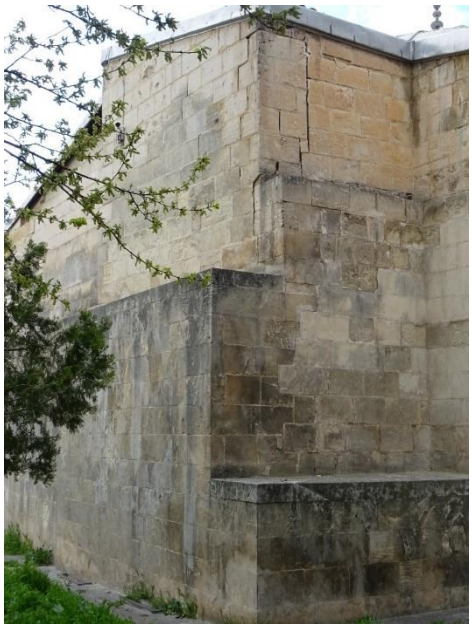

(a)

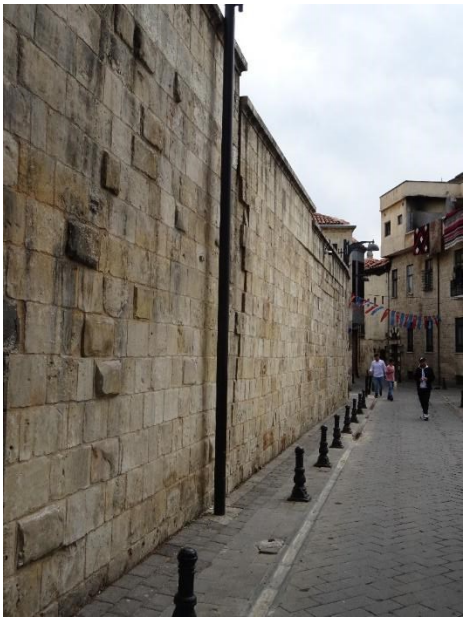

(b)

(c)

(d) (e)

(f)

(g)

(h)

(i)

Figure 5.6.18 Various degrees of damage due to out-of-plane action of the earthquake, in buildings (a) to (c) at Gaziantep, (d) to (i) Antakya

5.6.3.3 The detrimental effect of openings close to the corners of buildings

This is a specific and quite frequent damage that may cause partial collapse of the building. Indeed, the pier at the corner of the building is subjected to a combination of in- and out-of-plane actions, as well as to significant variation of its axial load during the earthquake. As a result, it may be disintegrated, or it may collapse. The effect of such a collapse on the overall stability of the building depends, among others, on the availability of other walls of significant sectional dimensions. The detrimental effect of openings close to the corners of buildings is illustrated in the photographs of Figure 5.6.19.

(a)

(b)

(c)

(d)

Figure 5.6.19 Unreinforced masonry building in Antakya. The detrimental effect of openings close to the corners.

5.6.3.4 Inadequate Interventions

The inspection of severely damaged buildings has revealed the, sometimes catastrophic, effect of inadequate interventions to unreinforced masonry buildings. Of course, there may be buildings adequately strengthened that did not undergo significant damage and, hence, the effect of interventions could not be detected and illustrated.

Several historical buildings seem to have been strengthened, especially in Antakya. It seems that the main intervention to those buildings was the replacement of the original timber roof by a reinforced concrete slab. The severe damage or the collapse due to the earthquake has allowed for the following observations to be made:

(a) There was no case in which strengthening of the vertical masonry elements was detected, whereas

Figure 5.6.20 Antakya, collapse of the upper storey, as a result of the action of the RC slab (upper photo: A.Sextos)

(b) the failure mode shows that the reinforced concrete slab was simply resting on the walls. Although the purpose of the intervention was to provide a stiff diaphragm at the top of the building, the addition of a significant mass, unconnected to the non-strengthened masonry walls of vulnerable construction typology has led to the partial or complete collapse of the upper storey of several buildings.

An example of the effect of the aforementioned intervention is shown in Figure 5.6.20, where the walls of the upper storey have collapsed, and its RC slab is sitting on the lower storey slab. A

similar case is shown in Figures 5.6.21, 5.6.23 and 5.6.24. In Figure 5.6.22, the walls at the façade of the building have collapsed out-of-their plane. The RC slab has lost its support.

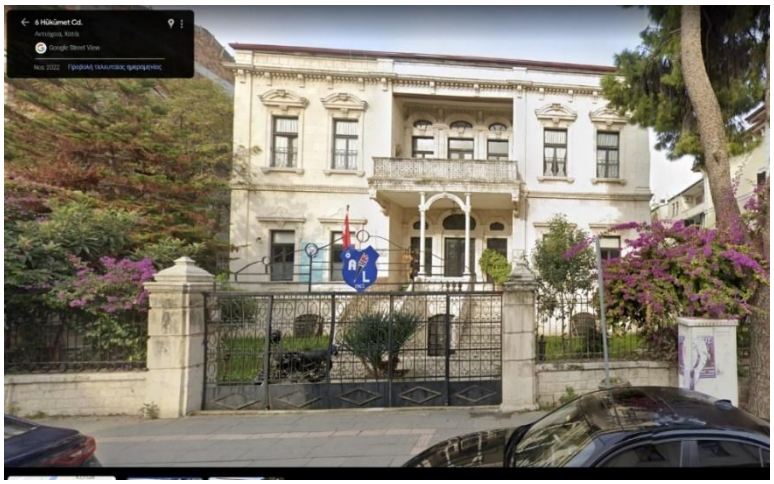

(a)

(b)

Figure 5.6.21 Antakya, a historic building (a) before the earthquake (Google map, street view) and (b) after the earthquake

Another case, that of a historic “han” (inn), is shown in Figure 5.6.25. The RC tie beam constructed at the top of the second floor has collapsed (Figure 5.6.25b), following the out-of-plane collapse of the façade wall. In the second photo of Figure 5.6.25b, one can see that the RC tie beam was constructed only on top of the interior leaf of the masonry wall. It seems that cement mortar was used as filling material over the vaults.

Finally, Figure 5.6.26 shows a case, where a RC slab was constructed at the top of the first floor. In the collapsed façade masonry wall, one can see the RC jacket (the small diameter reinforcing bars of the slab are anchored into the jacket). Furthermore, in the standing roof, one can distinguish a RC tie beam, clearly simply sitting on the collapsed façade wall.

(a)

(b)

Figure 5.6.22 Antakya, a historic building (a) before the earthquake (Google map, street view) and (b) after the earthquake

(a)

(b)

Figure 5.6.23 Antakya, the collapse of both storeys of a historic building (Protestant church). Fragments of RC slab(s) are visible on the ruins, (a) the building before the earthquake (Google map, street view), (b) after the earthquake

(a)

(b)

Figure 5.6.24 Antakya, historic building (a) before the earthquake (Google map, street view), (b) after the earthquake.

(a)

(b)

Figure 5.6.25 Old inn (han) in Antakya: (a) Before the earthquake (Google map, street view), (b) after the earthquake

Figure 5.6.26 Antakya, the effect of inadequate intervention using RC slab and jacket to masonry walls.

It should be noted that this type of interventions to existing masonry buildings, i.e., replacement of timber floors and roofs by RC slabs, jacketing of masonry walls (frequently, one-sided) and construction of RC tie-beams simply resting on masonry walls, was quite frequent in Europe and elsewhere some decades ago. The effect of those interventions on the seismic behaviour of masonry buildings, and-more specifically-on historical buildings and monuments, has led the competent authorities in several countries to discourage or even to prohibit the use of RC in interventions to masonry buildings.

An example of interventions using RC is shown in Figure 5.6.27: A RC slab has replaced the timber floor of the first storey. RC tie beams were provided to masonry at three levels, along with stiff RC lintels to the openings in both storeys. The photo shows that the roof is made of timber, and it is sitting on the RC tie beam. The three-leaf stone masonry is not taken care of. The intervention could not prevent the out-of-plane collapse of the upper storey masonry walls along two sides of the building, Partial collapse of the wall at the corner of the building did occur in the lower storey as well.

5.6.4 The behaviour of a historical construction system

As mentioned in Section 5.6.1, in the old part of Antakya, there are several two-storey buildings, in which the lower storey is made of stone masonry, while the upper storey is made of timber-

framed masonry. This is a historical structural system, found in other earthquake prone areas too, e.g., in the island of Lefkada, Greece (Figure 5.6.28).

Figure 5.6.27 Illica, Italy, after the 2016 Rieti earthquake: The effect of interventions to a masonry building

Figure 5.6.28 Lefkada-island, Greece: Typical historical building

(a)

(b)

(c)

Figure 5.6.29 Antakya, buildings constructed according to the historical structural system, (a) Typical building, (b) Building in continuous system. Most probably, the large doors in the ground floor are not original. The building may have survived thanks to the adjacent buildings, (c) The damage in the upper storey is due to the interaction of the building with the adjacent entrance to the Habib-i Nejjar Mosque.

In this structural system, stiffness and lateral resistance is provided by stone masonry at the ground floor. The weight of the upper storey, made of thin timber-framed masonry is significantly reduced (compared to the massive stone masonry walls). Nonetheless, the lateral stiffness of the upper storey walls is sufficient for shear distortion to be limited.

The seismic behaviour of this system is known to be adequate, and this was confirmed in several cases, in buildings at Antakya (Figure 5.6.29). Although we cannot know how many other buildings constructed according to this system have collapsed, it is to be admitted that the buildings shown in Figure 5.6.29, although not maintained, did survive amidst collapsed buildings. It is questionable whether those buildings can be preserved. Nonetheless, it may be assumed that their survival offered life protection to their inhabitants.

5.6.5 Adobe buildings

A small number of adobe buildings are still in use at Islahiye. Reportedly, their total number does not exceed twenty. The few inspected buildings (Figure 5.6.30) present damage typical for unreinforced masonry buildings, namely, vertical cracks in the walls due to out-of-plane actions and tendency of separation of perpendicular walls (Figure 5.6.30a), shear cracks (Figure 5.6.30b) and out-of-plane collapse of walls (Figure 5.6.30c).

(a)

(b)

(c)

Figure 5.6.30 Islahiye, adobe buildings and their damage.

5.6.6 Damage to monuments

The built cultural heritage in the affected area is rich in monuments, namely, castles, mosques, churches, etc. The team did not specifically focus on significant individual monuments, as in several cases-for safety reasons-the access to severely damaged or collapsed monuments was not permitted. Furthermore, with the exception of some damage, typical for all unreinforced masonry constructions, the affected monuments exhibited damage that cannot be interpreted unless more data are available (e.g., drawings, history of the monument, including previous damage and interventions, etc.). This is more so for monuments that have partially or completely collapsed. Thus, in this Section, only selected photographs are presented, showing the before and after earthquake state of the monuments the team has inspected, without entering to them though.

5.6.6.1 The Gaziantep Castle

The castle (Figure 5.6.31), dating back to the Roman era, was preserved in a seemingly good state, having been subjected to several interventions during its lifetime. However, the history of the monument, including events that have affected its structural behaviour is not known to the team. Extensive and severe damage has occurred, as shown in Figure 5.6.32. Shear cracks (Figure 5.6.32a) out-of-plane collapse of the exterior leaf of masonry (Figure 5.6.32b), disintegration of thick masonry elements (towers, Figure 5.6.32c). The masonry typology and the observed damage prove that strengthening of this vulnerable masonry was not among the measures taken to protect the monument against earthquakes.

Figure 5.6.31 The Gaziantep castle before the earthquake (source: Google map, street view)

(a)

(b)

(c)

Figure 5.6.32 Gaziantep Castle, Damage observed in various parts of the monument

5.6.6.2 Şirvani Mosque, Gaziantep

The 17th century mosque (Figure 5.6.33) was in good state before the earthquake. Its current state is apparently due to the collapse of the minaret (Figure 5.6.34). The current situation, and the limited access to the monument do not allow for further causes of damage to be identified, although there are some typical cracks in the walls due to in-plane shear. Furthermore, the damage to the perimeter masonry reveals the vulnerable (three-leaf) masonry typology identified in historical buildings as well.

Figure 5.6.33 Şirvani Mosque, Gaziantep, before the earthquake. Source: Google map, street view.

Figure 5.6.34 The mosque after the earthquake, damage due to the collapse of the minaret

5.6.6.3 The Greek Orthodox Church in Antakya (St. Paul's Church)

The construction of the Orthodox Church in Antakya was initiated in the 1860s. According to the official site of the Turkish Ministry of Culture, the church was destroyed due to the 1872 earthquake in the region (https://www.kulturportali.gov.tr/turkiye/hatay/gezilecekyer/ortodoks-kilisesi).Its reconstruction has started in the late 19th century and the church is open for worship since 1900.

Figure 5.6.35 The Greek Orthodox Church at Antakya, before the earthquake (source: Google map, street view)

Figure 5.6.36 The Greek Orthodox church at Antakya, after the earthquake (source: timesfreepress.com)

5.6.6.4 Habib-i Neccar Cami, Antakya

According to Türkiye Kültür Portalı, the mosque was built when Antakya was conquered by the Muslim Arabs in 638 AD (https://www.kulturportali.gov.tr/turkiye/hatay/gezilecekyer/habib-i-neccar-camii). It is considered to be the first mosque built within the borders of today's Turkey.

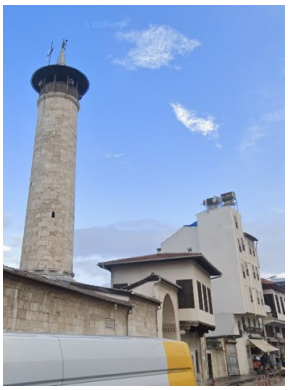

Figure 5.6.37 The Habib-i Neccar Cami before the earthquake (source: Google map, street view)

Figure 5.6.38 Aerial view of the monument after the earthquake (source: timesfreepress.com)

The monument was severely damaged (Figure 5.6.38). Although it is certain that the observed damage is due to the collapse of the minaret, one may observe the poor quality of masonry that was completely disintegrated, as well as damage typical for unreinforced masonry structures (e.g., shear cracks, Figure 5.6.39). It is admitted though that the current state of the monument does not allow for further interpretation of the damage and partial collapse.

Figure 5.6.39 Damage observed in the standing parts of the Habib-i Neccar Camii

References

5.1 Gulkan P., Aschheim M., Spence R.. World Housing Encyclopedia: Reinforced concrete frame building with masonry infills. Turkey. Rep. 64. [2002]. Earthquake Engineering Research Institute and Intern. Assoc. of Earthquake Engineering.

5.2 Toki, Ministry of Environment, Urbanisation and Climate Change, Housing Development Administration. https://www.toki.gov.tr/en/

5.3 Bikçe M., Erdem M. [2021]. Investigation of Construction Material Quality and Workmanship Defects of RC Buildings Collapsed and Severely Damaged in the 6.8 Mw Sivrice, Elaziğ, Turkey, Earthquake, January 2020, Bulletin of the New Zealand Society for Earthquake Engineering, 54(3), pp. 184-196.

5.4 Sabahoğlu A., Eryılmaz M.R., Bikçe M., Evaluation of Concrete Compressive Strength of Urban Transformation Buildings in Hatay, [2019], International Conference on Innovation, Sustainability, Technology and Education in Civil Engineering. Iskenderun (in Turkish).

5.5 Gunes, O., 2015. Turkey's grand challenge: Disaster-proof building inventory within 20 years. *Case Studies in Construction Materials 2*, 18–34.

5.6 Ay, B.Ö., Eroğlu Azak, T., Erberik, M.A., 2016. Evaluation of Changing Building Characteristics in Turkey. *ACE 2016, 12th International Congress on Advances in Civil Engineering*, Istanbul, Turkey.

5.7 Bilgi, E.M., Tümer, E.U, 2020. Building Typologies in Between the Vernacular and the Modern: Antakya (Antioch) in the Early 20th Century. *SAGE Open*, 1–18.

5.8 Cetin, KO, Mylonakis, G, Sextos, A, Stewart, JP (report coordinators), 2020. Seismological and engineering effects of the M 7.0 Samos Island (Aegean Sea) Earthquake. *GEER Report 069*, Hellenic Association of Earthquake Engineering, Earthquake Engineering Association of Turkey, Earthquake Foundation of Turkey, Earthquake Engineering Research Institute, Geotechnical Extreme Event Reconnaissance Association, https://doi.org/10.18118/G6H088.

5.9 Palieraki, V, Zeris, Ch, Vintzileou, E, and Adami, Ch-E, 2018. In-Plane and out-of Plane Response of Currently Constructed Masonry Infills. *Journal Engineering Structures,* 177, 103-116.

5.10 Qu, Z., Wang, F., Chen, X., Wang, X., Zhou, Z., 2023. Rapid report of seismic damage to hospitals in the 2023 Turkey earthquake sequences. Earthq. Research Advances, doi.org/10.1016/j.eqrea.2023.100234

5.11 REUTERS, https://www.reuters.com/world/middle-east/doctor-says-bodies-everywhere-collapsed-iskenderun-hospital-2023-02-07/

5.12 Seismic Isolation Engineering Inc., http://www.siecorp.com/.

5.13 Sumer, A., Phipps M., Lizundia B., Wray, G., Roufegarinejad, A., Henoch, R., Akinci, O., 2023. Impact of the Kahramanmaraş Earthquakes on Hospitals: A Preliminary Report from the EERI Reconnaissance Team

5.14 TIS https://www.tis.com.tr

5.15 Abrahamson, NA, Silva, WJ, and Kamai, R, 2014. Summary of the ASK14 ground motion relation for active crustal regions. *Earthquake Spectra,* 30, 1025-1055.

6. Critical Infrastructure

Chapter Author: ***Sotiria STEFANIDOU***

Infrastructure damage after the earthquake events in Turkey was reported extensive, mainly in Hatay, Kahramanmaras, and Gaziantep (Gunasekera et al., 2023). Damage observed to roadway bridges was mainly due to ground deformation and damage to roads/highways due to fault rupture on the surface. Extensive damage to railway track lines was also reported. Direct infrastructure damage was estimated to be approximately equal to US$6.4 billion (Gunasekera et al., 2023), while total (direct and indirect) losses are expected to be higher due to traffic disruption and the required time for recovery and reconstruction.

As already described in previous sections, the Greek reconnaissance team mainly focused on the inspection of buildings, performing post-earthquake rapid assessment. However, the bridges (reinforced concrete (RC), masonry, steel bridges) of the urban network of the cities visited (shown in Figure 6.1) were inspected, as well as the bridges of the interurban roadway network connecting the inspected cities. It is outlined that the inspection of bridges was not detailed and did not include bridges with extensive damage, that were reported and shown elsewhere (Çetin et al., 2023a), nor older bridges that were not seismically designed. Since the field trip was strictly scheduled, the team did not have the time to thoroughly inspect the bridges that were reported severely damaged. Furthermore, most of the collapsed or severely damaged bridges had already been removed or repaired at the time of the visit (2.5 months after the event).

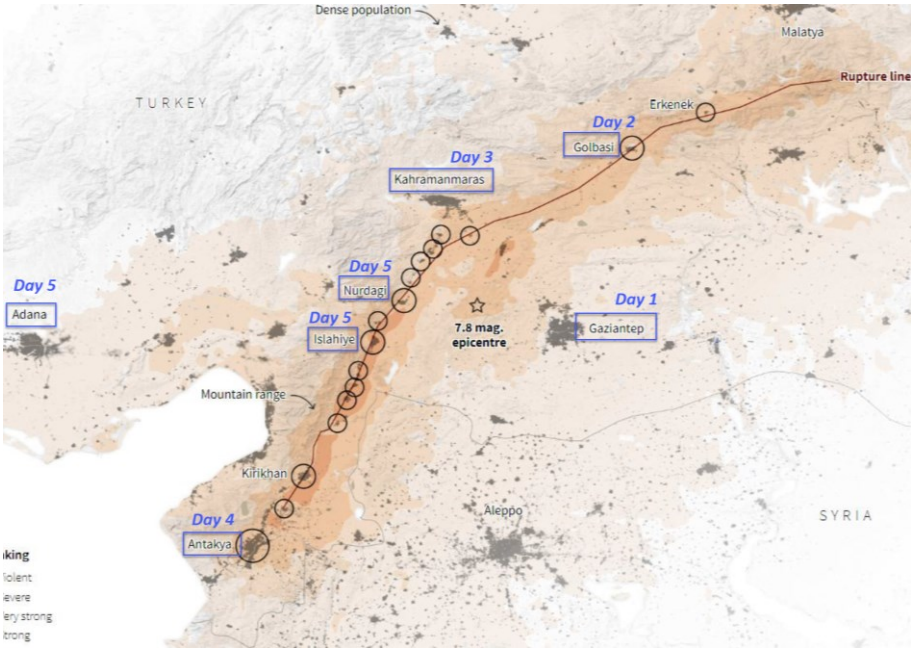

Figure 6.1 Interurban roadway network inspected

6.1 Bridges

All the bridges of the urban network inspected in Gaziantep were undamaged or exhibited minor damage due to small permanent bearing deformation; therefore, the functionality of the network was not disrupted, and the bridges were in normal service. The majority of the bridges were seismically isolated; therefore, no damage was generally observed to bridge piers. It should be outlined that the fundamental period (T) of the bridges is, in most cases, >1.0 sec; therefore, the spectral value for bridge structures was substantially lower than the relevant for low- or high-rise buildings (Figure 6.2). As depicted in Figure 6.2, the input seismic force for bridges in Gaziantep was approximately seven times lower than the relevant for 4-storey buildings (T~0.4sec).

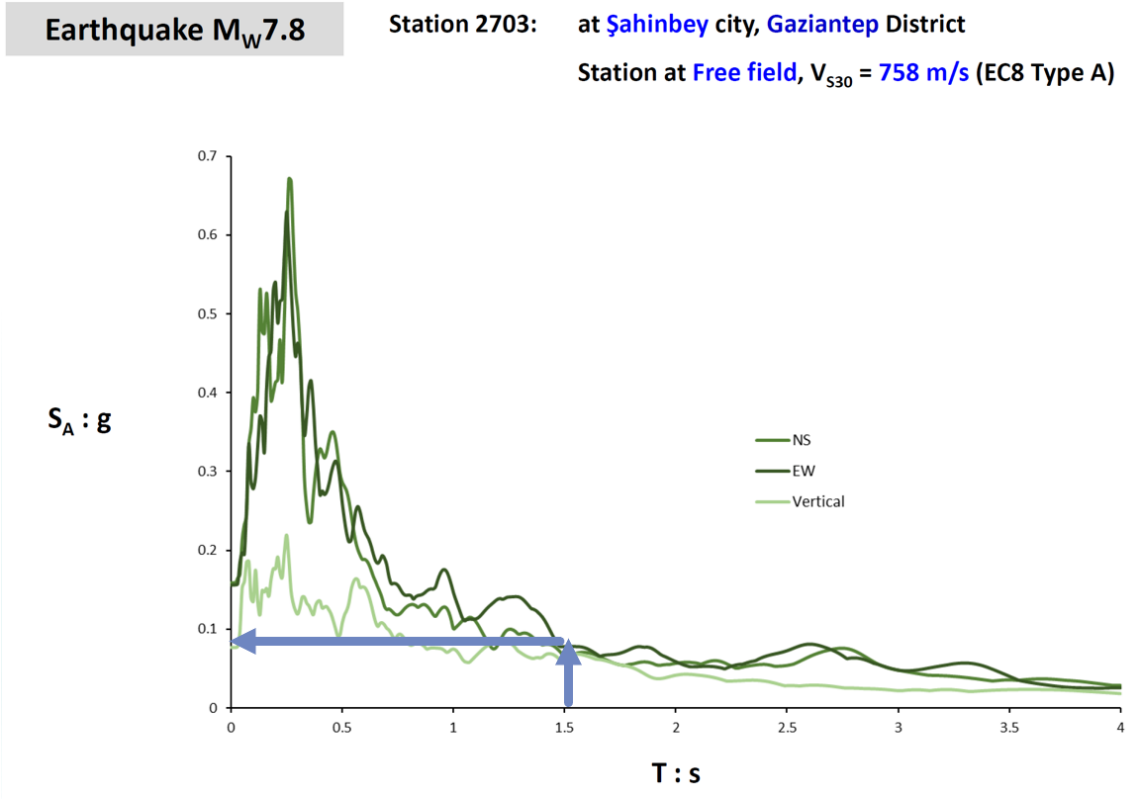

Figure 6.2 Elastic response spectra for the record of Gaziantep station and spectral value for RC bridges.

Two seismically isolated RC overpasses with simply supported and continuous decks respectively were inspected in Gaziantep and shown in Figures 6.3 and 6.4. Both bridges were not damaged and performed well during the earthquake events. In both cases, the wall-type and cylindrical piers performed elastically, while small permanent bearing deformations were inspected. No damage was observed at the abutments.

Figure 6.3 Simply supported, isolated RC bridge (overpass) in Gaziantep.

Figure 6.4 Continuous, seismically isolated RC bridge (overpass) in Gaziantep.

Bridges of the interurban roadway network connecting Golbasi and Kahramanmaras were inspected. The elastic spectra of the recording at Kahramanmaras station are presented in Figure 6.5. Obviously, the spectral values for bridges (T>1.0sec), and eventually the input seismic forces, are four times higher than the relevant ones at Gaziantep.

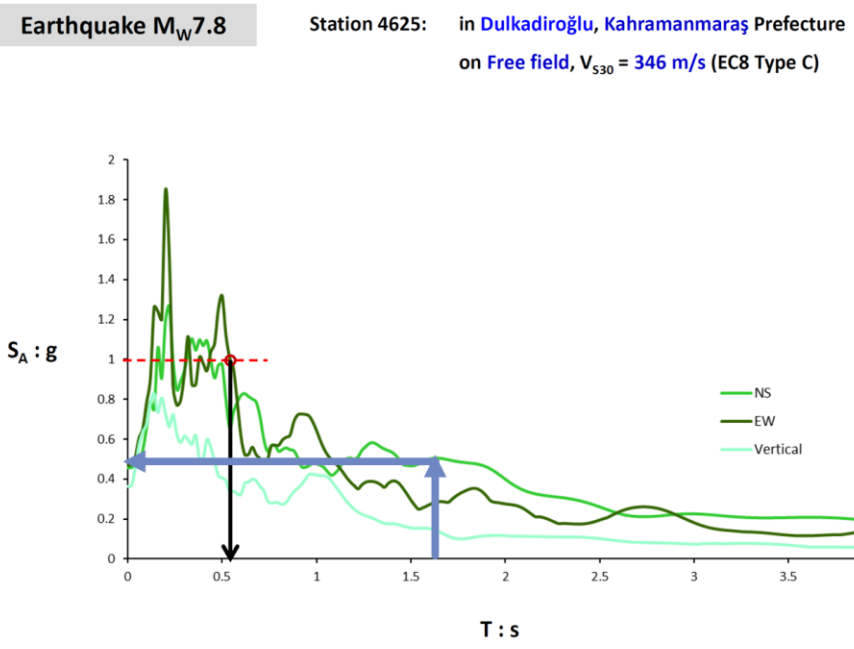

Figure 6.5 Elastic response spectra for the record of Kahramanmaras station and spectral value for RC bridges.

Figure 6.6 Shear key (stopper) failure of a seismically isolated bridge of Kahramanmaras interurban network

Minor damage was observed at the inspected bridges, related to the collapse and/or crushing of the seismic stoppers and shear keys, mainly attributed to extensive deformation along the transverse direction. Relevant damage modes were inspected at the seat-type abutments, along with embankment soil failure in some cases. An example of the inspected damage of the Golbasi to Kahramanmaras roadway network is presented in Figure 6.6 for a simply supported bridge. Shear key failure at the pier-to-deck connection shown in Figure 6.6 is the most frequent failure mode of the overpasses of the roadway network inspected.

As already stated, damage as a proportion of total building/infrastructure stock was greatest in Hatay. The Greek reconnaissance group focused on building inspection in Hatay; however, a roadway and a pedestrian bridge of the urban network were also inspected (Figure 6.7 and 6.8, respectively). Both bridges performed well; minor to moderate damage was observed at the roadway RC simply supported the bridge due to permanent soil displacements, while no structural damage was observed at the pedestrian steel truss bridge inspected.

Figure 6.7 Simply supported riverine bridge at Antakya

Figure 6.8 Steel truss pedestrian bridge at Antakya

In Adana, building stock and infrastructure damage was not reported as extensive compared to the other areas inspected. An old masonry bridge inspected with no structural damage is shown in Figure 6.9, and a railway bridge with simply supported steel deck in full service is shown in Figure 6.10.

Figure 6.9 Masonry bridge in Adana

Figure 6.10 Railway bridge with steel deck in normal service

More details regarding bridge damage observed, resulting in traffic disruption and replacement/recovery, are available elsewhere (Çetin et al., 2023a, Çetin et al., 2023b). In general, it is reported that newly constructed bridges performed well, however, the evaluation of the new and older bridges is a timely and demanding procedure due to the extended exposure and the limited accessibility in many cases; therefore, detailed inspection results are expected in the near future to evaluate the urban and interurban network seismic performance.

6.2 Tunnels

All the tunnels inspected at the roadway network connecting the inspected cities were undamaged and fully in service. Limited minor damage related to the crushing of concrete at the inner surface was reported in 1-2 cases; more data is available in Çetin et al., 2023a.

6.3 Railway tracks

Permanent ground displacements resulted in damage of railway tracks in many cases, as shown in Figure 6.11 at Golbasi.

Figure 6.11 Railway track damage

References

6.1 Gunasekera, R, Ishizawa, E, Oscar, A, Daniell, JE, Pomonis, A, Macabuag, JLDC, Brand, J, Schaefer, A, Romero, H, Roberth, A, Esper,S, Otálora, SG, Khazai, B, Cox, KD, 2023, Global Rapid Post-Disaster Damage Estimation (GRADE) Report : February 6, 2023 Kahramanmaraş Earthquakes - Türkiye Report (English). Washington, D.C. : World Bank Group.

6.2 Çetin, KO, Bray, JD, Frost, JD, Hortacsu, A, Miranda, E, Moss, RES, Stewart, JP, 2023, February 6, 2023 Türkiye Earthquakes: Report on Geoscience and Engineering Impacts. Earthquake Engineering Research Instute, LFE Program.

6.3 Çetin, KO, Ilgaç, M, Can, G, and Çakır, E, 2023, Preliminary Reconnaissance Report on February 6, 2023, Pazarcık Mw=7.7 and Elbistan Mw=7.6, Kahramanmaraş-Türkiye Earthquakes, Report No:METU/EERC 2023-01

6.4 Garini E., Gazetas G. (2023) “Preliminary Report on the M7.8 and M7.5 earthquakes of February 6, 2023 in Turkey-Syria, DOI 10.17605/OSF.IO/V4MSW

7. Rapid Visual Inspection of buildings

Chapter Authors: ***Anastasios SEXTOS*** *and* ***Aristidis PAPACHRISTIDIS***

Many methodologies are available for pre- and post-earthquake assessment of structures, while the most popular and widely used is the FEMA method for Rapid Visual Screening (RVS) or Rapid Visual Inspection (RVI) of Buildings (FEMA P-154 (2015), FEMA 356, (2000)). The NZSEE (New Zealand National Society for Earthquake Engineering), JBDPA (Japan Building Disaster Prevention Association, 1990) and the GNTD (Gruppo Nationale Per La Difesa Dai Terremoti, 1993) are also widely applied methodologies for Rapid Visual Screening. The RVI procedure prescribed by FEMA uses a methodology based on the building survey inspection and requires the filling of a data collection form based on visual observation of the building from the exterior, and if possible, the interior. The two-page data collection form includes building identification information (i.e. usage, area, floor number, etc.), a photograph of the building, sketches, and documentation of pertinent data related to seismic performance. Based on the data collected during the survey, a score is calculated that provides an indication of the expected seismic performance of the building. Simple survey procedures for seismic risk assessment are proposed and applied to urban building stocks to provide damage statistics [3].

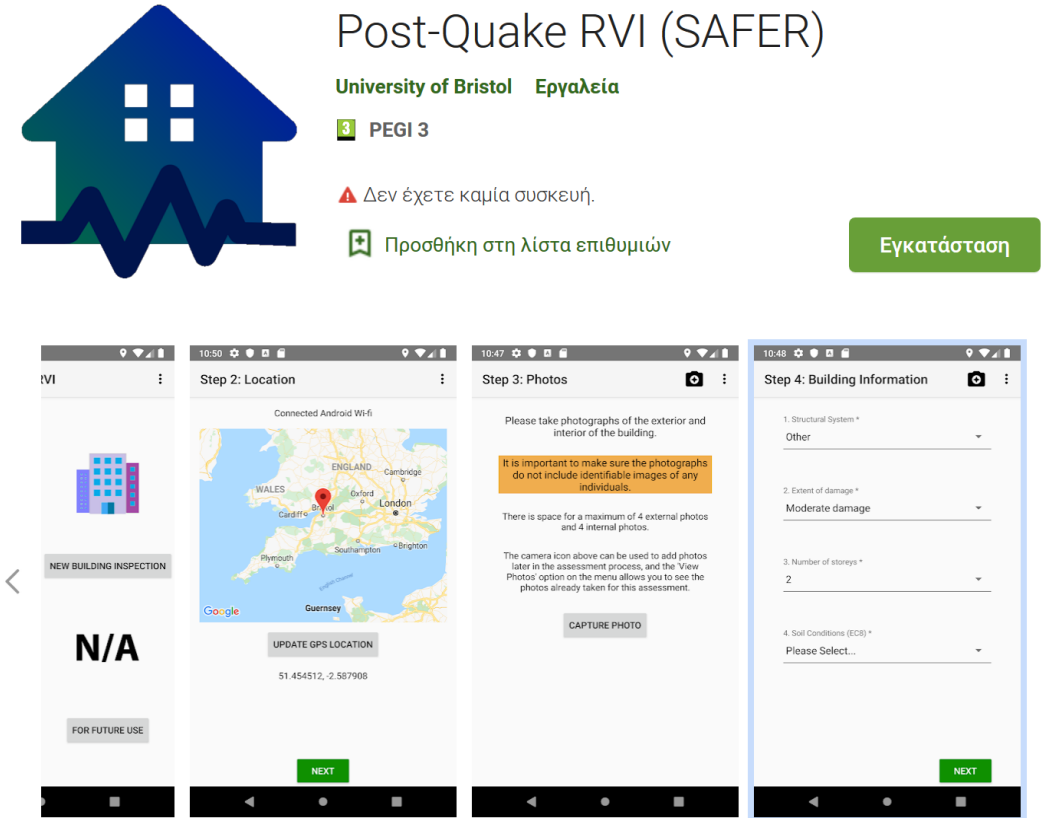

Figure 7.1 Post-Quake RVI (Safer) mobile app.

To perform Post-Quake RVI and store the relative information in an online database, the use of a tool for rapid visual survey was necessary. The TEE/NTUA/HAEE team, consisting of experienced civil engineers, used the Post-Quake RVI (SAFER) app (Figure 7.1). This is a tool developed by the University of Bristol following the 2016 central Italy earthquake [4,5]. For every building inspected, the app retrieves the GPS location [6], while the user stores (and the app wirelessly transmits) external and internal photos and general building information affecting its seismic performance (structural system, extent of damage, number of storeys, soil conditions, etc.). Furthermore, information related to the type of damage (i.e. beam flexural or shear damage, panel out-of-plane cracking, etc) is also collected for every building. The data of all buildings inspected is then saved and uploaded to a central data server, that is accessible through a dedicated WebApp. During the field mission, the data (summarized in Table 7.1) were harvested following inspection surveys of 238 buildings using the above app. The geographical distribution of the inspected buildings in space is highlighted in Fig. 7.2 for different structural typologies as are broken down in Fig. 7.3.

An important disclaimer that needs to be made is that the focus of the inspecting field team was mainly on severely damaged buildings. As a result, the statistical distribution and conclusions reflect the particular building sample only and should not be extrapolated to the entire set of structures of the visited towns and cities. This is particularly stressed considering that the number of buildings inspected is only a fraction of the actual building portfolio in the area.

Table 7.1: List of collected data using Post-Quake RVI (SAFER)

Location	GPS latitude/longitude, Country
Building Information	Structural System, Extend of damage, Number of Stories, Soil Conditions, Regularity in plan and elevation
Type of Damage	Settlement (S) Infill panel cracking in plane, Infill panel cracking out of plane, Beam flexure failure, Beam flexure shear, Column flexure failure, Column flexure shear, Shear wall failure flexure, Shear wall failure shear, Short column failure, Joint failure, Soft storey, Pounding
Other Information	Notes, Date/time, Username

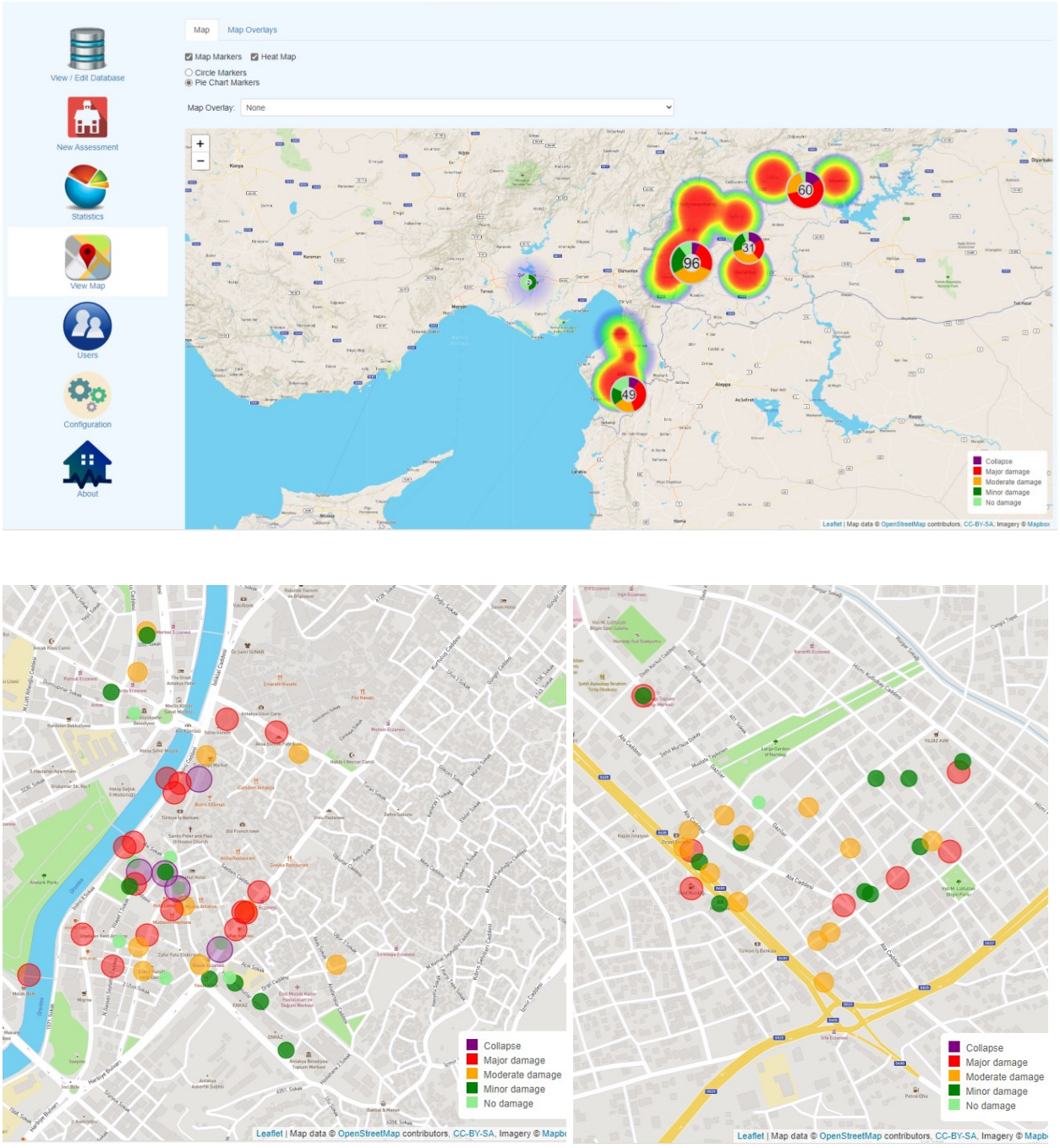

Figure 7.2 Indicative spatial distribution of the inspected buildings along with the assigned damage tagging in the affected area (Antakya on the left, Golbasi on the right).

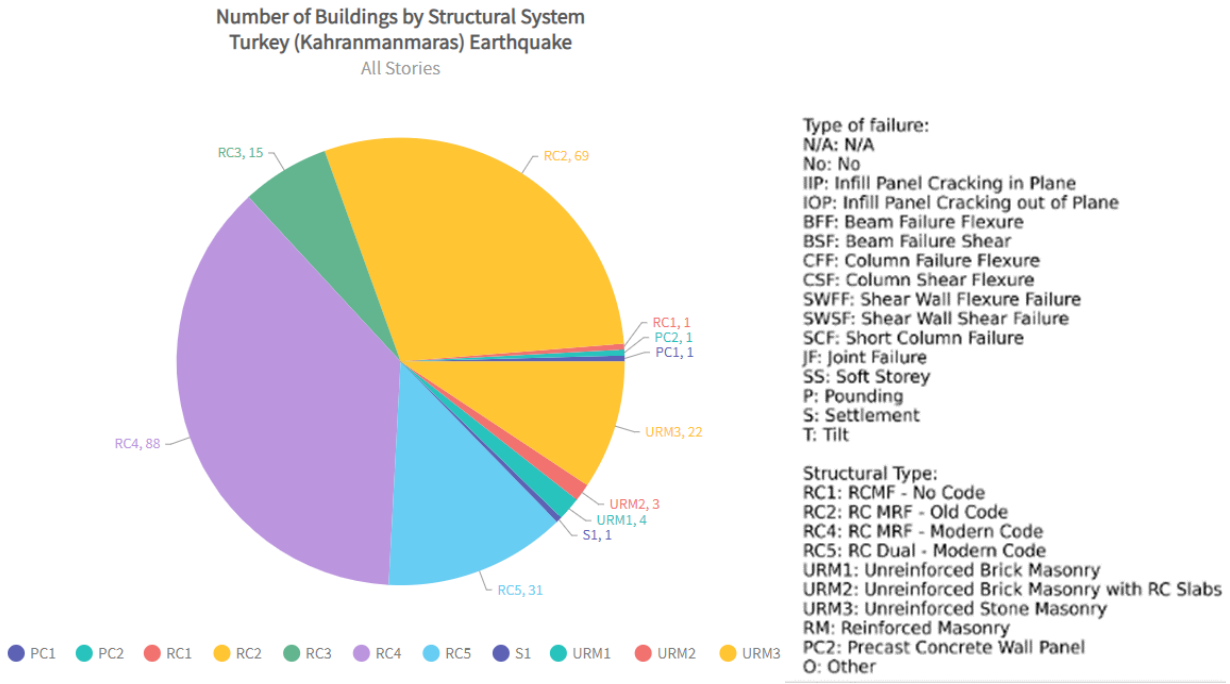

Figure 7.3 Classification of buildings inspected in terms of structural typology.

Approximately 500 buildings were also imported into the AFAD, Arc-GIS 123 Survey-based mobile phone app. The structural typology of the inspected buildings is depicted in Fig. 7.4; the categories of structural systems considered are similar to the ones prescribed in FEMA 154 ([7]. The majority of the 238 buildings inspected (approximately 80%) were reinforced concrete (RC) buildings constructed with different versions of the Turkish seismic code.

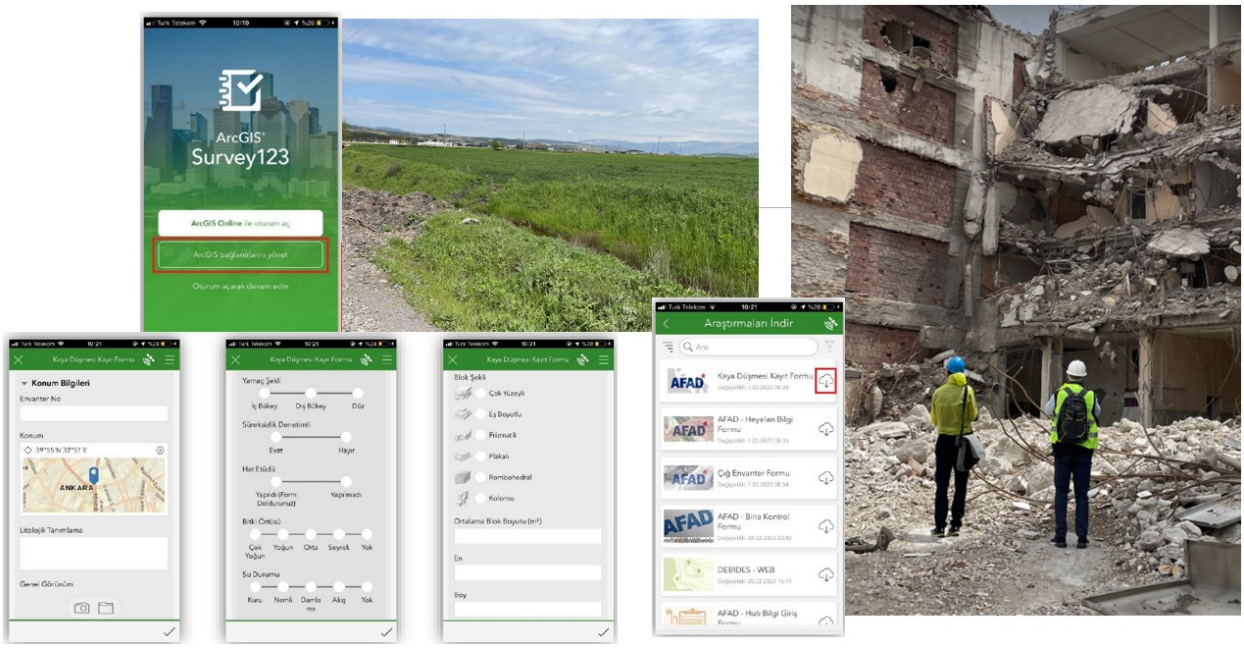

Figure 7.4 Rapid Visual Inspection using the AFAD mobile app.

The distribution of damage level per structural typology of the inspected sample of buildings is depicted in Fig. 7.4. It is interesting to note that there were RC buildings designed to modern seismic codes (RC4) that collapsed and even buildings with a dual (MRF and shear wall) structures that suffered severe damage. In fairness, one needs to appreciate the very strong earthquake ground motions that the buildings experienced during the sequence of two mainshocks and dozens of aftershocks that, to some extent, explain the severity of damage. Equally, it is important to stress the need for close quality control in terms of ensuring capacity design, which is the ultimate mechanism for collapse prevention. Overall, most RC buildings designed with old codes (RC2) and unreinforced brick masonry (URM1) suffered severe damage.

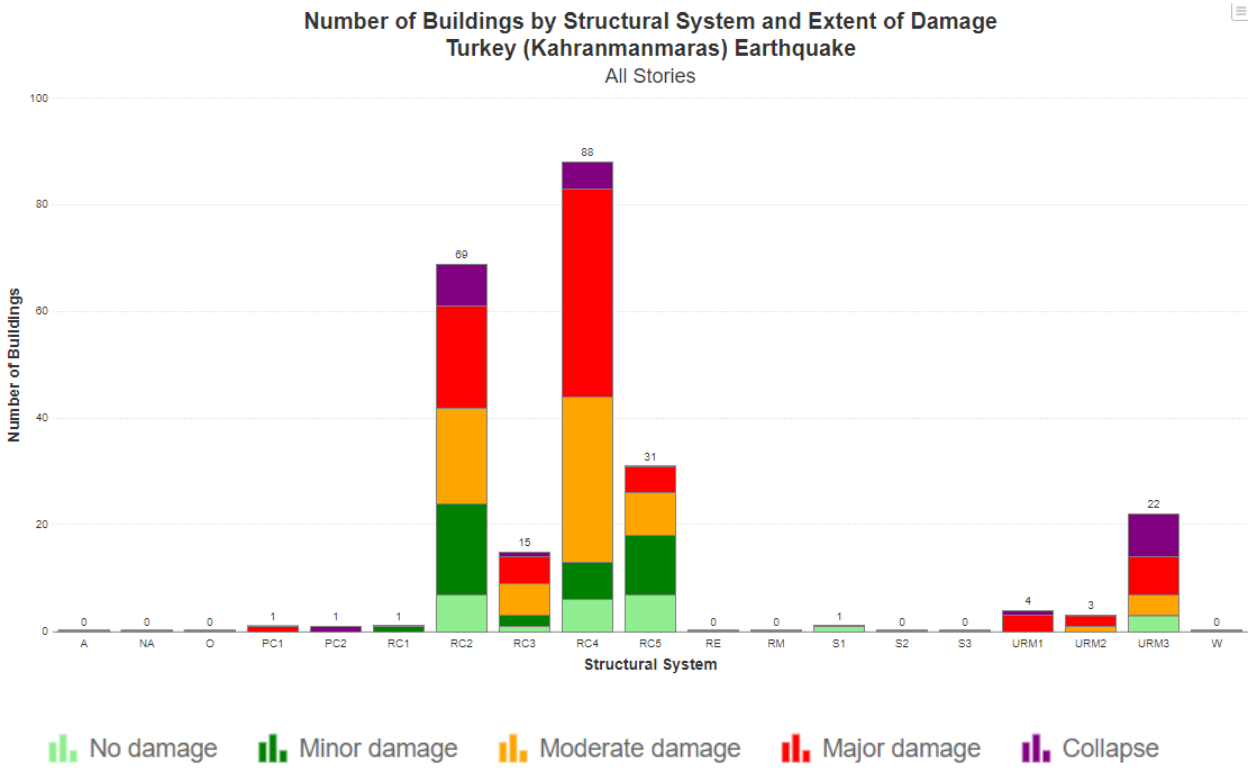

References

7.1 FEMA P-154. *Rapid visual screening of buildings for potential seismic hazards: A Handbook*. 2015. DOI: 10.4231/D3M90238V.

7.2 FEMA 356. *Prestandard and Commentary for the Seismic Rehabilitation of Buildings FEMA-356*. Federal Emergency Management Agency, Washington, D.C.: 2000.

7.3 Sucuoglu H, Yazgan U. Simple Survey Procedured for Seismic Risk Assessment in Urban Building Stocks. *Seismic Assessment and Rehabilitation of Existing Buildings* 2003(January). DOI: 10.1007/978-94-010-0021-5.

7.4 Sextos AG, De Risi R, Pagliaroli A, Foti S, Passeri F, Ausilio E, *et al.* Local Site Effects and Incremental Damage of Buildings during the 2016 Central Italy Earthquake Sequence. *Earthquake Spectra* 2018; **34**(4): 1639–1669. DOI: 10.1193/100317EQS194M.

7.5 Stewart JP, Zimmaro P, Lanzo G, Mazzoni S, Ausilio E, Aversa S, *et al.* Reconnaissance of 2016 Central Italy Earthquake Sequence. *Earthquake Spectra* 2018; **34**(4): 1547–1555. DOI: 10.1193/080317EQS151M.

7.6 Sextos AG, Kappos AJ, Stylianidis KC. Computer-aided pre- and post-earthquake assessment of buildings involving database compilation, GIS visualization, and mobile data transmission. *Computer-Aided Civil and Infrastructure Engineering* 2008; **23**(1). DOI: 10.1111/j.1467-8667.2007.00513.x.

7.7 FEMA P-154. *Rapid visual screening of buildings for potential seismic hazards: A Handbook*. 2015. DOI: 10.4231/D3M90238V.